Characterisation of organelle maintenance in *Saccharomyces cerevisiae*

Lakhan Ekal, BS-MS (Dual Degree)

This thesis is submitted to the University of Sheffield for the degree of Doctor of Philosophy

Department of Molecular Biology and Biotechnology

University of Sheffield

October 2018

Abstract

Eukaryotic cells harbour various membrane enclosed structures called organelles. These organelles perform a myriad of specialised functions to sustain cell metabolism under different growth conditions. Therefore, cells have evolved molecular mechanisms to closely monitor organelle dynamics and maintenance during cell growth and division.

Various human diseases are a consequence of dysfunctional organelle dynamics and maintenance. The budding yeast, *S. cerevisiae*, is one of the model organisms that is being studied extensively with respect to these processes and has led to identification of a variety of new factors and mechanisms that secure organelle function. Many of the fundamental principles of organelle dynamics and maintenance turn out to be conserved throughout eukaryotic evolution.

In the first part of the thesis I studied regulation of peroxisome fission which involves genetic analysis of dynamin like GTPase, Vps1 and a peroxisomal peripheral membrane protein, Pex27. Here, I showed that Pex27 and Vps1 act in the same pathway and physically interact *in vivo*.

Next, we sought to identify novel factors required for organelle maintenance in *S. cerevisiae*. For this I performed an SGA based genome wide high throughput microscopy screen and found Kin4 kinase as a regulator of peroxisome inheritance. Kin4 was further characterised to unravel its role in this process. Kin4 has a paralog, Frk1. Both Kin4 and Frk1 are required for transport of peroxisomes and vacuoles (yeast lysosome) to the emerging bud. Moreover, I showed that Kin4 and a PAK kinase, Cla4, regulate antagonistically the transport of both the organelles in a spatial and temporal manner.

These novel insights into the regulation of organelle transport and peroxisome fission in yeast have been discussed and can be explored further to understand molecular principles involved in organelle maintenance in general.

Acknowledgements

My tenure as a PhD student has helped me to grow as a good human being and has enhanced my appreciation towards science and research. I am thankful to all the people whose direct or indirect involvement made this possible and worthwhile.

I would like to express my deepest gratitude towards my supervisor, Dr. Ewald Hettema for his guidance, support and encouragement throughout the course of my PhD. I am thankful to him for believing in me and giving me ample opportunity to get exposure of scientific knowledge and research. His exceptional level of drive has made me learn the fine points, which I would have missed otherwise. I would also like to thank Dr. Donald Watson for his valuable support and guidance.

I am very lucky to have excellent lab mates who helped me throughout my project. I am thankful to Dr. James Nuttall, Dr. Jamie Greig and Dr. Nadal Al Saryi for introducing me to the lab techniques. Dr. John Hutchinson, for being helpful and for involving me in several university socials. Special thanks to Dr. Paul Galvin for helping me with microscopy imaging and Dr. Murtakab, Georgia and Anson for their companionship.

I take this opportunity to thank Prof. Maya Schuldiner, Dr. Einat Zalckvar and lab members (Weizmann Institute of Science, Rehovot, Israel) for providing me an excellent platform to carry out the genome wide screens.

A special thanks to Dr. Ram Kumar Mishra, Mansi Gujrati, Aseem Shrivastava and Animesh Mishra for their valuable inputs in my PhD fellowship applications and constant support.

I owe more than whatever I have thought of to my family for their unconditional love and support.

Table of contents

Abbreviations

°C	Degrees Celsius
aa	Amino acids
ADP	Adenosine diphosphate
APS	Ammonium persulphate
ATP	Adenosine triphosphate
C-terminal	Carboxyl-terminal
DNA	Deoxyribonucleic acid
dATP	Deoxyadenosine triphosphate
dCTP	Deoxycytidine triphosphate
dGTP	Deoxyguanosine triphosphate
dH_2O	Deionised water
dNTPs	Equimolar mixture of dATP, dTTP, dCTP, dGTP
DTT	Dithiothreitol
dTTP	Deoxythymidine triphosphate
DRP	Dynamin related protein
E. coli	*Escherichia coli*
ECL	Enhanced chemiluminescence
EDTA	Ethylenediaminetetraacetic acid
ER	Endoplasmic reticulum
GFP	Green fluorescent protein
GSH	Glutathione
GST	Glutathione *S*-transferase

H. polymorpha	*Hansenula polymorpha*
HcRed	*Heteractis crispa* red fluorescent protein
h	Hour(s)
HRP	Horseradish peroxidase
IgG	Immunoglobulin G
IPTG	Isopropythio-β-D-galactoside
IRD	Infantile Refsum disease
M	Molar
min	Minute(s)
mKate2	monomeric far-red fluorescent protein
mM	Millimolar
mNG	monomeric Neon Green
mPTS	Peroxisomal membrane protein targeting signal
mRNA	Messenger RNA
mRuby2	monomeric bright red fluorescent protein
NaCl	Sodium chloride
NALD	Neonatal adrenoleukodystrophy
N-terminal	Amino-terminal
nt	Nucleotide(s)
OD_{600}	Optical density at 600nm
ORF	Open reading frame
PEG	Polyethylene glycol
PBD	Peroxisome biogenesis disorder

PCR	Polymerase chain reaction
PED	Peroxisomal enzyme deficiency
PMP	Peroxisomal membrane protein
PTS	Peroxisome targeting signal
S. cerevisiae	*Saccharomyces cerevisiae*
SDS	Sodium dodecyl sulphate
SDS-PAGE	Sodium dodecyl sulphate-polyacrylamide gel electrophoresis
sec	Second(s)
TEMED	N, N, N-Tetramethylethlenediamine
WB	Woronin body
WSC	Woronin sorting complex
WT	Wild type
ZS	Zellweger syndrome
ZSD	Zellweger spectrum of disorders
α	Alpha
β	Beta
β-ME	β-mercaptoethanol
γ	Gamma
μ	Micro
μM	Micromolar
Δ	Delta
geneΔ	*GENE* deletion mutant

Amino acids

Ala	A	Alanine
Cys	C	Cysteine
Asp	D	Aspartic acid
Glu	E	Glutamic acid
Phe	F	Phenylalanine
Gly	G	Glycine
His	H	Histidine
Ile	I	Isoleucine
Lys	K	Lysine
Leu	L	Leucine
Met	M	Methionine
Asn	N	Asparagine
Pro	P	Proline
Gln	Q	Glutamine
Arg	R	Arginine
Ser	S	Serine
Thr	T	Threonine
Val	V	Valine
Trp	W	Tryptophan
Tyr	Y	Tyrosine
	X	Any

The list of figures

Chapter 1

Chapter 2

Chapter 3

Chapter 4

Chapter 5

Chapter 6

The list of tables

Chapter 1

Chapter 2

Chapter 3

Chapter 4

Chapter 1 Introduction

1.1 Peroxisomes

Peroxisomes are ubiquitous single membrane bound eukaryotic organelles. They can perform a myriad of activities but they share fundamental functions including β-oxidation based fatty acid degradation and detoxification of toxic peroxides over all eukaryotes (Fidaleo, 2010; Lazarow and Fujiki, 1985; van den Bosch et al., 1992). In mammals, they are mainly responsible for β-oxidation of very long chain and branched fatty acids whereas short, medium and long chain fatty acids are processed in mitochondria. The cascade of reactions in β-oxidation is the same for peroxisomes and mitochondria but they differ in substrate specificity. In yeast and plants β-oxidation is solely dependent on peroxisomes (Fidaleo, 2010). They are partially involved in biosynthesis of cholesterol, docosahexaenoic acid (DHA) and plasmalogens. Plasmalogens are ether lipids and critical component of myelin sheath in nerve cells. Moreover, peroxisomes contain most of the enzymes for cholesterol degradation to bile acids (Pedersen, 1993). They also have enzymes like catalase, manganese superoxide-dismutase and copper–zinc superoxide-dismutase required for the decomposition of peroxides and superoxides. These activities prevent further damage to biomolecules by these toxic oxides. In yeast along with β-oxidation, degradation of methanol and amino acids and biosynthesis of lysine are other processes that are carried out in peroxisomes (Al-Saryi et al., 2017; Brown and Baker, 2003).

Various modified forms of peroxisomes have been identified in different organisms that perform specialised functions **(Table 1.1)**.

Table 1.1 Specialised peroxisomes and their functions (Platta and Erdmann, 2007).

Organism	**Name**	**Functional process**
Trypanosoma and Leishmania	Glycosome	Glycolysis
Plants	Glyoxysome	Glyoxylate cycle
Neurospora crassa	Woronin bodies	Seal hyphal pores under stress

1.2 Disorders related to peroxisomes

Peroxisomes are vital for sustaining metabolism and subsequently survival of an organism. Therefore, defects in peroxisome functions have been shown to cause various disorders. These disorders are the consequence of mutations in over 30 genes that are somehow associated with

peroxisome biogenesis and functions (Wanders, 2018). Peroxisome related disorders have been categorised in two groups, i) peroxisome biogenesis disorders (PBDs) and ii) peroxisomal enzyme deficiencies (PEDs). Zellweger spectrum of disorders (ZSDs) constitute the majority of PBDs. Previously, Zellweger syndrome (ZS), neonatal adrenoleukodystrophy (NALD) and infantile Refsum disease (IRD) were used to categorise most PBDs. Now they are considered as different severities along a spectrum with ZS being to most severe form followed by NALD and IRD. Heimler syndrome is a recent addition to ZSDs and it is considered clinically mild. PBDs are autosomal recessive disorders and mainly involve abnormalities in brain development, craniofacial dysmorphia, hypotonia, liver and kidney dysfunction. Biochemically, there is an accumulation of fatty acids and reduced plasmalogens synthesis and an absence of peroxisomes (Fidaleo, 2010; Klouwer et al., 2015; Steinberg et al., 2006; Wanders, 2018). In the peroxisomal matrix a myriad of biochemical reactions takes place and they involve more than fifty enzymes. PEDs, depending on the enzyme deficiency, present as disorders with overlap of symptoms to ZSDs. They are a consequence of dysfunctional enzymes involved in β-oxidation, ether phospholipid synthesis, α-oxidation and peroxide detoxification (Fidaleo, 2010; Klouwer et al., 2015; Wanders, 2018).

1.3 *PEX* genes and their role in peroxisome biogenesis

The biogenesis process of peroxisomes involves multiple events including peroxisome membrane synthesis, protein transport and peroxisomal fission. The genes responsible for peroxisome biogenesis are called *PEX* genes; which encode peroxin proteins. There are about 30 known *PEX* genes in budding yeast, *S. cerevisiae*. They can be further subdivided into smaller groups according to their role in the above processes **(Table 1.2)** and the functions associated with each gene have been tabulated in **Table 1.3**.

Table 1.2 Genes associated with peroxisome maintenance.

Genes	**Process affected**
PEX1, 2, 4, 5, 6, 7, 8, 9, 10, 12, 13, 14, 15, 17, 18, 20,21, 22	Matrix protein import
PEX3, 19	Membrane Formation/ER to peroxisome transport
PEX11, 25, 27, 28, 29, 30, 31, 32, 34, 35, VPS1, DNM1	Number and morphology
INP1, INP2	Inheritance

Table 1.3 The known *PEX* genes in *S. cerevisiae* and functions associated with them modified from (Smith and Aitchison, 2013).

Peroxin	**Functional categories**
Targeting of matrix proteins	
Pex5	PTS1 cargo, shuttling receptor
Pex7	PTS2 cargo, shuttling receptor
Pex18	PTS2 cargo, co-receptor
Pex21	PTS2 cargo, co-receptor,
Pex9	PTS1 cargo, shuttling receptor
Matrix protein import machinery	
Pex13, Pex14, Pex17	Receptor docking complex
Pex8	Docking and export complex conjugation, importomer assembly
Pex4	Receptor export (ubiquitylation), ubiquitin conjugating enzyme
Pex22	Receptor export (ubiquitylation), Pex4 anchor
Pex2, Pex10, Pex12	Receptor export (ubiquitylation), form the RING finger complex
Pex1, Pex6	Receptor export (recycling), AAA-type ATPase
Pex15	Receptor export (recycling), membrane receptor for Pex1 and Pex6
Direct targeting of PMPs	
Pex3	Receptor docking
Pex19	Soluble chaperone and receptor
Formation of peroxisomal membrane from the ER	
Pex3, Pex19	Form a complex required for the *de novo* generation of peroxisomes
Pex25	Required for the *de novo* generation of peroxisomes, recruits Rho1
Pex30	Regulate the *de novo* generation of peroxisomes
Fission	
Pex11	Membrane elongation recruits the fission machinery,
Pex25	Membrane elongation and remodelling
Pex27	Positive regulator of fission
Pex34	Positive regulator of fission, part of a tether with mitochondria
Regulation of peroxisome biogenesis	
Pex28, Pex29, Pex31, Pex32	Form a complex with reticulon homology domain-containing proteins and establish peroxisome contact sites at ER subdomains
Pex35	Interacts with Arf1 and regulates peroxisome abundance

Peroxisome membranes are rich in phospholipids mainly phosphatidyl choline and phosphatidyl ethanolamine and the endoplasmic reticulum (ER) is site for their biosynthesis (Lazarow and Fujiki, 1985). Pex3 has been implicated in lipid delivery from ER to peroxisomes (Hoepfner et al., 2005). The delivery for lipids from ER to peroxisomes can be independent of vesicular transport (Raychaudhuri and Prinz, 2008). Deletion of *PEX3* and or *PEX19* cause lack of peroxisomal structures in *S. cerevisiae* (Hettema et al., 2000). Although it was reported that pre-peroxisomal structures containing Pex13 and Pex14 in *H. polymorpha pex3Δ* and *pex19Δ* cells have been observed (Knoops et al., 2014). Similar pre-peroxisomal structures containing Pex13, Pex14 were also observed in *S. cerevisiae pex3Δ* cells. Furthermore, Pex4, Pex22, Pex5, Pex7 and Pex25 were also found in the same membrane fractions (Wroblewska et al., 2017). Interestingly most of the *pex25Δpex34Δ* cells lack detectable mature peroxisomes when grown on glucose containing medium (Tower et al., 2011). But whether pre-peroxisomal structures (with Pex proteins) are present in these cells is not yet described. In a recent study Pex30 along with seipin (Sei1) have been suggested to organise a subdomain in ER with distinct lipid composition from ER and this subdomain contribute to the *de novo* formation of peroxisomes (Joshi et al., 2018; Wang et al., 2018). Peroxisomal membrane proteins (PMPs) can be sorted to peroxisomal membrane in different pathways depending upon involvement of Pex19 (Hettema et al., 2014). PMPs that are recognised by Pex19 and delivered to peroxisomes via docking on Pex3 belongs to Class I (Jones et al., 2004). Pex3 is a classic example of a Class II PMP that is translocated to peroxisomes by means of Pex19 but does not need docking. Since Pex13 and Pex14 are found in pre-peroxisomal structures in *H. polymorpha pex3Δ* and *pex19Δ* cells and *S. cerevisiae pex3Δ* cells, both constitute Class III PMPs (Hettema et al., 2014; Knoops et al., 2014; Wroblewska et al., 2017). How these proteins are inserted into these membranes and what the origin of these membranes is, is still unclear.

Peroxisomal matrix protein import is dependent on two receptor proteins Pex5 and Pex7; which recognise peroxisomal targeting sequences (PTS) 1 and 2, respectively, on peroxisomal matrix proteins. The consensus sequences for PTS1 and PTS2 are (S/A/C)(K/R/H)(L/M/I) and (R/K)(L/V/I)X5(H/Q)(L/A), respectively. The PTS1 is present at the C-terminus of the protein whereas PTS2 is at the N-terminus. Most of the matrix proteins are imported via the PTS1 dependent pathway (Subramani, 1993; Titorenko and Rachubinski, 2001). Recently Pex9, a Pex5 paralog, has been identified which is required for import of malate synthase (Mls1 and Mls2) when cells were grown on oleate containing medium (Effelsberg et al., 2016; Yifrach et al., 2016). The PTS receptors recognize cargo in the cytosol. The cargo-loaded receptor is

directed to the peroxisomal membrane and binds to the docking complex (Pex13/Pex14/Pex17). It assembles with Pex14 to form a transient pore and cargo proteins are transported into the peroxisomal matrix. Cargo release might involve the function of Pex8 or Pex14. After that the receptor is mono-ubiquitinated at a conserved cysteine by the E2-enzyme complex Pex4/Pex22 in tandem with E3-ligases of the RING-complex (Pex2, Pex10, Pex12). The ubiquitinated receptor is released from the peroxisomal membrane in an ATP-dependent manner by the AAA-peroxins Pex1 and Pex6, which are anchored to the peroxisomal membrane via Pex15. Finally, the ubiquitin moiety is removed, and the receptor enters a new round of targeting and import **(Figure 1.1)**.

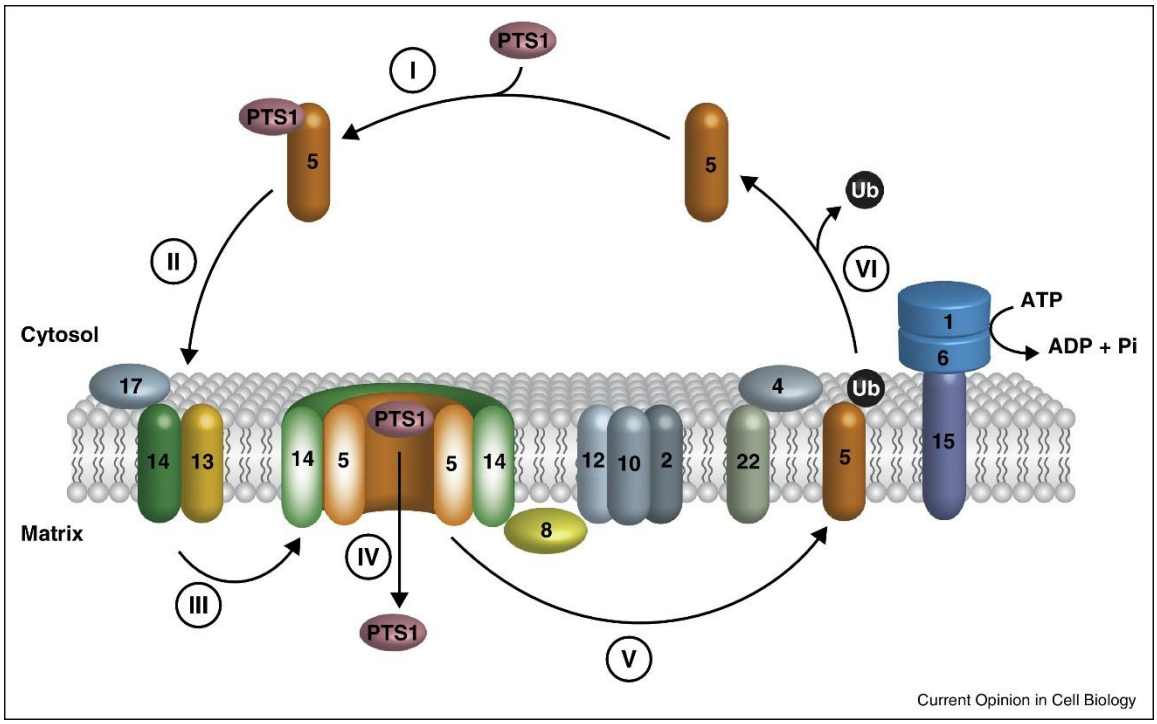

Figure 1.1 Schematic representation for the cascade of events involved in import of peroxisomal matrix proteins (Hettema et al., 2014). There are six major steps in matrix protein import including cargo recognition by receptor (I), docking at the peroxisome membrane (II), pore formation (III), cargo release (IV), followed by ubiquitination of receptor (V) and removal from the peroxisomal membrane for recycling (VI).

Pex11 family proteins have been well characterised for their role in peroxisome proliferation. In mammals there are three isoforms of Pex11 α, β and γ; whereas in most fungal species Pex11, Pex25 and Pex27 constitute to Pex11 family, reviewed in (Kiel et al., 2006). Here, Pex25 and Pex27 are paralogs. There are three subsequent events involved in peroxisome multiplication; elongation, constriction and fission. Pex11 family proteins, mainly Pex11 performs elongation step. Pex11 causes tubulation of peroxisomes in yeast by means of an

amphipathic helix, present near the N-terminus of the protein. A peptide consisting of this amphipathic helix can modulate liposomes *in vitro* (Opalinski et al., 2011). In mammals all three Pex11 (α, β and γ) isoforms have this helix (Yoshida et al., 2015) whereas in yeast it is restricted to Pex11. However, Pex25 has been shown to induce peroxisome elongation upon overexpression (Huber et al., 2012). Peroxisome elongation is followed by constriction. For constriction, no molecular player has been identified or assigned yet. The dynamin related protein (Drp) GTPases play role in peroxisome fission. In yeast Dnm1 and Vps1 (Vacuolar Sorting Protein 1) and in mammals Dlp1 act as Drps (Hoepfner et al., 2001; Kuravi et al., 2006; Li and Gould, 2003). Dnm1 and Dlp1 (Drp1) are targeted to the peroxisomal membranes via tail anchored Fis1 (Fission 1) whereas Vps1 works independent of Fis1. Furthermore, in *S. cerevisiae* Dnm1 requires an auxiliary component either Caf4 or Mdv1 for its recruitment (Kaur and Hu, 2009; Motley et al., 2008). In mammals Mff (Mitochondria Fission Factor) is also a tail anchored protein that promotes peroxisome fission along with mitochondrial fission (Gandre-Babbe and van der Bliek, 2008). Here, Mff also recruits Dlp1 and siRNA mediated knockdown of Mff leads to peroxisome tubulation in mammalian cell line (Otera et al., 2010). In *H. polymorpha,* Dnm1 is more prominent in peroxisome fission but in *S. cerevisiae* Vps1 based fission is dominant over Dnm1 system (Motley et al., 2008; Nagotu et al., 2008). Remarkably, Pex11β can interact with Fis1 via its C-terminus and also it is found in complex with Fis1 and Dlp1 (Kobayashi et al., 2007). In conclusion Pex11 appears to be the initiator of the fission process. Pex11 achieves this by modulating the membrane and then may recruit Fis1, which further can target Drps to an active site of fission **(Figure 1.2)**. Furthermore, in *H. polymorpha* Pex11 is required for Dnm1 GTPase activity at the peroxisomal membrane *in vivo* and has been shown to enhance GTPase activity *in vitro* (Williams et al., 2015).

Pex34 is a membrane protein and is partially redundant with Pex25 since *pex34Δ* and *pex25Δ* (not all) cells have peroxisomes but most of *pex25Δpex34Δ* cells have no detectable peroxisomes (Tower et al., 2011). In a recent study Pex34 has been shown to form a tether between peroxisomes and mitchondria (Shai et al., 2018). Pex35 is a novel Pex protein and it has been impicated to regulate peroxisome abundance via interaction with Arf1 GTPase (Yofe et al., 2017). Pex28, Pex29, Pex30, Pex31 and Pex32 have been implicated in peroxisome biogenesis and they regulate peroxisome number, size and shape but their exact mechanistic roles have not been characterised yet (Vizeacoumar et al., 2004; Vizeacoumar et al., 2003). Though, Pex30 with seipin and Pex29 and Pex30 with reticulons have been reported to play

role in peroxisome biogenesis at the ER (Joshi et al., 2018; Mast et al., 2016; Wang et al., 2018).

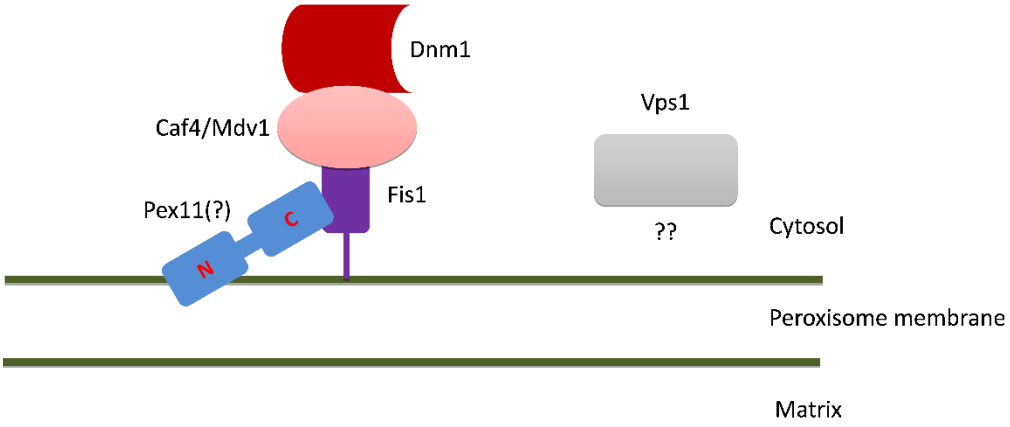

Figure 1.2 The proposed model for recruitment of fission machinery in *S. cerevisiae*. Peroxisomal Dnm1 requires a multitude of factors for its recruitment and activity including Pex11, Fis1 and Mdv1/Caf4. No auxiliary factors have been identified for Vps1 dependent peroxisome fission, although this is the main DRP required for this process.

1.4 Models for peroxisome biogenesis

The biogenesis of peroxisomes has been central to peroxisome research for many years. The first profound review by Lazarow and Fuzuki (1985) on biogenesis stated that peroxisomes form by growth and fission from pre-existing one. It proposed explicitly that peroxisomes do not form via a *de novo* process under any circumstances. The basis behind this theme was that all peroxisomal proteins are synthesized on free poly ribosomes and that they are recruited to peroxisomes post-translationally. Moreover, not a single protein undergoes ER based post translational modification. In addition, by that time mutants lacking peroxisomal membrane structure had not been discovered (Lazarow and Fujiki, 1985). But with more detailed studies it became subjective because certain mutant cells (*pex3Δ* and *pex19Δ* cells) were found to lack detectable peroxisomal membranes (Hettema et al., 2000) and the structures do appear again upon reintroduction of wild type genes (Hohfeld et al., 1991). This indicates that they can form *de novo* too and several studies have been reported that *de novo* formation occurs from the ER (Hoepfner et al., 2005). Although some studies suggest that *de novo* formation occurs in all cells (Kim et al., 2006; Sugiura et al., 2017; van der Zand et al., 2012), the majority of studies in yeast indicate that the preferred mode of multiplication is via fission (Knoblach et al., 2013; Knoops et al., 2015; Menendez-Benito et al., 2013; Motley et al., 2015; Motley and Hettema, 2007); and that *de novo* formation can be observed in cells temporarily devoid of peroxisomes (Motley et al., 2015; Motley and Hettema, 2007).

Various models for peroxisome biogenesis have been proposed **(Figure 1.3)** (Hettema et al., 2014). All these models are based on vesicular transport from ER to (pre)peroxisomes. *In vitro*, budding assays, have shown generation of similar vesicles is dependent on Pex19. However, essential molecular machinery apart from Pex19 have not been characterised. Although, ESCRT-III complex affects budding *in vitro*, deletion of components of this complex has got no strong defect *in vivo* in peroxisome morphology when cells were grown on glucose containing medium (Mast et al., 2018). Peroxisomes are no longer considered as isolated structures in the cell but rather there are several reports that suggest that they are connected to other organelles like mitochondria and ER through tethers and contacts sites. Peroxisome-mitochondria (PerMit) contact sites play role in metabolic exchanges during β-oxidation (Shai et al., 2018). Moreover, in general contact sites are emerging as potential sites for membrane biogenesis for organelles (Dimmer and Rapaport, 2017; Mast et al., 2016; Shai et al., 2016).

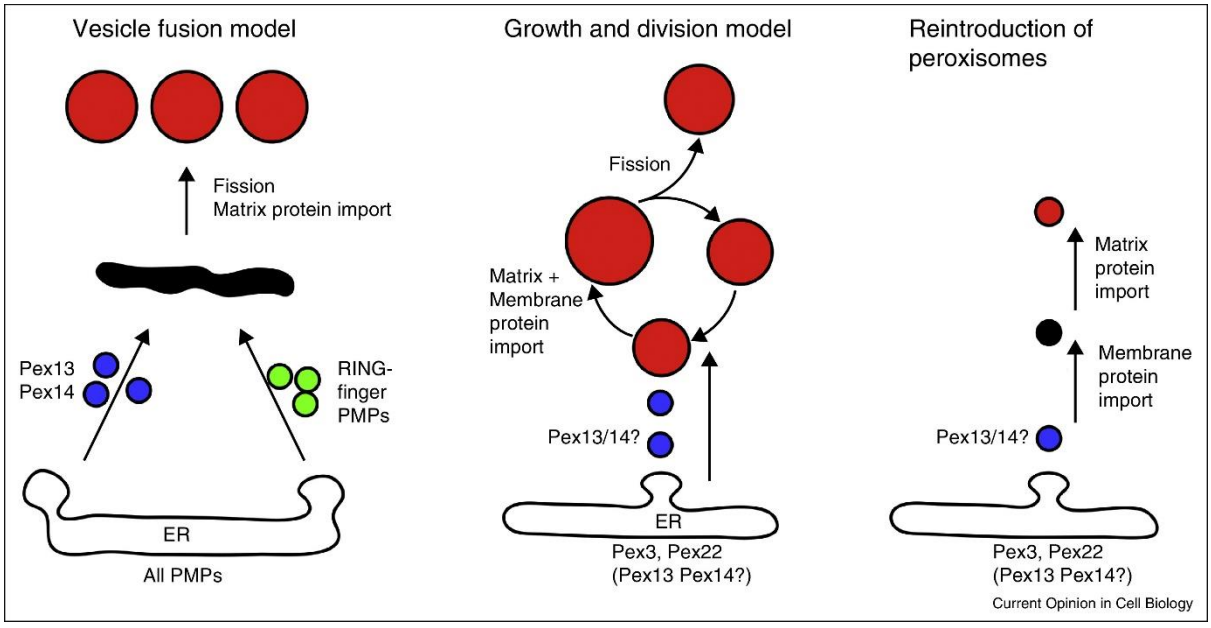

Figure 1.3 Peroxisome biogenesis models. 'Vesicle fusion' and 'growth and division' models proposed for peroxisome biogenesis in wild type cells. The fusion model proposes that all PMPs insert into the ER where they assemble into two distinct vesicles that upon release fuse and form a pre-peroxisome. This pre-peroxisome imports matrix proteins and divides to give rise to multiple mature peroxisomes. The growth and division model propose that peroxisomes receive newly synthesised matrix and membrane proteins. They acquire lipids from the ER via vesicular transport and these vesicles may carry a subset of PMPs. When peroxisomes reach a certain size, they divide. The 'reintroduction model' is for mutants lacking peroxisomes after the complementation (Hettema et al., 2014).

1.5 Maintenance of peroxisomes in *S. cerevisiae*

In *S. cerevisiae*, there are four processes that determine peroxisome number and morphology, i) fission, ii) *de novo* formation, iii) pexophagy, and iv) inheritance **(Figure 1.4)**. In wild type cells under normal conditions there is no strong evidence for *de novo* peroxisome formation whereas fission process has been shown to control the peroxisome number by several independent reports (Knoblach et al., 2013; Lazarow and Fujiki, 1985; Menendez-Benito et al., 2013; Motley et al., 2015; Motley and Hettema, 2007).

Pexophagy is a selective form of autophagy for peroxisomes. It plays an important role in peroxisome turnover during starvation (Hutchins et al., 1999; Klionsky, 1997). Atg36 is the peroxisomal receptor for autophagy that interacts with components of the autophagy machinery, Atg11 and Atg8. Pex3 recruits Atg36 on peroxisomes and this Pex3 dependent recruitment is required for pexophagy (Motley et al., 2012a, b). Starvation induced pexophagy requires the activity of a kinase, Hrr25; where Hrr25 has been shown to modulate Atg36 phosphorylation *in vivo* under these conditions (Tanaka et al., 2014).

Peroxisomes are inherited with high fidelity by segregation between mother and daughter cell and will be discussed further in organelle inheritance section.

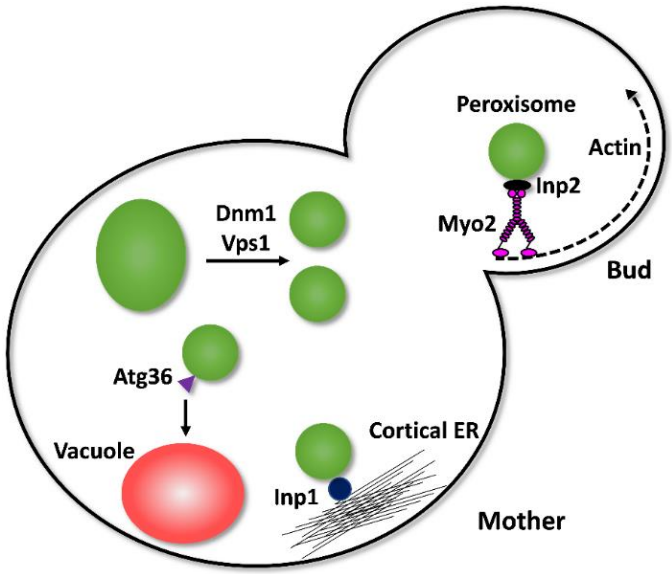

Figure 1.4 Peroxisome fission, segregation and pexophagy maintain peroxisomes in *S. cerevisiae*. Vps1 and Dnm1 divide peroxisomes resulting in an increase in peroxisome number. Atg36 activation reduces peroxisomes by targeting them to the vacuole for degradation. Inp1 and Inp2 contribute to proper segregation during asymmetric growth and division of the cell. Inp1 tethers some peroxisomes to the mother cell periphery. Inp2 recruits the ClassV unconventional Myosin Myo2 to peroxisomes and to mediate transport to the daughter cell.

1.6 Organelle inheritance

A key aspect of eukaryotic cells is the presence of membrane bound organelles. These lipid enclosed structures, despite housing different chemical micro-environments, have evolved to co-exist and still perform various specialised functions. A full complement of organelles is important for cellular functions. The organelles that contain genetic material, mitochondria, chloroplast and the nucleus are essential for the cell survival. These organelles must be inherited as they cannot be formed *de novo*. On the other hand, some organelles such as vacuoles and peroxisomes can form *de novo,* but this is not energetically favourable compared to the process of replication of pre-existing organelles followed by their partition. Hence, several molecular mechanisms have been employed by cells to tightly regulate organelle partition between two daughter cells during cell division (Knoblach and Rachubinski, 2015a; Nunnari and Walter, 1996; Warren and Wickner, 1996).

The asexual reproduction of the budding yeast *S. cerevisiae* involves asymmetric growth and division of the cell. During cell growth, the concomitant actions of organelle retention in the mother and transport to the emerging bud help to inherit preconceived equity of organelle content. Therefore *S. cerevisiae* has become an important model system to unravel the basic molecular principles of the organelle segregation.

The organelle carrier machinery includes the classV myosin proteins, Myo2 and Myo4. These myosin motors are fuelled by hydrolysis of ATP. They transport organelles on actin tracks by means of their N-terminal domains. To load the cargoes, Myo2 and Myo4 recognise receptors on the organelles via their C-terminal cargo binding domain (CBD) (Knoblach and Rachubinski, 2015a; Sellers and Veigel, 2006). Myo2 is essential for cell growth whereas Myo4 is not. Myo2 delivers most of the organelles like Golgi bodies, lipid bodies, mitochondria, nuclei, peroxisomes, vacuoles and secretory vesicles. Myo4 transports cortical ER (cER) and a subset of mRNAs (Knoblach and Rachubinski, 2015a) **(Figure 1.6)**.

1.6.1 Peroxisome inheritance

Although peroxisomes can form *de novo in S. cerevisiae*, they are maintained by the process of growth and division of pre-existing peroxisomes. Inp1 and Inp2 are directly involved in the inheritance of peroxisomes during cell growth.

Inp1 was discovered to be peroxisomal in a global localisation studies (Huh et al., 2003). Inp1 is a peripheral membrane protein. It was implicated in peroxisome retention because *inp1Δ* mother cells frequently lack peroxisomes in contrast to the buds. Moreover, overexpression of

INP1 retained most of the peroxisomes in the mother cell (Fagarasanu et al., 2005). Further studies revealed that the peroxisomal membrane protein Pex3 physically interacts with Inp1 and recruits it to the peroxisomes. Also, Pex3 mutants that do not bind Inp1 but are still functional in peroxisome biogenesis, show a defect in peroxisome inheritance (Munck et al., 2009). In split-GFP assay, Inp1 was shown to function as a tether between two Pex3 molecules one located at the peroxisomal membrane and one at cortical ER. In addition, two distinct Pex3 binding sites in Inp1, present at N and C-terminal domains are predicted to play a role in tether formation. The cortical ER in conjugation with plasma membrane forms distinct patches where Pex3-Inp1 complexes can anchor peroxisomes and prevents their transport to the bud (Knoblach et al., 2013).

Inp2 is an integral peroxisomal membrane protein that acts as Myo2 receptor. Inp2 interacts with the Myo2 CBD and mediates peroxisome movement to the bud (Fagarasanu et al., 2006). Specific amino acid residues like Y1415, W1407, Q1447, Y1483 and Y1484 in Myo2 CBD have been identified that are important for Inp2 binding. Mutations in these residues specifically impair the interaction with Inp2 and subsequently affect peroxisome transport to the bud. The protein levels of Inp2 are regulated as the cell cycle progresses. It reaches its peak around 100min after release from G1 arrest (Fagarasanu et al., 2006). A subset of peroxisomes contains Inp2 and this subset is transported to the bud. In cells with Myo2-Y1483A mutant, where peroxisomes fail to be transported to the bud, all peroxisomes in the mother cell contain Inp2 and there is an increase in Inp2 protein levels compared to the wild type cells (Fagarasanu et al., 2009). Pex19 also has been shown to contribute to the peroxisome delivery in the bud by binding Myo2 (Otzen et al., 2012). In *H. polymorpha*, Pex19 is essential for interaction of Inp2 with Myo2 (Saraya et al., 2010).

Peroxisomes undergo division once per cell cycle. In *dnm1Δvps1Δ* cells peroxisome fission is abolished and therefore in these cells one elongated peroxisome is observed near the bud neck (Kuravi et al., 2006). On the elongated tubules, Inp1 is located at the tip extended in the mother and Inp2 decorates the opposite end in the bud (Knoblach et al., 2013). The shape and position of the peroxisomes change with an additional deletion of either *INP1* or *INP2* genes (Motley and Hettema, 2007). Based on the above observations it has been proposed that the peroxisome inheritance and fission are coupled with each other (Knoblach et al., 2013) **(Figure 1.5)**.

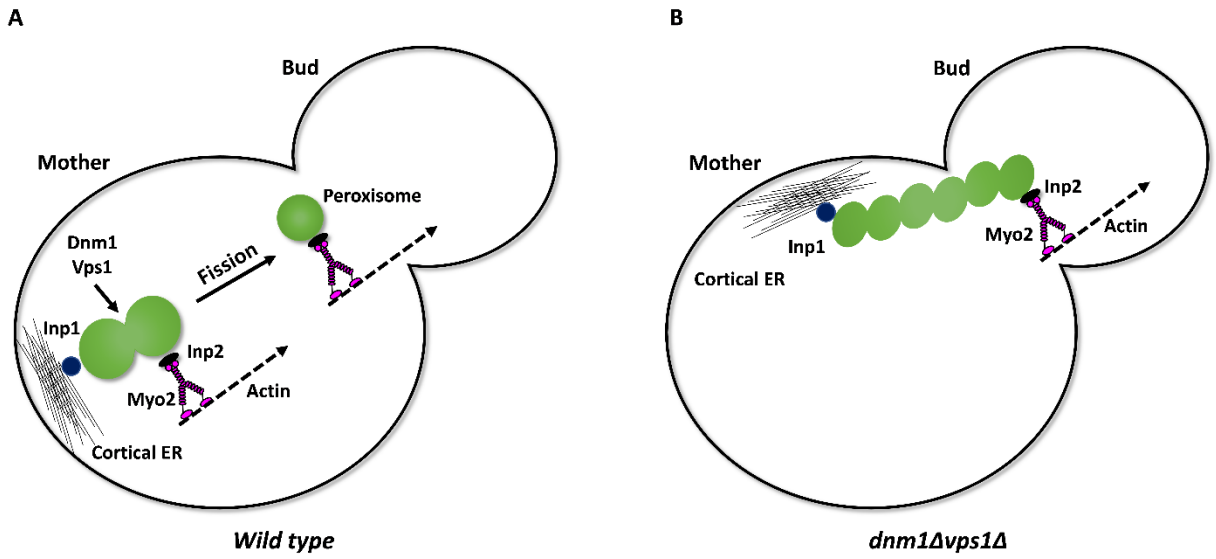

Figure 1.5 Proposed model where peroxisome segregation is coupled to fission. (A) In wild type cells the Inp2-Myo2 complex forms on peroxisomes in the mother cell and upon fission the released peroxisome is directed towards the bud. (B) In *dnm1Δvps1Δ* cells fission is blocked and both retention and transport machinery compete for the same peroxisome which is why the peroxisome is stuck at the bud neck and eventually undergoes division during cytokinesis **(Chapter 4, Figure 4.1)**.

1.6.2 Vacuole inheritance

Vacuoles are the yeast equivalent to lysosomes. They are essential for cell cycle progression (Jin and Weisman, 2015). The mechanisms underlying the inheritance of vacuoles have been unravelled most among all yeast organelles. From the inception to culmination almost every factor has been characterised in vacuole movement (Chapter 5, Figure 5.1). Vacuoles form segregation structures which are pulled from the tip by Myo2 motors into the emerging bud during G1 phase.

Vacuole transport begins with Cdk1-dependent phosphorylation of Vac17, the Myo2 receptor, and Myo2. This phosphorylation is crucial for the interaction between Vac17 and Myo2 (Legesse-Miller et al., 2006; Peng and Weisman, 2008). Once the organelle reaches the bud tip Vac17 is degraded and the vacuoles are released from Myo2 into the bud (Tang et al., 2003; Yau et al., 2017). Vac8, an armadillo repeat protein, plays a vital role in the vacuole maintenance. Vac17 interacts concomitantly with Myo2 and Vac8 and forms the vacuole carrier complex. In *vac8Δ* cells vacuole inheritance is completely abolished (Wang et al., 1998). Apart from its role in inheritance, Vac8 is also involved in vacuole fusion (Pan and Goldfarb, 1998), protein targeting from the cytosol to the vacuole (Wang et al., 1998) and with Nvj1 in nuclear-vacuole junction formation (Pan et al., 2000).

In cells with an inheritance defect the cell cycle halts in G1 phase until a vacuole is formed *de novo* in the bud. Pep12 and Vps45 proteins are required for the *de novo* vacuole formation. Once the mature vacuole is formed the TORC1-Sch9 pathway signalling triggers resumption of the cell cycle (Jin and Weisman, 2015).

In a recent study, Vac17 has also been reported as an asymmetry generating factor required for protein aggregate fusion with vacuoles. This phenomenon has a positive impact on the replicative life span of the cell (Hill et al., 2016).

1.6.3 Inheritance of mitochondria and other organelles

Multiple pathways are employed to assure mitochondrial partition during every cell division. In *S. cerevisiae*, like other organelles mitochondria are also actively transported along the actin cables to the bud during asymmetric cell growth (Simon et al., 1997). Association of Arp2 with mitochondria is also essential for directed mitochondrial movement. Arp2, an actin related protein, is a part of Arp2/3 complex that acts as a nucleation site for actin filament formation (Boldogh et al., 2001; Fehrenbacher et al., 2004). Mmr1 and Ypt11 are redundant in the transport function and they both interact with Myo2. In *mmr1Δypt11Δ* cells mitochondrial inheritance is completely abolished, which induces cell death. Mmr1 is a peripheral membrane protein and Ypt11 is a GTPase (Chernyakov et al., 2013; Itoh et al., 2004; Itoh et al., 2002). There are three known mechanisms for the mitochondrial retention by anchoring in the mother cell. Num1, Mfb1 and the ERMES complex are integral parts of the anchors. Num1, by means of its pleckstrin homology (PH) domain plays a major role in tethering mitochondria to the cell cortex. Mdm36, mediates the linkage of Num1 to mitochondria. Mdm10, Mdm12, Mdm34 (Mitochondrial proteins) and Mmm1 (ER protein) constitute the ERMES complex. The ERMES connects mitochondria to the cortical ER (Knoblach and Rachubinski, 2015a). Mfb1 is vital for the retention of high functioning mitochondria at the mother cell tip (Pernice et al., 2016).

Myo2 is essential for transport of secretory vesicles to the site of bud growth (Johnston et al., 1991). Multiple players including Ypt31, Ypt32, Sec4 and Sec15 interact with Myo2 and mediate polarised movement of secretory vesicles (Jin et al., 2011; Lipatova et al., 2008). Ypt11 is involved in inheritance of mitochondria and late Golgi elements (Arai et al., 2008; Chernyakov et al., 2013; Itoh et al., 2002). Interaction of Ypt11 with Ret2, a Golgi resident protein, is required for proper Golgi segregation (Arai et al., 2008). Like other organelles lipid droplets are also actively transported to the emerging bud in a Myo2 dependent manner

(Knoblach and Rachubinski, 2015b). However, the receptor(s) for Myo2 (if any) on lipid droplets have not been identified yet. Myo4 plays a vital role in delivery of mRNAs and the cortical ER to the bud (Bobola et al., 1996; Estrada et al., 2003). In both cases She3 acts as an adaptor for Myo4 and hence She3 is required for mRNA and cortical ER transport. Apart from She3, She2 is also required for transport of mRNAs. She2 binds to certain mRNAs and this association facilitates recognition by the She3-Myo4 complex (Bohl et al., 2000; Estrada et al., 2003; Long et al., 2000; Takizawa and Vale, 2000).

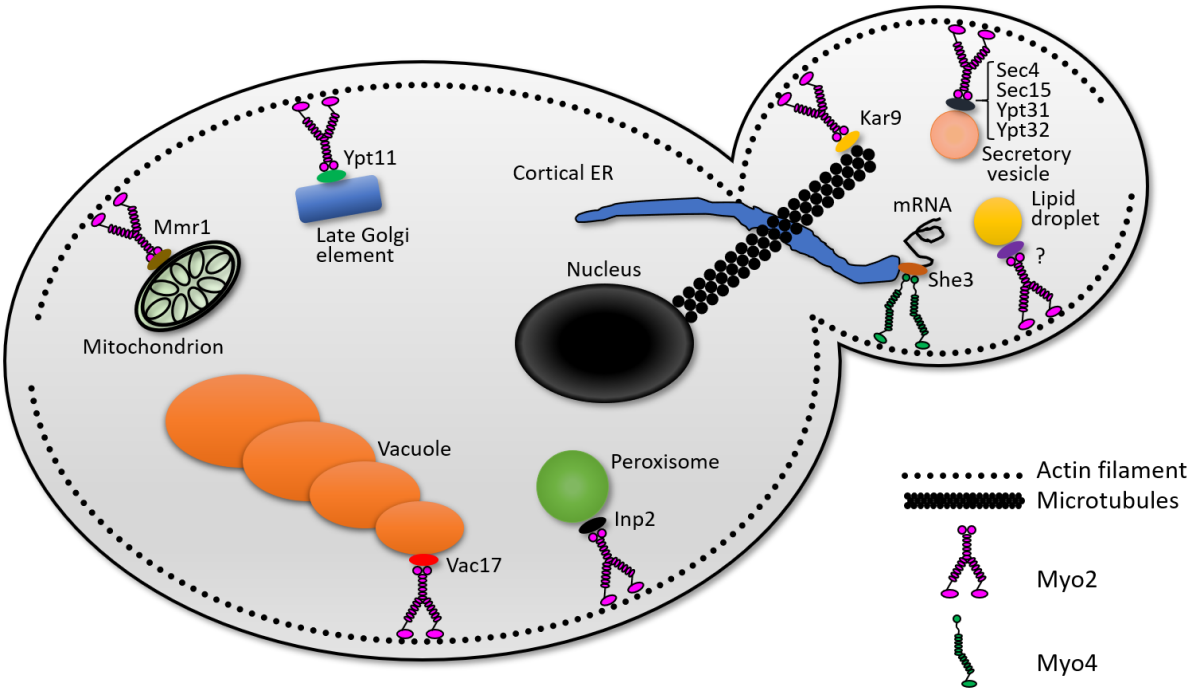

Figure 1.6 Organelle inheritance in *S. cerevisiae*. Class V myosins Myo2 and Myo4 play vital role in organelle transport along actin cables to the emerging bud. Myo2 has two separate regions that constitute the CBD (Catlett et al., 2000). Based on the interaction with these sites, Myo2 receptors are grouped into two subsets. Mmr1 and Vac17 compete for one site and Inp2, Kar9, Sec4 and Rab GTPases share another site (Eves et al., 2012; Fagarasanu et al., 2009).

1.7 Nuclear inheritance and SPoC

In budding yeast, mitosis is the process of equal splitting of duplicated nuclear chromosomes between mother and daughter cell. The Spindle pole body (SPB), the centrosome equivalent in yeast, acts as a microtubule organising centre and is duplicated prior to inception of nuclear inheritance (Adams and Kilmartin, 2000; Yamamoto et al., 1990). Duplicated SPBs mediate the alignment of the mitotic spindle along the cell polarity axis. Moreover, Dyn1 and Kar9 are required to maintain the spindle alignment and subsequent nuclear inheritance. Here, Kar9 is a Myo2 receptor and Dyn1 is a microtubule based motor protein (Eshel et al., 1993; Hwang et al., 2003; Li et al., 1993; Miller and Rose, 1998). Unlike other organelles, nuclear inheritance

requires both actin and the microtubule cytoskeleton. Dyn1 needs association with microtubules for its function whereas for Kar9 bridges astral microtubules and actin filaments. The Myo2-Kar9 complex directs the astral microtubules towards the cell cortex along the actin filaments **(Figure 1.6)**. Bim1, a microtubule binding protein, is required for Kar9 localisation along microtubules (Beach et al., 2000; Miller et al., 2000; Miller and Rose, 1998).

Two checkpoints, the spindle assembly checkpoint (SAC) and the spindle position checkpoint (SPoC), make sure that the chromosome segregation occurs properly; reviewed in (Caydasi and Pereira, 2012). The SAC comes into play when the microtubules fail to connect to the kinetochores in a bipolar fashion during metaphase before cells enter into anaphase (Musacchio and Salmon, 2007). On the other hand, the SPoC does not allow cells to undergo mitotic exit if spindle alignment is not maintained parallel to the cell polarity axis during anaphase (Caydasi et al., 2010a).

The key factor in the SPoC is a kinase, Kin4; which was discovered as a negative regulator of mitotic exit in response to spindle misalignment. Kin4 does not play any role in the SAC (D'Aquino et al., 2005; Pereira and Schiebel, 2005). Kin4 contributes to SPoC via phosphorylation of Bfa1; which in complex with Bub2 acts as a GAP for Tem1 GTPase; the mitotic exit network (MEN) activator (Bardin et al., 2000; Maekawa et al., 2007). The kinase activity of Kin4 is positively regulated by another upstream kinase, Elm1 (Caydasi et al., 2010b; Moore et al., 2010) and localisation during SPoC by a phosphatase, Rts1 (Chan and Amon, 2009). Elm1 phosphorylates Kin4 at Thr209 position, present in the kinase activation loop. Since Kin4 can inhibit the activation of MEN, overexpression of Kin4 causes a block in cell cycle progression and therefore growth but overexpression of T209A mutant form does not (Caydasi et al., 2010b; Moore et al., 2010). Kin4 is localised to the mother cell cortex throughout the cell cycle but in addition, it is also observed on the spindle pole bodies, at the bud tip during G1 and at the bud neck in late anaphase (D'Aquino et al., 2005; Pereira and Schiebel, 2005).

Lte1 is a negative regulator of Kin4 and resides at the bud cortex. It physically interacts with Kin4 and inhibits Kin4 function in the bud (Bertazzi et al., 2011; Falk et al., 2011). Being an inhibitor of Kin4, Lte1 promotes MEN activation indirectly. Recent studies have revealed a direct role in MEN activation independent of Kin4 inhibition. The PAK kinase Cla4 acts upstream to Lte1 in MEN. Another PAK kinase, Ste20 activates MEN directly, probably via inactivation of Bfa1-Bub2, GAP complex. In the absence of Spo12, an important player in

FEAR (Cdc14 early anaphase release) network Kin4 becomes almost dispensable for SPoC (Caydasi et al., 2017; Falk et al., 2016) **(Figure 1.7)**.

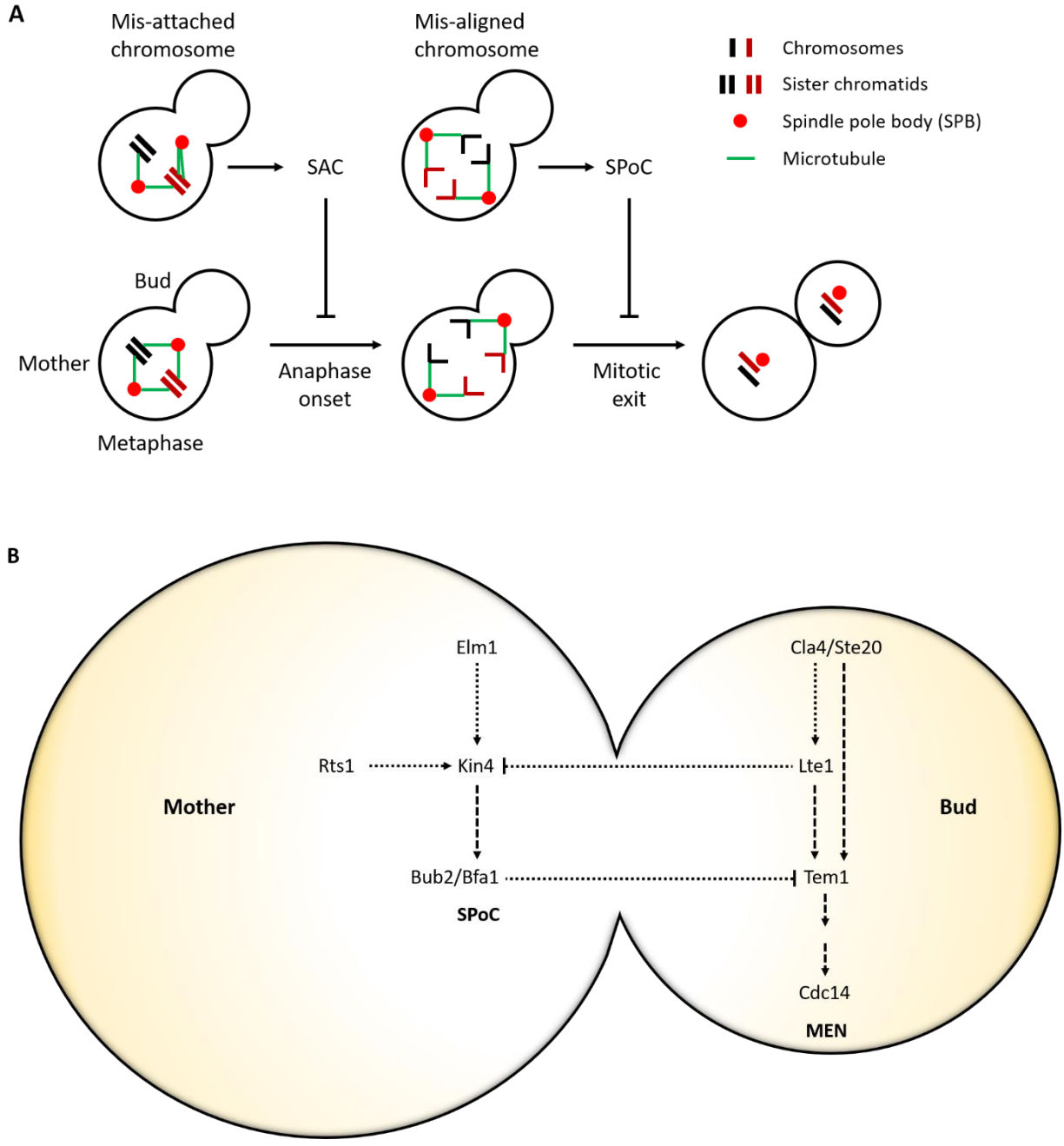

Figure 1.7 Schematic representation of checkpoints involved in the regulation of chromosome segregation. (A) The spindle assembly checkpoint (SAC) is activated upon improper attachment of microtubules to kinetochores which prevents transition from metaphase to anaphase. The spindle position checkpoint (SPoC) halts the cell cycle in late anaphase via inhibition of the mitotic exit network (MEN) in response to a misaligned mitotic spindle in the mother cell. (B) Molecular players involved in SPoC and MEN and their spatial distribution.

1.8 Aims and objectives and overview of the project

The main **aim** of the research was to characterise new mechanisms underlying peroxisome maintenance. This was done by,

1) investigating candidate genes for their function in peroxisome multiplication and

2) a genetic screen to identify novel factors required for peroxisome inheritance and *de novo* formation.

The candidate approach uncovered a role for Pex27 in Vps1-dependent peroxisome fission (Chapter 3). The genetic screen identified Kin4 as a new factor required for peroxisome segregation (Chapter 4). We found that Kin4 also regulates vacuole segregation. As various aspects of spatiotemporal regulation of vacuole transport have been described and many reagents are available to study this process in detail, we diverted our research focus to vacuole inheritance (Chapter 5). Our findings with respect to vacuole inheritance also informed us about the role of Kin4 in peroxisome inheritance (Chapter 6).

Chapter 2 Materials and methods

2.1 Chemicals and enzymes

Most of the chemicals, primers and materials used during this study were supplied by Sigma-Aldrich (now MERCK). Restriction enzymes and respective buffers were provided by New England Biolabs (NEB). PCR buffers, dNTPs and DNA polymerases were supplied by Bioline UK.

Miniprep kits and Gel Extraction kits were provided by Bioline and Qiagen, respectively. Growth media components were supplied by Difco Laboratories and ForMedium. D-Glucose was provided by Fisher Scientific UK.

Equipment used for DNA and protein work were provided by BioRad and buffers for protein work by Geneflow.

2.2 Strains and plasmids

2.2.1 Strains

Table 2.1 The yeast strains used in this study. The gene deletions or modifications were performed as described in (Longtine et al., 1998). *sp: Schizosaccharomyces pombe*, *cg: Candida glabrata*.

Strain name	Genotype	Source
SGA strain (YMS1169)	*his3Δ1 leu2Δ0 met15Δ0 ura3Δ0 his3Δ1::TEF2pr-Cherry::URA3 can1Δ::STE2pr-spHIS5 lyp1Δ::STE3pr-LEU2*	Maya Schuldiner
dnm1Δvps1Δ (YEH738) SGA screen query strain	*YMS1169 dnm1Δ::cgMET15 vps1Δ::mNG-PTS1-natMX6*	This study
dnm1Δvps1Δpex5Δ	*YMS1169 dnm1Δ::cgMET15 vps1Δ::mNG-PTS1-natMX6 pex5Δ::kanMX4*	This study
dnm1Δvps1Δpex13Δ	*YMS1169 dnm1Δ::cgMET15 vps1Δ::mNG-PTS1-natMX6 pex13Δ::kanMX4*	This study
dnm1Δvps1Δinp1Δ	*YMS1169 dnm1Δ::cgMET15 vps1Δ::mNG-PTS1-natMX6 inp1Δ::kanMX4*	This study
dnm1Δvps1Δinp2Δ	*YMS1169 dnm1Δ::cgMET15 vps1Δ::mNG-PTS1-natMX6 inp2Δ::kanMX4*	This study
dnm1Δvps1Δkin4Δ	*YMS1169 dnm1Δ::cgMET15 vps1Δ::mNG-PTS1-natMX6 kin4Δ::kanMX4*	This study
dnm1Δvps1Δkin4Δinp1Δ	*YMS1169 dnm1Δ::cgMET15 vps1Δ::mNG-PTS1-natMX6 kin4Δ::kanMX4 inp1Δ::hphMX6*	This study
dnm1Δvps1Δkin4Δinp2Δ	*YMS1169 dnm1Δ::cgMET15 vps1Δ::mNG-PTS1-natMX6 kin4Δ::kanMX4 inp2Δ::hphMX6*	This study

dnm1Δvps1Δbfa1Δ	*YMS1169 dnm1Δ::cgMET15 vps1Δ::mNG-PTS1-natMX6 bfa1Δ::kanMX4*	This study
dnm1Δvps1Δbub2Δ	*YMS1169 dnm1Δ::cgMET15 vps1Δ::mNG-PTS1-natMX6 bub2Δ::kanMX4*	This study
BY4741	*MATa his3Δ1 leu2Δ0 met15Δ0 ura3Δ0*	Euroscarf
bfa1Δ	*BY4741 bfa1Δ::kanMX4*	Euroscarf
bub2Δ	*BY4741 bub2Δ::kanMX4*	Euroscarf
elm1Δ	*BY4741 elm1Δ::kanMX4*	Euroscarf
frk1Δ	*BY4741 frk1Δ::kanMX4*	Euroscarf
kin4Δ	*BY4741 kin4Δ::kanMX4*	Euroscarf
kar9Δ	*BY4741 kar9Δ::kanMX4*	Euroscarf
frk1Δkin4Δ	*BY4741 frk1Δ::kanMX4 kin4Δ::hphMX6*	This study
frk1Δkin4Δvac17Δ	*BY4741 frk1Δ::kanMX4 kin4Δ::hphMX6 vac17Δ::natMX6*	This study
frk1Δkin4Δdma1Δ	*BY4741 frk1Δ::kanMX4 kin4Δ::hphMX6 dma1Δ::his3MX6*	This study
frk1Δkin4Δinp1Δ	*BY4741 frk1Δ::kanMX4 kin4Δ::hphMX6 inp1Δ::his3MX6*	This study
WT MYO2-3HA	*BY4741 MYO2::MYO2-3HA-his3MX6*	This study
frk1Δkin4Δ MYO2-3HA	*BY4741 frk1Δ::kanMX4 kin4Δ::hphMX6 MYO2::MYO2-3HA-his3MX6*	This study
WT MYO2-GFP	*BY4741 MYO2::MYO2-GFP-his3MX6*	This study
frk1Δkin4Δ MYO2-GFP	*BY4741 frk1Δ::kanMX4 kin4Δ::hphMX6 MYO2::MYO2-GFP-his3MX6*	This study
PEX22-TAP	*BY4741 PEX22::PEX22-TAP-HIS3*	(Ghaemmaghami et al., 2003)
PEX27-TAP	*BY4741 PEX27::PEX27-TAP-HIS3*	(Ghaemmaghami et al., 2003)
BY4742	*MATα his3Δ1 leu2Δ0 lys2Δ0 ura3Δ0*	Euroscarf
dnm1Δ	*BY4742 dnm1Δ::kanMX4*	Euroscarf
inp2Δ	*BY4742 inp2Δ::kanMX4*	Euroscarf
pex3Δ	*BY4742 pex11Δ::kanMX4*	Euroscarf
pex11Δ	*BY4742 pex11Δ::kanMX4*	Euroscarf
pex25Δ	*BY4742 pex25Δ::kanMX4*	Euroscarf
pex27Δ	*BY4742 pex27Δ::kanMX4*	Euroscarf
vac17Δ	*BY4742 vac17Δ::kanMX4*	Euroscarf
vps1Δ	*BY4742 vps1Δ::kanMX4*	Euroscarf
dnm1Δvps1Δ	*BY4742 dnm1Δ::kanMX4 vps1Δ::his3MX6*	Euroscarf
dnm1Δvps1Δ	*BY4742 dnm1Δ::kanMX4 vps1Δ::loxP*	Lab stock
dnm1Δvps1Δkin4Δ	*BY4742 dnm1Δ::kanMX4 vps1Δ::loxP kin4Δ::hphMX6*	This study
dnm1Δvps1Δfrk1Δ	*BY4742 dnm1Δ::kanMX4 vps1Δ::loxP frk1Δ::natMX6*	This study
dnm1Δvps1Δkin4Δfrk1Δ	*BY4742 dnm1Δ::kanMX4 vps1Δ::loxP kin4Δ::hphMX6 frk1Δ::natMX6*	This study

myo2Δ pRS416-MYO2 (URA3)	*BY4742 myo2Δ::KanMX4, pRS416-MYO2 (URA3)*	(Fagarasanu et al., 2009)
frk1Δkin4Δmyo2Δ pRS416-MYO2 (URA3)	*BY4742 frk1Δ::natMX6 kin4Δ::hphMX6 myo2Δ::KanMX4, pRS416-MYO2 (URA3)*	This study
myo2Δ pRS413-MYO2 (HIS3)	*BY4742 myo2Δ::KanMX4, pRS413-MYO2 (HIS3)*	This study
frk1Δkin4Δmyo2Δ::KanMX4, pRS413-MYO2 (HIS3)	*BY4742 frk1Δ::natMX6 kin4Δ::hphMX6 myo2Δ::KanMX4, pRS413-MYO2 (HIS3)*	This study
myo2::KanMX4, pRS413-myo2-D1297N (HIS3)	*BY4742 myo2Δ::KanMX4, pRS413-myo2-D1297N (HIS3)*	This study
frk1Δkin4Δmyo2Δ pRS413-myo2-D1297N (HIS3)	*BY4742 frk1Δ::natMX6 kin4Δ::hphMX6 myo2Δ::KanMX4, pRS413-myo2-D1297N (HIS3)*	This study
dnm1Δvps1Δpex27Δ	*BY4742 dnm1Δ::kanMX4 vps1Δ::loxp pex27Δ::his3MX6*	This study
dnm1Δpex11Δ	*BY4742 dnm1Δ::kanMX4 pex11Δ::his3MX6*	This study
dnm1pex27Δ	*BY4742 dnm1Δ::kanMX4 pex27Δ::his3MX6*	This study
vps1Δpex11Δ	*BY4742 vps1Δ::kanMX4 pex11Δ::his3MX6*	This study
vps1Δ	*BY4742 vps1Δ::kanMX4 PEX11::PEX11-mNG-HIS3*	This study
vps1Δ	*BY4742 vps1Δ::kanMX4 PEX27::PEX27-mNG-HIS3*	This study
dnm1Δvps1Δ PEX11-mNG	*BY4742 dnm1Δ::kanMX4 vps1Δ::loxP PEX11::PEX11-mNG-HIS3*	This study
dnm1Δvps1Δ PEX27-mNG	*BY4742 dnm1Δ::kanMX4 vps1Δ::loxP PEX27::PEX27-mNG-HIS3*	This study
dnm1Δpex27Δ PEX11-mNG	*BY4742 dnm1Δ::kanMX4 pex27Δ::hphMX6 PEX11::PEX11-mNG-HIS3*	This study
TEF2-mCherry (N' mCherry Matα)	*his3Δ1 leu2Δ0 met15Δ0 ura3Δ0 can1Δ::GAL1pr-SceI::STE2pr-SpHIS5 lyp1Δ::STE3pr-LEU2*	(Yofe et al., 2016)
TEF2-mCherry-CLA4	*N' mCherry Matα CLA4::natMX6-TEF2-mCherry-CLA4*	(Yofe et al., 2016)
TEF2-mCherry-FRK1	*N' mCherry Matα FRK1::natMX6-TEF2-mCherry-FRK1*	(Yofe et al., 2016)

Table 2.2 The *E. coli* strains used in this study.

Strain	Genotype	Usage	Source
DH5α	*supE44 ΔlacU169 (ϕ80 lacZ ΔM15) hsdR17 recA1 endA1 gyrA96 thi-1 relA1*	Plasmid amplification and recovery of plasmid DNA from *S. cerevisiae* following *in vivo* homologous recombination.	Hanahan, (1983)
BL21 DE3	*hsdS gal (λcIts857 ind1 Sam7 nin5 lacUV5-T7 gene 1)*	Expression of 6xHis fusion proteins.	Studier and Moffat, (1986)

2.2.2 Plasmids

Plasmids used in this study are tabulated in the **Table 2.3**. Plasmids were made by either a homologous recombination-based approach in *S. cerevisiae* or by conventional restriction digestion and ligation followed by transformation into *E. coli* method. For the yeast plasmids, the parental vectors Ycplac33 and Ycplac111 (Gietz and Sugino, 1988) were used to insert promoters (*GAL1/10*, *HIS3* and *TPI1*) between EcoRI and SacI sites, tags (N-terminal tags between SacI and BamHI sites and C-terminal tags between PstI and HindIII sites) and open reading frames (introduced into the remaining restriction sites in the multiple cloning sites).

Table 2.3 The list of plasmids used in this study.

Plasmid Name	Vector backbone	Promoter	Insert	Source
pAS5	Ycplac33	*HIS3*	*Hc-Red-PTS1*	Lab stock
pAS63	Ycplac111	*HIS3*	*Hc-Red-PTS1*	Lab stock
pAUL3	Ycplac33	*HIS3*	*mNG-PTS1*	Lab stock
pAUL4	Ycplac111	*HIS3*	*mNG-PTS1*	Lab stock
pAUL7	Ycplac111	*GAL1/10*	*mNG-PTS1*	Lab stock
pAUL19	pFA6a	*TPI1*	*mNG-PTS1-natMX6*	Lab stock
pAUL28	Ycplac33	*HIS3*	*mKate2-PTS1*	Lab stock
pEH 012	Ycplac33	*TPI1*	*GFP-PTS1*	Lab stock
pEH 073	Ycplac33	*HIS3*	*Mito-GFP*	Lab stock
pEH 077	Ycplac111	*TPI1*	*3xHA-DNM1*	Lab stock
pEH 079	Ycplac111	*TPI1*	*3xHA-VPS1*	Lab stock
pKA1078	Ycplac33	*VPS1*	*VPS1-GFP*	Kathryn Ayscough
pMS79	pCG	*MET15*	*MET15*	Maya Schuldiner
pLE 007	Ycplac33	*PEX27*	*PEX27*	This study
pLE 044	pFA6a	-	*mNG-HIS3*	This study
pLE 047	Ycplac111	*TPI1*	*PEX11*	This study
pLE 048	Ycplac111	*TPI1*	*PEX27*	This study
pLE 049	Ycplac33	*INP2*	*INP2-GFP*	This study
pLE 050	Ycplac33	*GAL1/10*	*KIN4*	This study
pLE 051	Ycplac33	*GAL1/10*	*FRK1*	This study
pLE 052	Ycplac111	*GAL1/10*	*KIN4*	This study
pLE 053	Ycplac111	*GAL1/10*	*FRK1*	This study
pLE 054	Ycplac111	*VAC17*	*VAC17-GFP*	This study
pLE 056	Ycplac111	*VPH1*	*VPH1-GFP*	This study
pLE 057	Ycplac111	*ERG6*	*ERG6-GFP*	This study
pLE 058	Ycplac111	*KIN4*	*KIN4-GFP*	This study
pLE 059	Ycplac111	*FRK1*	*FRK1-GFP*	This study
pLE 060	Ycplac111	*KIN4*	*KIN4-T209A-GFP*	This study
pLE 061	Ycplac111	*FRK1*	*FRK1-T209A-GFP*	This study
pLE 079	Ycplac111	*VAC17*	*VAC17-S222A-GFP*	This study

pLE 080	Ycplac111	*VAC17*	*VAC17-T240A-GFP*	This study
pLE 082	Ycplac33	*GAL1/10*	*GST-KIN4*	This study
pLE 087	pET28a	*T7*	*VAC17 (1-195aa)*	This study
pLE 088	pET28a	*T7*	*VAC17 (97-355aa)*	This study
pLE 092	pRS413	*MYO2*	*MYO2*	Lois Weisman
pLE 093	pRS413	*MYO2*	*MYO2-D1297N*	Lois Weisman
pLE 098	Ycplac33	*GAL1/10*	*GST-KIN4-T209A*	This study
pLE 102	pRS416	*RRP4*	*GFP-TUB1*	This study
pLE 104	Ycplac33	-	*TEV-2XProtA*	This study
pLE 107	Ycplac33	*INP2*	*INP2-TEV-2XProtA*	This study
pLE 108	Ycplac33	*VAC17*	*VAC17-TEV-2XProtA*	This study
pLE 114	Ycplac33	*VAC17*	*VAC17-S222A-TEV-2XProtA*	This study
pLE 121	Ycplac33	*VAC17*	*VAC17-T240A-TEV-2XProtA*	This study

2.3 DNA procedures

2.3.1 Polymerase chain reaction (PCR)

PCR was routinely used to amplify specific regions of genomic DNA or whole plasmids during Site Directed Mutagenesis (SDM). For proofreading PCR Accuzyme DNA polymerase was used instead of MyTaq DNA polymerase. Promega/Biovision Pfu was used for mutagenesis PCR.

Table 2.4 PCR reaction mixture composition.

Component	Accuzyme pol.	MyTaq pol.	Pfu pol.
Template	1 µl (gDNA or plasmid)	1 µl (gDNA or plasmid)	1 µl (30-50ng plasmid)
Reaction buffer	5µl 10x Accuzyme buffer	10µl 5x MyTaq buffer	2.5µl 10x Pfu buffer
Forward primer	5µl of 5µM	5µl of 5µM	1µl of 5µM
Reverse primer	5µl of 5µM	5µl of 5µM	1µl of 5µM
dNTPs	4µl of 2.5mM	-	4µl of 2.5mM
$MgCl_2$	2µl of 50mM	-	-
DNA pol.	0.5µl of 2.5U/µl	0.2µl of 5U/µl	0.5µl of 2U/µl
ddH_2O	27.5µl	27.8µl	15µl
Total volume	50µl	50µl	25µl

Reactions were run in a thermocycler as follows:

Steps	Accuzyme pol.	MyTaq pol.	Pfu pol.
Initial denaturation	95°C 2min	95°C 2-3min	94°C 2min
Denaturation	95°C 30sec	95°C 30sec	94°C 30sec
Annealing	50-55°C 30sec	50-55°C 30sec	50-55°C 1min
Elongation	74°C 2min/kb	72°C 30sec/kb	68°C 2min/kb
Final elongation	74°C 10min	72°C 10min	68°C 20min
Termination	10°C *	10°C *	10°C *

* Not limited time

Depending upon the nucleotide composition of the primers, the annealing temperature was set for PCR reaction. To get approximate annealing temperature following equation was used: (T_A°C) = (T_M°C) - 5°C where (T_M°C) = 4 x (#G + #C) + 2 x (#A + #T); where T_A and T_M are annealing and melting temperature respectively. Mostly, 5µl of PCR product was loaded on an agarose gel to see if a product of the required size had been produced. The primers used for various PCRs in this study are put in **(Table 2.5)**.

Table 2.5 The primers used in this study. Here, 'F' and 'R' stand for 'forward' and 'reverse' respectively.

Name code	Sequence (5' to 3')	Description
VIP3328 F	GAGTTTATCATTAAGTAGCTACCAGCGAATCTAAA TACGACGGATAAAGACACAGGAAACAGCTATGACC	*DNM1* knockout primer using pCG-MET15
VIP3329 R	ATCACGCCCGCAATGTTGAAGTAAGATCAAAAATGA GATGAATTATGCAAGTTGTAAAACGACGGCCAGT	*DNM1* knockout primer using pCG-MET15
VIP3330 F	GTGCCGATGTTATTGTACCG	Primer 500bp upstream to *DNM1* ORF
VIP3331 R	GGTCATAGCTGTTTCCTGTG	Knockout check PCR primer
VIP3332 F	ACTGGCCGTCGTTTTACAAC	Knockout check PCR primer
VIP3333 R	CTCGTTGATATTAGCATACACC	Primer 500bp downstream to *DNM1* ORF
VIP3340 F	ACCAAAATAAGGACCGTACGAAAACTGCACATTT TATATTATCAGATATCGAATTCCATCAGGTTGGTGG	*VPS1* knockout primer using mNG-PTS1-cloNAT
VIP3342 R	GAGAAATACTCAAAACCAAGCTTGAGTCGACCGGTA TAGATGAGGAAAACGCATAGGCCACTAGTGGATCTG	*VPS1* knockout primer using mNG-PTS1-cloNAT
VIP009 F	GCATCTAGATCTGTTATCAATAGAGGTCAAAAGG	Primer 1300bp upstream to *VPS1* stop codon
VIP012 R	AACCAAGCTTGAGTCGACCG	Primer 40bp downstream to *VPS1* stop codon
VIP982 F	ACGGTGGAAACAGGTCCAG	Primer 500bp upstream to *VPS1* ORF
VIP2029 F	AAGGTCTACATTTTTCGTCTGATAACTCTCAGGAAAT TAAACAAAGTGGTCAGCTGAAGCTTCGTACGC	*INP1* knockout primer
VIP2030 R	ACTTTGGTTTACACCTACATTCATTTGTGCAGTTATG CTTTGAACTTCATGCATAGGCCACTAGTGGATCTG	*INP1* knockout primer
VIP261 F	GTAAAACGACGGCCAGTGAATTC ATTGCTGACCATTTGGTTGG	Primer 500bp upstream to *INP1* ORF
VIP147 F	CAAGTTTGTTTTTACTTACTTGTGAAACGTTTGTTGA TTAACTTAATAATGCAGCTGAAGCTTCGTACGC	*INP2* knockout primer
VIP148 R	GAAAATATGATTAAAGTGTAATTAGTTATTTCAAAGT ACATATTAAAATATATTGTGTTCAATATCCTTTTGACC	*INP2* knockout primer
VIP1706 F	GCGTTCTTGTAACCAAATTTC	Primer 500bp upstream to *INP2* ORF
VIP2034 F	CACGACGGTTGTAAAACGACGGCCAGTGAATTC AAAAGTTCAAAACAGTAACTCGC	Primer to amplify *INP2* ORF with promoter
VIP2035 R	TGCACCCGCCCCTGCTCCCTGCAGTGAATCATT TCCTAGTAATCCTTTTAATTC	Primer to amplify *INP2* ORF with promoter

VIP3428 F	CCGGTGTTGTCACATCTATCCTTGGTATGCAAGACAT GTGGAAAGCTACAGGTGACGGTGCTGGTTTA	Primer to tag *PEX11* with mNG in genome
VIP230 R	TCAAACATAAGCGGAGAATAGCCAAATAAAAAAAA AAGATGAAAAGAAAGGCATAGGCCACTAGTGGATC	Primer to tag *PEX11* with mNG in genome
VIP3429 F	TGGTTAAACTTTGGATAACAACAAAGAGGTCACTTT GCTCTTCAAAAGATGGTGACGGTGCTGGTTTA	Primer to tag *PEX25* with mNG in genome
VIP232 R	ATTCGCCACATATATATGTACATATCTATATGTATAC ATATTTTTATATAGCATAGGCCACTAGTGGATC	Primer to tag *PEX25* with mNG in genome
VIP3430 F	TATGGAACCGAGCCAAAGTCACTTCGGCTAATGAA CATACAAGCGCTGTTGGTGACGGTGCTGGTTTA	Primer to tag *PEX27* with mNG in genome
VIP3431 R	AACTAAAAAAACGAAATAAAGAGGGATGCAACGA ACTTGGTCATCTGTTGGCATAGGCCACTAGTGGATC	Primer to tag *PEX27* with mNG in genome
VIP3445 F	GGTTTAATTAACATGGTGAGCAAGGGCGAGG	Primer to clone mNG into pFA6a-HIS3 backbone
VIP3446 R	GGTGGCGCGCCTTACTTGTACAGCTCGTCCATG	Primer to clone mNG into pFA6a-HIS3 backbone
VIP3459 F	TCATCGCATAATATTCTATCAGGACATTCCGTATA CCTGAATATATATACCAGCTGAAGCTTCGTACGC	*KIN4* knockout primer
VIP3460 R	TATCACTCTATAATATAATGTAATTGTCGATATAAC TATGTACTGAAAACGCATAGGCCACTAGTGGATCTG	*KIN4* knockout primer
VIP3461 F	CCGGAGCTCTGCCTTTTTTCTTTCTCTGCC	Primer 500bp upstream to *KIN4* ORF
VIP3488 F	CGCGAGCTCGGAGCAAGAGATAGTCTGAG	Primer 500bp upstream to *BFA1* ORF
VIP3489 F	CGCGAATTCCTTCCACTGCGTCGTATCCC	Primer 500bp upstream to *BUB2* ORF
VIP3490 F	CGCGAGCTCCGCAGGGGAAGGGATTCAC	Primer 500bp upstream to *RTS1* ORF
VIP3491 F	CGCGAGCTCGAAGATGCAAGCAATTCCCG	Primer 500bp upstream to *ELM1* ORF
VIP3517 F	TCAAGGAGAAAAAACTATAGAGCTCATGG CTTCTGTACCTAAACGC	Primer to clone *KIN4* under *GAL1* promoter
VIP3518 R	CCTGCAGGTCGACTCTAGAGGATCCTCAA ACCCTCATGCTCCTTC	Primer to clone *KIN4* under *GAL1* promoter
VIP3519 F	TCAAGGAGAAAAAACTATAGAGCTCATG TCGTACACCAATAAACGTC	Primer to clone *FRK1* under *GAL1* promoter
VIP3520 R	CCTGCAGGTCGACTCTAGAGGATCCCTCT AGATTTTCATACTTCTTC	Primer to clone *FRK1* under *GAL1* promoter
VIP3527 F	AACGACGGCCAGTGAATTCGAGCTCCTTT TGAAGGAGCCACTTGG	Primer to amplify *VAC17* ORF with promoter
VIP3528 R	CCGCCCCTGCTCCCTGCAGGTCGACAAAC AGCAGTTCTGTATTCAAAGC	Primer to amplify *VAC17* ORF with promoter
VIP3540 F	CTAAGAGAATAGTTGACCTTGTTGCCCAACAAGTCG TTCAAGACGGCCACCGGATCCCCGGGTTAATTAAC	Primer to tag *MYO2* with GFP in genome
VIP3541 R	ATTTCTTTTTTTAGCATTCATGTACAATTTTGTTTCT CGCGCCATCAGTTGCATAGGCCACTAGTGGATC	Primer to tag *MYO2* with GFP in genome
VIP3546 F	AACGACGGCCAGTGAATTCGAGCTCTGGGAAGC CAATTGAAAAGG	To amplify *VPH1* ORF with promoter
VIP3547 R	TTGCACCCGCCCCTGCTCCCTGCAGGCTTGAAGC GGAAGAGCTTG	To amplify *VPH1* ORF with promoter

VIP3558 F	TTGTAAAACGACGGCCAGTGAATTCCAACCAAA CAGCTAGGGCTG	To amplify *ERG6* ORF with promoter
VIP3559 R	CACCCGCCCCTGCTCCCTGCAGTTGAGTTGCTTC TTGGGAAG	To amplify *ERG6* ORF with promoter
VIP3560 F	AACGACGGCCAGTGAATTCGAGCTCTGCCTTTT TTCTTTCTCTGCC	To amplify *KIN4* ORF with promoter
VIP3561 R	TTGCACCCGCCCCTGCTCCCTGCAGAACCCTCA TGCTCCTTCTTTTG	To amplify *KIN4* ORF with promoter
VIP3562 F	AACGACGGCCAGTGAATTCGAGCTCGGTTTAG CCCCTACTGTATAC	To amplify *FRK1* ORF with promoter
VIP3563 R	TTGCACCCGCCCCTGCTCCCTGCAGGATTTTCA TACTTCTTCTTTTG	To amplify *FRK1* ORF with promoter
VIP3581 F	GAAGATAACGAATTAATGAAAGCTTCTTGTGG TTCGCCCTGTTATGC	To mutate *KIN4* Thr 209 to Ala
VIP3582 R	GCATAACAGGGCGAACCACAAGAAGCTTTCA TTAATTCGTTATCTTC	To mutate *KIN4* Thr 209 to Ala
VIP3583 F	GCTCACGAAACGAATTAATGAAGGCGTCATG TGGCTCTCCATGCTACG	To mutate *FRK1* Thr 209 to Ala
VIP3584 R	CGTAGCATGGAGAGCCACATGACGCCTTCAT TAATTCGTTTCGTGAGC	To mutate *FRK1* Thr 209 to Ala
VIP3603 F	ATTCAATTGGCCATTACTTCTATATACTGATTTAG AGTGCCAAAAATTTACAGCTGAAGCTTCGTACGC	*FRK1* knockout primer
VIP3604 R	TTTTTCATATGATAAGTGGATATTATTGTCAAATGA GATAGGTATTATCTGCATAGGCCACTAGTGGATCTG	*FRK1* knockout primer
VIP3503 F	CCGGAGCTCGGTTTAGCCCCTACTGTATAC	Primer 500bp upstream to *FRK1* ORF
VIP3605 F	TAAGATAGATAAGAAACAGCTCGCATAAGGAAACA AGGACACATCGATTACAGCTGAAGCTTCGTACGC	*VAC17* knockout primer
VIP3606 R	AATAAACATTTGGAGCAAAAGAAGAGTAGGTTAGGT AAAGGAGGCATTAAGCATAGGCCACTAGTGGATCTG	*VAC17* knockout primer
VIP3617 F	CTTCAAAAATAGACAAAGACTTGCGTTG ACCTTCTTTGATGAAATGG	To mutate *VAC17* Ser 222 to Ala
VIP3618 R	CCATTTCATCAAAGAAGGTCAACGCAAG TCTTTGTCTATTTTTGAAG	To mutate *VAC17* Ser 222 to Ala
VIP3619 F	GATTTTGATTCTGATCAAGATGCTATCAT TCTACCAAACATAAGTACC	To mutate *VAC17* Thr 240 to Ala
VIP3620 R	GGTACTTATGTTTGGTAGAATGATAGCA TCTTGATCAGAATCAAAATC	To mutate *VAC17* Thr 240 to Ala
VIP3659 F	TCAAGGAGAAAAAACTATAGAGCTCATG TCCCCTATACTAGGTTATTGG	Primer to amplify GST to clone it upstream *KIN4* ORF
VIP3660 R	CGTTTAGGTACAGAAGCCATATCCGATTT TGGAGGATGGTC	Primer to amplify GST to clone it upstream *KIN4* ORF
VIP3674 F	CGCGGATCCATGGCAACCCAAGCCCTAG	To amplify *VAC17* 1-195aa
VIP3675 R	CGCGTCGACTTAATGTGATTTGGCTGCACGTAAAG	To amplify *VAC17* 1-195aa
VIP3676 F	CGCGGATCCGAATTCCAGGATATCACTTTGAG	To amplify *VAC17* 97-355aa
VIP3677 R	CGCGTCGACTTAAAGATTTGTGTTGTTCTCTTTTACC	To amplify *VAC17* 97-355aa
VIP3692 F	GCATGGATGAACTATACAAGAATTCAATGAGAGAA GTTATTAGTATTAATGTCGGTCAAGCTGGTTGTC	To amplify *TUB1* ORF
VIP3693 R	CGAGGTCGACGGTATCGATAAGCTTGGGTGATGTA AGAATCTGATG	To amplify *TUB1* ORF

VIP3696 F	GTCGACCTGCAGGGAGCAGGGGCGGGTGCAAGCG AGAATTTGTATTTTCAGGG	To amplify TEV-2xProtA tag with GAGAGA linker
VIP3697 R	AAAAAATTGATCTATCGATAAGCTTGCCTCACTG ATGATTCGCGTC	To amplify TEV-2xProtA tag with GAGAGA linker
VIP313 F	TGTCTCCATCTACTACTTCAAAGACTTCATCAAGT AATAGTATAATCAATCAGCTGAAGCTTCGTACGC	*PEX11* knockout primer
VIP314 R	TCAAACATAAGCGGAGAATAGCCAAATAAAAAAAA AAGATGAAAAGAAAGCATAGGCCACTAGTGGATCTG	*PEX11* knockout primer
VIP537 F	AGAACCCGAAGCGATGGG	Primer 100bp upstream to *PEX11* ORF
VIP317 F	ATTTGAAGGTAGACTATGACCTTTGTGTTAACTTGG ACAATCGTTTTATCCAGCTGAAGCTTCGTACGC	*PEX27* knockout primer
VIP318 R	AACTAAAAAAACGAAATAAAGAGGGATGCAACGA ACTTGGTCATCTGTTGCATAGGCCACTAGTGGATCTG	*PEX27* knockout primer
VIP021 F	CTGGAATTCTCATCATTTGCGTCATCTTC	Primer 500bp upstream to *PEX27* ORF
VIP3439 F	CAAAAAACACATACATAAACGAGCTCAAAATGG TCTGTGATACACTGG	To amplify *PEX11* ORF
VIP038 R	GGGGTCGACCTATGTAGCTTTCCACATGTC	To amplify *PEX11* ORF
VIP2971 F	GTTGTAAAACGACGGCCAGTGAATTCCCTTGC GTTTCAGCTTCCAC	To amplify *PEX27* ORF with promoter
VIP2972 R	CCAAGCTTGCATGCCTGCAGGTCGACTCAAAC AGCGCTTGTATGTTC	To amplify *PEX27* ORF
VIP325 F	CACATACATAAACGAGCTCAAA ATGACATCCGATCCTGTTAATAC	To amplify *PEX27* ORF
VIP1078 F	CAGATCCACTAGTGGCCTATGC	Knockout check PCR primer
VIP1079 R	GCGTACGAAGCTTCAGCTG	Knockout check PCR primer
VIP142 R	CTGCAGCGAGGAGCCGTAAT	Knockout check PCR primer
VIP272 R	CCCATTAACATCACCATC	Primer anneals at GFP N-ter
VIP418 F	GTATTACTTCTTATTCAAATG	Primer anneals in *GAL1* promoter
VIP3466 F	GGTGGTGGCGACCATCCTCC	Primer anneals at GST C-ter
VIP081 F	GTATTACTTCTTATTCAAATG	Primer anneals in *TPI1* promoter

2.3.2 Plasmid miniprep

E. coli DH5α cells with plasmid were grown overnight in 3-5ml of 2TY medium containing an appropriate antibiotic. Plasmid DNA was isolated from the culture using the mini prep kit (Bioline) following manufacturer's instructions.

2.3.3 Agarose gel electrophoresis

PCR product, plasmid, digested PCR (or plasmid) and gel-extracted DNA samples were examined by agarose gel electrophoresis. Generally, 1% agarose gels were prepared by melting 0.5g of agarose in 50ml of 1X TBE and adding ethidium bromide to a final concentration of 0.5µg/ml. Samples were loaded after mixing with DNA Loading Buffer at 1X final concentration. A DNA marker (Bioline Hyper ladder I) was run alongside the DNA samples to

estimate the size of DNA fragments. Gels were run in 1X TBE buffer at a constant voltage of 90-95V. DNA bands were examined using an ultraviolet transilluminator imaging system (Gene Genius).

6X DNA loading buffer: 0.25% bromophenol blue (w/v), 30% glycerol (v/v), 0.25% xylene cyanol FF (w/v).

10X TBE buffer: 0.9M Tris-Borate, 10mM EDTA, pH 8.0.

2.3.4 DNA digestion and gel extraction

The digestion was performed using restriction endonucleases in CutSmart buffer. Typically, 0.5µg DNA was digested in a 25µl reaction volume containing 1µl of restriction enzyme and 2.5µl of the 10X CutSmart buffer. The final volume was achieved by adding ddH_2O. The digestion mixtures were incubated at 37°C for periods varying from 2h to overnight. If the digested DNA was required, then the digestion mixture was run onto the agarose gel. The bands of interest were excised from the gel by viewing using a long wavelength UV transilluminator. After that, DNA fragments were extracted using the QIAquick Gel Extraction Kit (Qiagen) according to manufacturer's instructions.

2.3.5 DNA ligation

Generally, 10µl DNA ligation reaction consisted of: 1µl of 10X ligase buffer, 3-5µl of digested PCR product, 2µl of linearized vector (20-25ng) and 1µl of T4 DNA ligase (NEB). The reaction tubes were left at room temperature (or at 25°C) for at least 2h and then transformed into chemical competent *E. coli* cells.

2.3.6 Homologous recombination-based cloning

The homologous recombination-based DNA editing was employed for gene cloning, to introduce tags, genes or both in a vector. The insert (promoters, ORFs and tags) to be cloned was amplified by PCR using primers designed to anneal to the start and the end of a region of interest and to have ~20 nucleotides as flanking regions identical to each side of the desired insertion sites in the vector. PCR fragment and linearized vector were transformed to yeast and upon homologous recombination the vector is circularised, a procedure also referred to as gap-repair **(Figure 2.1)**. Recombinant plasmid carrying cells were identified by growth on selective medium.

2.3.7 Site directed mutagenesis

Site directed mutagenesis was performed using Pfu DNA polymerase (Promega/Biovision) **(Table 2.4)**. The obtained PCR product was subjected to DpnI digestion for 1h at 37°C. Then,

5µl of PCR was analysed by agarose gel electrophoresis. 1µl of the reaction mixture was transformed into electrocompetent *E. coli.* cells. Few individual colonies were grown in liquid cultures for plasmid miniprep purification. The DNA sequence of the clones was subsequently determined to check for the presence of desired mutation.

A)

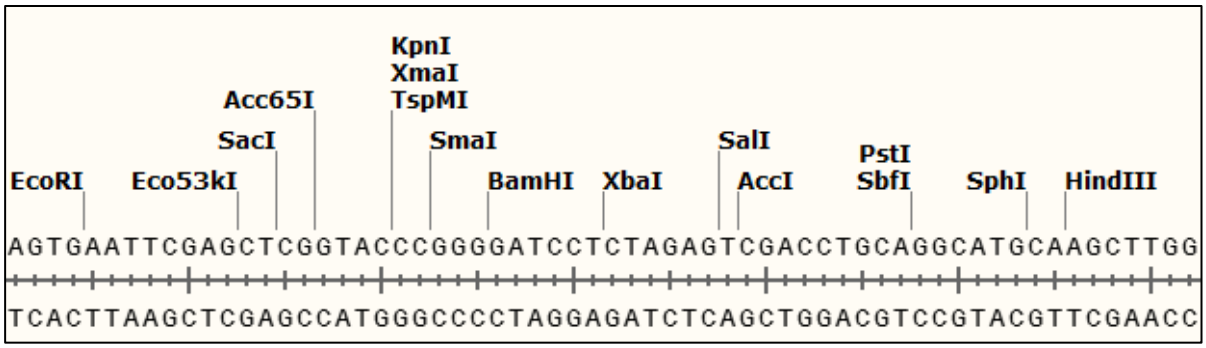

B)

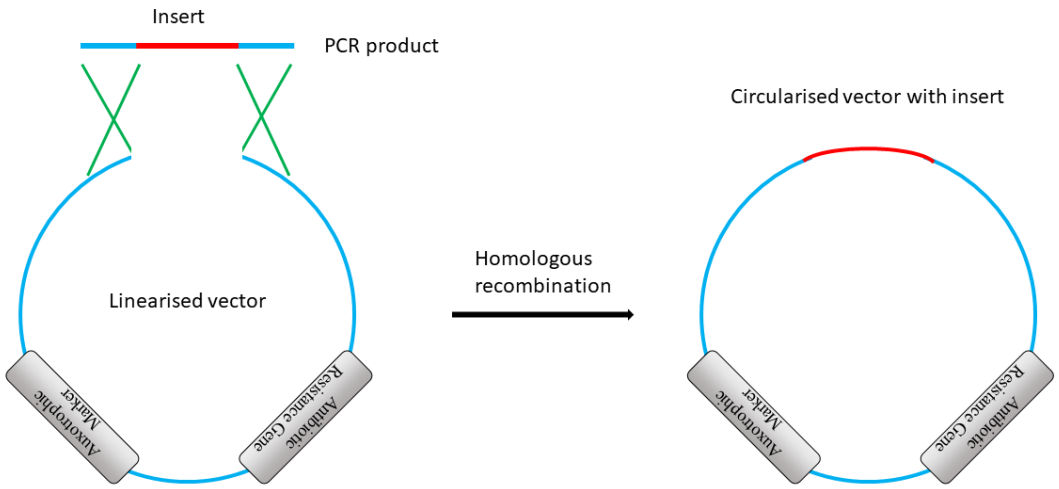

Figure 2.1 Plasmid construction by homologous recombination in *S. cerevisiae*.
(A) The multiple cloning sites (MCS) present in the Ycplac33 and Ycplac111 vectors. (B) The PCR product consists of insert (red) and nucleotide overhangs (blue) are 18-20nt long. These overhangs are identical nucleotide sequences between the PCR product and a linearized plasmid. Once transformed into yeast the linearized vector and the PCR product undergo homologous recombination and that results in the circularised plasmid with insert.

2.3.8 DNA sequencing

To confirm the sequence of the plasmid clones, they were sequenced by Sanger sequencing method, the service provided by Source Bioscience. The obtained sequence data was analysed using SnapGene and ClustalW multiple sequence alignment online tool (http://www.genome.jp/tools-bin/clustalw).

2.4 Growth Media

All the components of cell growth media were dissolved in Millipore water. The sterilisation of culture media was carried out by autoclaving at 121°C. Where antibiotic-resistance selection was required, the appropriate antibiotics were added to their final concentration once the media had cooled down to ~50°C after sterilisation.

Table 2.6 The culture media and their constituents.

Culture media	Components with concentration
2TY	Bacto tryptone (1.6%), yeast extract (1%), NaCl (0.5%). If antibiotic-resistance selection was required, Ampicillin (75µg/ml) or Kanamycin (50µg/ml) were added.
YPD	Yeast extract (1%), peptone (1%), D-glucose (2%).
Yeast minimal media 1 (YM1)	Ammonium sulphate (0.5%), yeast nitrogen base (0.17%), either glucose or raffinose or galactose (2%). Adjusted to pH 6.5.
Yeast Minimal Media 2 (YM2)	Ammonium sulphate (0.5%), yeast nitrogen base (0.17%), either glucose or raffinose or galactose (2%), casamino acids (1%). Adjusted to pH 6.5.
Amino acid and nucleic acid base	As required following amino acids were added to YM1 and YM2 medium; 100x stocks (0.2% histidine, 0.3% leucine, 0.3% lysine, 0.2% methionine, 0.2% tryptophan, 0.2% uracil)
Dropout supplements	Instead of adding individual amino acid sometimes dropout supplements; for e.g. -Leu-Ura-His, -Ura-His, from ForMedium were used to prepare YM1 dropout media
Solid Media	Agar (2%) was added to the dissolved growth liquid medium which was then autoclaved. The medium was cooled and poured into sterile petri dishes (Sterilin) and further allowed to set at room temperature. Once set, plates were stored at 4^{o}C.
SGA sporulation medium	1% potassium acetate, 0.1% yeast extract, 0.05% glucose, 0.01% amino-acids supplement powder mixture for sporulation (contains 2g histidine, 3g leucine, 2g lysine, 2g uracil).
SD -Ura-Met-Leu-Arg-Lys + canavanine + thialysine	0.5% Ammonium sulphate, 0.17% yeast nitrogen base w/o amino acids, amino acids supplement powder mixture (-Ura-Met-Leu-Arg-Lys), canavanine (50mg/L) and 0.5ml thialysine (50mg/L), glucose (2%).
SD-(MSG) -Ura-Met-Leu-Arg-Lys + canavanine + thialysine	1g MSG (L-glutamic acid sodium salt hydrate, Sigma), 0.17% yeast nitrogen base w/o amino acids, amino acids supplement powder mixture (-Ura-Met-Leu-His-Arg-Lys), canavanine (50mg/L) and 0.5ml thialysine (50mg/L), glucose (2%).
5-FOA plates	4% agar solution was autoclaved and cooled down to 50°C. Added filter sterilised 1% ammonium sulphate, 4% glucose, 0.2% 5-FOA, 0.05% Uracil in equal volumes. Added other amino acids as required.

2.5 Yeast protocols

2.5.1 Yeast growth maintenance

All yeast strains were grown on either liquid or solid media **(Table 2.6)** incubated at 30°C. Amino acids, adenine and uracil were added to the plates for the strains with auxotrophies as required. Antibiotics were used to select for resistance conferring selection cassettes. Glycerol stocks were prepared in 15% (v/v) glycerol and stored at -80°C. For yeast strains with a reporter gene under control of the *GAL1/10* promoter, cells were grown overnight in 2% raffinose (or sucrose) containing selective medium. Then, cells were transferred to YM2 2% galactose medium to induce gene expression for the times indicated.

2.5.2 One step transformation

Yeast strains were grown overnight in appropriate liquid media (mostly YPD). 200µl from overnight culture was centrifuged for 1min at 12,000rpm in an Eppendorf microfuge and supernatant was removed. 1µl of plasmid DNA (100-300ng), 5µl (50µg) of single stranded DNA and 50µl of one step buffer were added to the above tube and was given a short spin to collect all the components to the bottom. The mixture was then resuspended by means of the cut tip followed by vortexing. The tube was incubated at room temperature for more than 3h with occasional vortexing. Further, the tube was heat shocked at 42°C for 30min and the cell suspension was plated on appropriate selective media. The plates were incubated at 30°C for 2-3 days to obtain transformants.

One step buffer: 0.2M LiAc pH 5.0, 40% (w/v) PEG (Polyethylene glycol) 3350, 0.1M DTT.

2.5.3 High efficiency transformation

High efficiency yeast transformations were performed according to the lithium acetate procedure (Gietz and Woods, 2006). The yeast strains were grown overnight in the YPD liquid media. Next day, secondary yeast culture was started with 0.1OD and allowed to grow to mid-log phase (~0.5-0.6OD). Cells (5ml per transformation) were harvested at 3000rpm for 5min by centrifugation. The supernatant was discarded, and cells were washed twice with 1ml of freshly prepared 1X TE/LiAc solution. Then, the cells were resuspended in 50µl of 1X TE/LiAc solution then 2-10µl (0.5µg-1µg) of DNA (PCR product and/or plasmid) and 5µl (50µg) of single stranded DNA were added to it. Next, 300µl sterile 40% PEG solution was added to above mixture and further mixed by vortexing. The tubes were incubated at room temperature for 1hour and subsequently they were transferred to a hot water bath at 42°C for 15min for heat shock. Then cells were spun down for 2min at 5000rpm and supernatant was removed. Finally, cells were resuspended in 50µl 1X TE, and plated on selective media and

incubated at 30°C for 2-3 days. Those instances where the antibiotic resistance markers were used (like cloNat, G418, Hygromycin B), cells were first recovered for 3-4h in liquid YPD medium before being spread onto YPD plates containing an appropriate antibiotic.

1X TE/LiAc: For 10ml-1ml of 10X TE, 1ml of 1M LiAc (Lithium acetate) pH7.5, 8ml of ddH_2O.

PEG 40% w/v: For 5ml-500µl of 10X TE, 500µl of LiAc, 4ml of 50% PEG 3350.

10X TE: 100mM Tris pH8.0, 10mM EDTA pH8.0.

2.5.4 Yeast genomic DNA isolation

Yeast strains were grown overnight in 3ml liquid media and harvested at 12000rpm for 1min in an Eppendorf microfuge and resuspended in 1ml of sterilised water. In some cases, the cells were scraped from agar plates and resuspended in 1ml sterilised water. The cells were centrifuged at 12000rpm for 1min, the supernatant was discarded, and the cells were resuspended in the remaining volume. 200µl of TENTS, 200µl of 425-600µm glass beads and 200µl phenol:chloroform:isoamyl alcohol (25:24:1) were added. Then, the cells were lysed using a mini bead beater (Biospec Products) at full speed for 45sec; the mixture was centrifuged at 12000rpm for 30s. 200µl of TENTS was added to the above tube and suspension was vortexed. The samples were centrifuged at 12000rpm for 5min and ~350µl of supernatant was transferred to a fresh tube. 200µl of phenol:chloroform:isoamyl alcohol was added and the samples were vortexed and centrifuged as above. 300µl of the supernatant was transferred to a clean tube, and DNA was precipitated by adding 1/10 volume of 3M NaAc pH 5.2 and 2.5X volume 100% ethanol and incubated at -20^{0}C for 30min. The samples were centrifuged at 12000rpm for 15min and washed with 100% ethanol. The samples were centrifuged at 12000rpm for 1min and the supernatant was removed. The pellet was resuspended in 200µl 1X TE + 2µl RNase (100µl RNase/TE (10µg/ml)). The tubes were left at room temperature for 10min. The DNA precipitation step was performed as described above. The pellet was washed with 70% ethanol. Finally, the pellet was dried at 56°C and resuspended in 50-100µl of 1xTE.

TENTS: 20mM Tris-HCl pH 8.0, 1mM EDTA, 100mM NaCl, 2%(v/v) Triton X-100, 1%(w/v) SDS.

1X TE: 10mM Tris-Cl pH8.0, 1mM EDTA.

2.5.5 Pulse chase experiment

Pulse-chase experiments were used to follow the localisation of fluorescently tagged proteins under control of the *GAL1/10* promoter. For rapid induction of expression, cells were grown overnight in raffinose (or glucose 2% w/v) selective medium at 30°C with shaking. The cells

were diluted 1:10 in galactose (2% w/v) containing selective medium and incubated for 2h. After that, the cells were spun down and resuspended into fresh selective medium with glucose to shut down the *GAL1/10* promoter-based expression. The cells were imaged at regular intervals.

2.5.6 FM4-64 staining

To stain the vacuolar membrane, the lipophilic dye FM4-64 (Invitrogen) was used (Vida and Emr, 1995). The cells were grown to log phase and then pelleted down (1-2ml) and resuspended into 200µl YPD containing FM4-64 (1ng/µl final concentration). The resuspended cells were incubated at 30°C for an hour and then pelleted down. The supernatant was removed, and the cells were washed thrice in appropriate minimal medium. Subsequently, the cells were resuspended in 200µl of medium and added to 3-4ml of fresh medium and incubated at 30°C for 3-4h and imaged using a fluorescence microscope.

2.5.7 Epitope tagging in genome and gene deletion

PCR was used to amplify the tags with selection marker or knockout cassette selection marker. The forward primer contains 50 nucleotides (orange) of identity to the region upstream of ORF stop codon (for tagging) or start codon (for gene deletion). The reverse primer contains 50 nucleotides (green) downstream identical to the sequence of ORF stop codon. PCR fragment was transformed to yeast and was grown on desired selective medium. Correct clones were identified by PCR to confirm the modification into the genome **(Figure 2.2 A, B)**.

2.5.8 SGA screen

To perform the SGA screen, the triple gene deletion library was prepared by means of SGA methodology and the obtained mutants were subsequently imaged by epifluorescence microscopy (Cohen and Schuldiner, 2011) **(Figure 2.3)**. Briefly, the query strain, *dnm1Δvps1Δ* carrying mNG-PTS1 and cytosolic mCherry was crossed with single gene deletion and DAmP libraries on YPD rich medium plates. The diploids were selected on SD medium and then shifted to nitrogen starvation medium for 5 days to induce sporulation. Further, the haploid (*MATα*) cells were selected on SD selective medium. Finally, two rounds of selection were performed to obtain desired mutants. The mutants were grown in SD medium overnight and then 5h during day in fresh medium before visualising by Olympus microscope with 60X Air lens and images were captured with camera (ORCA-ER, Hamamatsu). The microscopy images were analysed manually using Fiji-ImageJ software. The mutant library generation and microscopy analysis is done as (Cohen and Schuldiner, 2011).

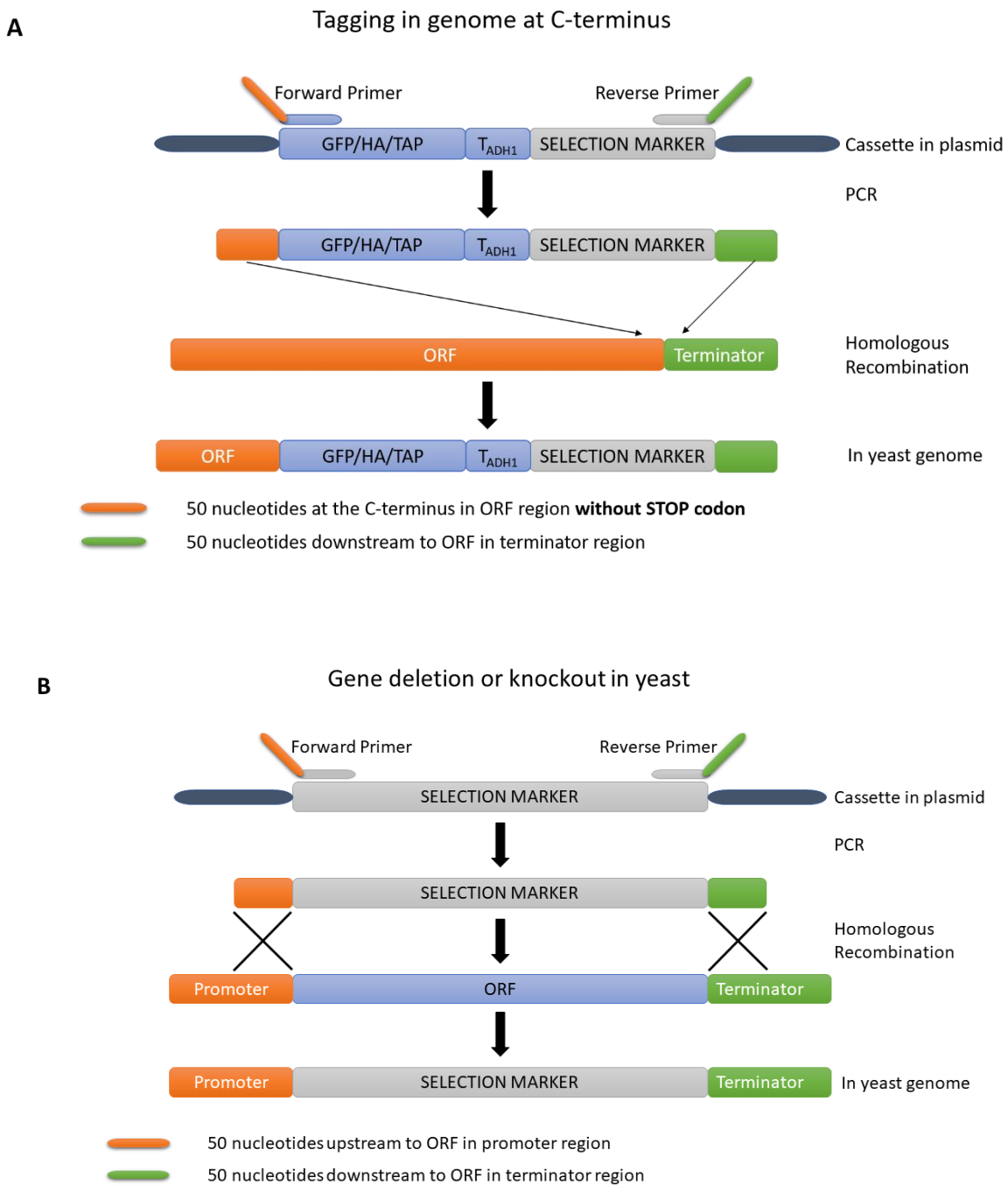

Figure 2.2 Schematic representation of the methods used to modify genes in the genome for either epitope tagging at the C-terminus of ORF (A) or gene deletion (B). PCR products were transformed by means of 'high efficiency transformation' protocol to obtain desired genetically modified strains. T_{ADH1} indicates *ADH1* terminator.

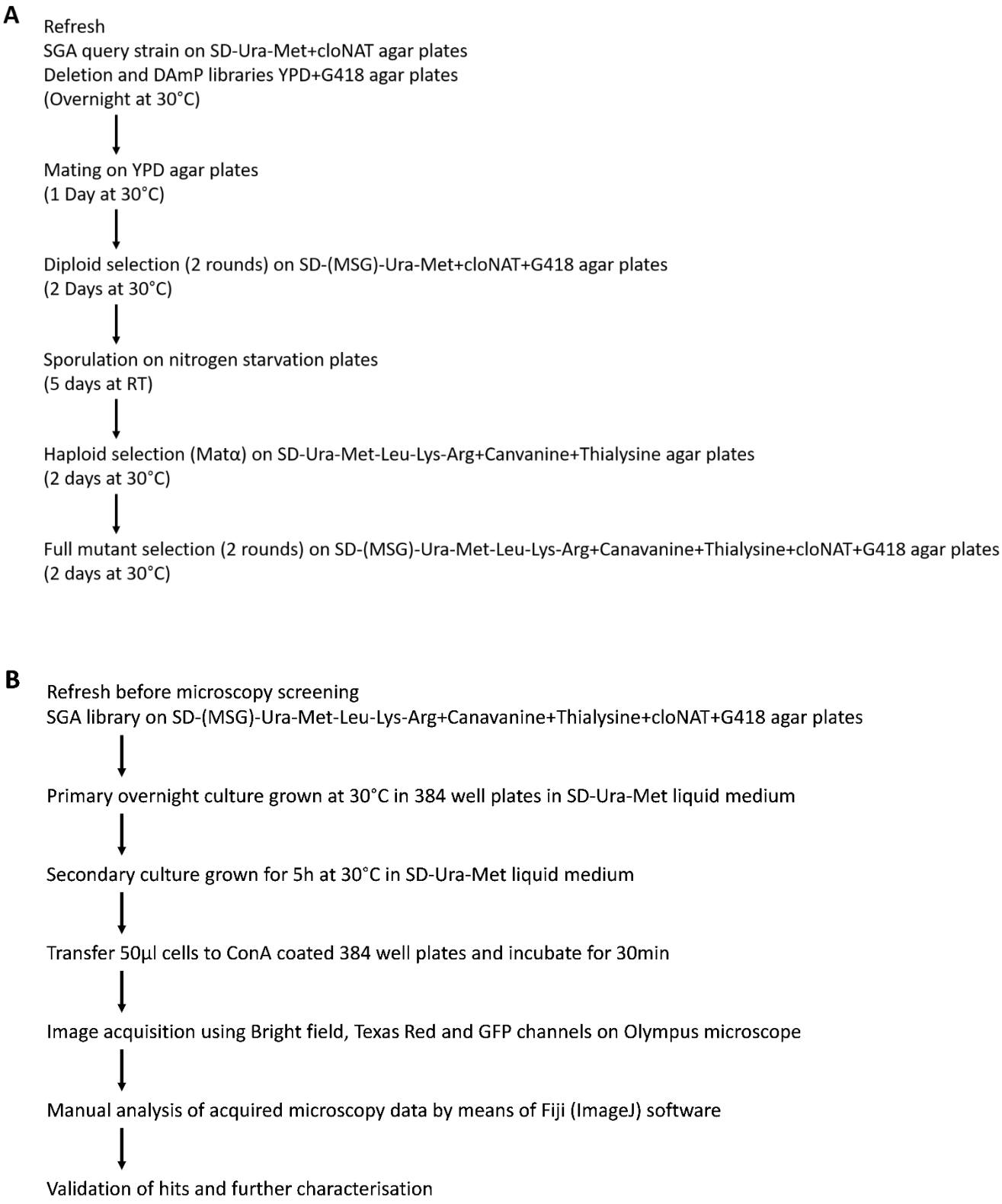

Figure 2.3 The flow chart for steps involved in SGA mutant library construction (A) followed by microscopy imaging (B).

2.6 *E. coli* protocols

2.6.1 Preparation of chemical competent *E. coli* DH5α cells

E. coli DH5α competent cells were prepared by the rubidium chloride method (Hanahan, 1983). Overnight cultures in 2TY liquid medium were prepared from a single colony of DH5α from a 2TY plate and incubated at 37°C. 200ml of 2TY medium in 1L conical flask was inoculated to start a secondary culture with $0.05OD_{600}$ and grown at 30°C with shaking until mid-log phase (~$0.5\text{-}0.6OD_{600}$). The culture was incubated on ice to cool down for 15min. Then cells were centrifuged at 3000rpm (Sigma 4-16K) for 10min at 4°C. The supernatant was removed, and the bacterial cells were resuspended in 75ml of ice-cold solution I and chilled on ice for 20min. The cells were pelleted down by centrifugation at 3000rpm for 10min at 4°C. The pellet was resuspended in 16ml ice cold solution II and aliquoted 200µl of cell suspension in each pre-cooled 1.5ml Eppendorf tubes. The aliquots were flash-frozen in liquid nitrogen and stored at -80°C.

Solution I: 100mM rubidium chloride, 50mM manganese chloride, 10mM calcium chloride, 30mM potassium acetate, 15% w/v glycerol, pH 5.8.

Solution II: 10mM MOPS, 10mM rubidium chloride, 75mM calcium chloride, 15% w/v glycerol, pH 6.8.

2.6.2 *E. coli* transformation

The *E. coli* competent cells (DH5α) were thawed on ice. 1µl of plasmid or 10µl of ligation mixture was added to 50µl or 100 of cells, respectively. Cells were incubated on ice for 30min. The cells were subsequently heat shocked at 42°C for 1min and incubated for 2-3min on ice. Subsequently, 900µl of 2TY media was added and incubated at 37°C for 45min. The cell transformation mixtures were centrifuged at 10000rpm for 1min and 900µl of supernatant was discarded. The cell pellet was resuspended in the remaining medium and plated onto 2TY agar media with the appropriate antibiotic.

2.6.3 Preparation of electroporation competent cells

1L of 2TY medium was inoculated from overnight grown cells to start a secondary culture starting with $0.05OD_{600}$. The cells were grown at 30°C with shaking to ~$0.5\text{-}0.6OD_{600}$. The culture was left on ice to chill for 15min and then the cells were harvested by centrifugation at 3,000rpm for 15min. After harvesting, the supernatant was discarded, and the pellet was resuspended in 500ml ice-cold 10%(v/v) glycerol. The cells were harvested again as above and resuspended in 250ml ice cold 10%(v/v) glycerol. The harvesting was done for a third time and the cells were resuspended in 50ml ice cold 10%(v/v) glycerol. Finally, the cells were spun

down by centrifugation at 3000rpm for 15min and the supernatant was discarded. The cell pellet was resuspended in 750µl 10%(v/v) ice cold glycerol. The cells were aliquoted (40µl in each tube) in 1.5ml Eppendorf tubes and flash-frozen into the liquid nitrogen and stored at -80°C. All centrifugation steps were carried out at 4°C.

2.6.4 *E. coli* transformation by electroporation

1µl yeast genomic DNA was added to 40µl of *E. coli* DH5α electrocompetent cells, which were thawed on ice. Cells were mixed and transferred to a chilled electroporation 2mm cuvette (Geneflow). The cuvette was placed in the electroporation chamber and was given a pulse using setting EC2 (V=2.5kV) on the electroporator (MicroPulser by BIORAD). After the pulse, 600µl of 2TY media was added immediately and the cells were transferred to a fresh 1.5ml Eppendorf tube. The tube was left shaking at 37°C for 30min and the cells were centrifuged at 5000rpm for 5min. The cell pellet was taken with cut tip and spread onto 2TY agar plate with the desired antibiotic. The plates were incubated overnight at 37°C.

2.7 Protein procedures

2.7.1 SDS-PAGE

Sodium dodecyl sulphate polyacrylamide gel electrophoresis (SDS-PAGE) was performed as described in (Sambrook and Russell, 2006). 8-12% gels were prepared using the constituents given in the following table.

Table 2.7 The constituents and their volumes for SDS-PAGE gel.

Components	**Resolving gel (12%)**	**Stacking Gel (4%)**
Protogel (Acrylamide, Bis-acrylamide mix) 30% stock	4ml	0.67ml
Resolving buffer 4X stock	2.5ml	-
Stacking buffer 4X stock	-	1.25ml
APS 10% (w/v) stock	100µl	50µl
TEMED 1000X stock	10µl	5µl
ddH_2O	3.39ml	3.025ml
Total Volume	**10ml**	**5ml**

Protein loading dye (4X): 250mM Tris pH6.8, 9.2% (w/v) SDS, 40% (w/v) Glycerol, 0.2% (w/v) Bromophenol brilliant blue, 100mM DTT.

2.7.2 Protein purification protocol

2.7.2.1 Primary, secondary culture growth and induction

Primary cultures were inoculated from single bacterial colony in 2ml Luria Broth containing appropriate antibiotic and incubating the culture overnight at 37ºC with constant shaking at 200rpm. The following day, secondary cultures were inoculated in 100ml Luria Broth using 1ml of overnight culture (1% inoculum) and the secondary cultures were incubated at 37ºC and 200rpm until OD_{600} reaches to 0.8-1.0. Prior to induction of protein 1ml bacterial culture was removed as an uninduced sample. Protein induction was performed mostly by adding Isopropyl-β-D-galactopyranoside (IPTG) to 1mM final concentration. Most of the protein inductions were carried out by shifting culture to 30ºC for 4h after IPTG addition. At the end of protein induction cells are harvested by centrifugation at 8000rpm for 15min at 4ºC. Bacterial pellet thus obtained was either used immediately or stored at -80ºC for later use.

2.7.2.2 6xHis-tagged protein purification

$(His)_6$-tagged proteins were affinity purified over (Ni-NTA)-agarose resin from Sigma Aldrich. Bacterial pellets stored at -80ºC were thawed and lysed on ice by resuspension in lysis buffer containing lysozyme. Eventual lysis of bacterial lysates was obtained by sonication of lysate until it appeared clear (45% amplitude, Pulse 20sec on and 10sec off). A 50µl sample was collected at this point as whole cell lysate. The lysate was cleared by a high-speed centrifugation spin at 11000rcf for 30min at 4ºC. The clear supernatant was collected and 50µl sample was collected at this point representing total soluble proteins. The remaining clear supernatant was transferred to the column containing Ni-NTA agarose beads that were washed and equilibrated in wash buffer. $(His)_6$-fusion proteins were allowed to bind the beads by keeping for 1h on a rotamer at 4°C. Unbound material was collected through a poly prep column (from BioRad) and 50µl sample was collected at this point as flow through. The beads bound with proteins were washed extensively with 10 bed volumes of wash buffer. After all washes; bound proteins were eluted from beads by incubating with elution buffer (pH adjusted to ~8.0). The column was kept on ice for 15min with intermittent tapping and eluted proteins were collected by gravity flow. Various samples collected at earlier stages were analysed on SDS-PAGE gel to check protein purification stability and quality.

Lysis buffer: 50mM NaH_2PO_4, 300mM NaCl, 10mM Imidazole, pH8.0. pH was adjusted with NaOH. Further added 5mM β-ME, 4mM AEBSF or PMSF, Lysozyme was added (1µg/ml of lysis buffer).

Wash buffer: 50mM NaH_2PO_4, 300mM NaCl, 25mM Imidazole, pH to 8.0.

Elution buffer: 50mM NaH_2PO_4, 300mM NaCl, 250mM Imidazole, pH 8.0 including 0.5% (v/v) Triton X-100 in certain cases.

2.7.3 TCA extraction

Overnight yeast cultures were grown and $10OD_{600}$ units of cells were harvested at 12000rpm for 1min. The pellet was re-suspended into 500µl of TCA lysis buffer and left the mixture on ice for 10min. Subsequently, 71µl of 40% (w/v) TCA (Trichloro acetic acid) solution was added to above mixture. Then centrifugation was carried out at 13000rpm for 5min at 4°C. The supernatant was aspirated off as much as possible leaving behind the precipitated protein. The pellet was neutralised by adding 10µl of 1M Tris Base, pH 9.4. Then 90µl of 1X SDS loading dye was added to above mixture and boiled for 10min at 95°C. Sample were ready to use for SDS-PAGE.

TCA lysis buffer: 0.2M NaOH and 0.2% β-ME.

2.7.4 Western blot analysis

Samples are prepared using 4X SDS Laemeli buffer and then loaded on SDS-PAGE gel. Gels were run at constant voltage (100-150V) and proteins were transferred onto nitrocellulose membranes using a wet transfer apparatus (Bio-Rad). All protein transfers were performed at constant current (200mA) for 120min. The nitrocellulose membranes cut to required size were pre-treated by soaking them transfer buffer for 1-3min, in 1X transfer buffer until used. After protein transfer, membrane was blocked with 5% (w/v) skimmed milk in TBST buffer for 1h at room temperature (Or overnight at 4°C). After blocking, the membrane was incubated with primary (usually for 1h at room temperature and occasionally overnight at 4°C) and secondary antibodies (1h at room temperature). Antibodies were used at given dilutions: anti-HA antibody (1:5000), anti-His antibody (1:10000), anti-GFP antibody (1:3000) and anti-Protein A antibody (1:2500), anti-rabbit or anti-mouse antibody (1:10000). After each of the antibody incubations membranes were washed 3 times for 10min each with TBST. Blot was developed using Enhanced Chemi-Luminescence (ECL) substrates.

PRB (Protein Running Buffer) 10X: 30.28g Tris Base, 144.13g Glycine, 1% (w/v) SDS. Top up to 1L.

Transfer buffer: 15.13g Tris Base, 56.25g Glycine, 4L dH_2O, 1L Methanol.

TBS 10X: 24.23g Tris HCl, 80.06 g NaCl. Mix in 800 ml ddH_2O. Adjust pH to 7.6 with HCl. Top up to 1 L.

TBST: For 1 L; 100ml of 10X-TBS + 900ml ddH_2O + 1ml Tween20.

2.7.5 GST-tagged protein purification from yeast

Kin4 was tagged with GST at N-terminus under *GAL1/10* promoter on plasmid. The transformants with *GAL-GST-KIN4* plasmid were grown overnight in YM2-Ura (+2% Sucrose) medium. Next day secondary culture was started with OD_{600} 0.3 into fresh YM2-Ura (+2% Sucrose) medium and after 2h galactose (2% final concentration) was added to the medium to induce the expression of the protein. The induction was carried out for 6h. Approximately $500OD_{600}$ units of cells were harvested by centrifugation for 5min at 3000rpm. The cell pellet was washed once with 1X PBS and stored at -80°C. In all the above steps, the cells were grown at 30°C and 200rpm shaking.

The frozen cell pellets once thawed were resuspended in the 5ml of cold lysis buffer. The suspension was distributed equally into 5 screw cap tubes containing 400ul of prewashed glass beads to each tube. The cells were lysed in bead beater (1min on+2min off on ice X 4 times). The cell extract was centrifuged at 13000rpm at 4°C for 10min. The supernatants were pooled together and transferred to the prewashed GSH-Sepharose beads and incubated at 4°C for 1h. The beads were washed thrice with wash buffer. Finally, the beads were resuspended into the kinase storage buffer and stored at -20°C.

Lysis buffer: 50mM Tris-Cl pH7.5, 250mM NaCl, 1% Nonidet P-40, 1mM DTT, 1mM EDTA, 10mM NaF, 50mM β-glycerophosphate, 1mM sodium orthovanadate and protease inhibitor cocktail.

Wash Buffer: 50mM Tris-Cl pH7.5, 250mM NaCl, 1% Nonidet P-40 and1mM DTT.

Storage buffer: 50mM Tris-Cl pH7.5, 100mM NaCl, 2mM DTT and 25% glycerol.

2.7.6 *In vitro* kinase assay

GST-Kin4 and 6xHis-Vac17 fragments were purified from the yeast and *E. coli*, respectively. 1μg of His-Vac17 and ~0.25μg of GST-Kin4 were added to the kinase assay buffer; here GST-Kin4 was bound to GSH-sepharose beads. [γ^{32}P]-ATP was used to analyse the phosphorylation of Vac17 fragments. The reaction mixture was incubated at 30°C with gentle shaking for 30min and was further stopped by the addition of 5X SDS protein loading buffer. The samples were boiled for 5min at 100°C before loading on the SDS-PAGE gel. The gel was subsequently stained and dried on the blotting paper. And after that it was exposed to the x-ray film at -80C using an intensifying screen and the film was developed after 2-3days.

Kinase assay buffer: 50mM Tris pH7.5, 100mM NaCl, 2mM $MgCl_2$, 2μCi [γ^{32}P]-ATP and 100μM cold ATP.

2.7.7 Co-immunoprecipitation from yeast cell lysate

For immunoprecipitation experiments logarithmically growing 50-60OD_{600} cells were harvested and washed once with 50mM HEPES-KOH pH7.6 before freezing at -80°C. The cell pellet was thawed and resuspended in 600µl of cold lysis buffer. Subsequently, 400µl of acid washed glass beads were added to the above mixture. The cells were lysed by means of glass bead beater for 2X 30sec rounds at top speed and 2min on ice after each round. The tubes were centrifuged for 5min at 13000rpm at 4°C. Approximately 400µl supernatant was collected and replaced with 400µl of lysis buffer and the tubes were beaten and followed by centrifugation again as mentioned above. The supernatants were pooled together and further cleared by centrifugation (5min at 13000rpm at 4°C). The clear supernatant was transferred to the affinity purification beads pre-equilibrated in lysis buffer. From cell lysate samples 45µl was taken before and after treatment with affinity beads as input and unbound material respectively. The tubes were incubated on a rotating wheel at 4°C for 2h and then washed three times with lysis buffer supplemented with 10% glycerol and no protease inhibitors. Then the beads were transferred to the fresh tube and washed once more before adding 100µl 1x protein loading dye. The samples were boiled at 95°C for 10min and analysed by western blot.

Lysis buffer: 50mM HEPES-KOH, pH 7.6, 150mM KCl, 100mM β-glycerol phosphate, 25mM NaF, 1mM EGTA, 1mM $MgCl_2$, 0.15% Tween-20, 1mM PMSF (or Protease inhibitor cocktail).

Wash buffer: 50mM HEPES-KOH, pH 7.6, 150mM KCl, 100mM β-glycerol phosphate, 25mM NaF, 1mM EGTA, 1mM $MgCl_2$, 0.15% Tween-20, 10% Glycerol.

2.8 Microscopy

Cell cultures were grown to log phase (OD_{600}~0.5-0.6) from overnight culture and visualised using an epifluorescence microscope. Live cells grown in minimal medium were imaged with an Axiovert 200M (Carl Zeiss MicroImaging, Inc.) microscope equipped with an Exfo X-cite 120 excitation light source, band pass filters (Carl Zeiss MicroImaging, Inc. and Chroma Technology Corp.), plan 63X/1.4 NA oil apochromat or an α plan-Fluar 100X/1.45 NA oil objective lens (Carl Zeiss MicroImaging, Inc.), and a digital camera (Orca ER; Hamamatsu). Image acquisition was performed using either Volocity software (Improvision) or ZEN (by Zeiss) software at room temperature. Fluorescence images were collected as 0.25 or 0.5µm z stacks, merged into one plane after contrast enhancing in Openlab, and further processed either in Adobe Photoshop or in ImageJ-win64. From the bright field images collected one image

where the cells are in focus was added into the blue channel in Adobe Photoshop. Further, this image was modified to highlight the circumference of the cell.

For time lapse imaging, a 2% agarose gel pad containing medium was prepared into a glass bottom 35mm μ-dish (Ibidi). The cells were grown logarithmically and 20μl culture was put under the gel pad and spread uniformly by gently pressing the gel pad from the top. The time lapse program was set using ZEN software for given number of cycles with 5-10min time interval between image acquisition.

2.9 Bioinformatics analysis

The Saccharomyces Genome Database (SGD) was used as main source for all DNA and protein sequences. Protein BLAST (http://blast.ncbi.nlm.nih.gov/Blast.cgi) search was performed using the gene sequences from *S. cerevisiae* as query to find out the most probable homologues. Multiple sequence alignment was performed by means of CLUSTALW-GenomeNet (https://www.genome.jp/tools-bin/clustalw) to identify conserved amino acid residues.

Chapter 3 A role for Pex27 in Vps1 dependent peroxisome fission

3.1 Introduction

In *S. cerevisiae*, peroxisomes are essential when cells are grown on oleate (fatty acid) as sole carbon source and are non-essential during growth on glucose containing medium (Kunau et al., 1995). During growth on glucose, peroxisome multiply by fission also called replicative multiplication. On oleate, peroxisomes proliferate and the membrane protein Pex11 plays an important role in this process (Erdmann and Blobel, 1995; Marshall et al., 1995). In mammals, Pex11 acts in concert with the dynamin-related protein (Drp), Dlp1 in peroxisome fission. Dlp1 is also required for fission of mitochondria (Li and Gould, 2003; Pitts et al., 1999). Also, in the methylotrophic yeast *H. polymorpha*, a single Drp, Dnm1, mediates fission of mitochondria and peroxisomes, with peroxisome fission also dependent upon Pex11 (Nagotu et al., 2008; Williams et al., 2015). However, in *S. cerevisiae*, two Drps, Dnm1 and Vps1 function in peroxisome fission. Dnm1 and Pex11 contribute to peroxisome fission during oleate induced peroxisome proliferation (Erdmann and Blobel, 1995; Kuravi et al., 2006; Marshall et al., 1995). However, Vps1 plays a major role in peroxisome replicative multiplication when cells are grown on glucose containing medium and proliferation in not induced **(Table 3.1)** (Hoepfner et al., 2001). Though overexpression of *DNM1* can compensate for a *VPS1* deficiency (Motley et al., 2008). Vps1 was originally found to be involved in transport between endosomes and the late Golgi but is also required for endocytosis (Smaczynska-de et al., 2010; Vater et al., 1992; Wilsbach and Payne, 1993). How Vps1 is recruited to the various sites of its function is poorly understood but for endocytosis the chronological order in which Vps1 appears at the endocytosis site is known and there it is implicated in membrane invagination step (Smaczynska-de et al., 2010).

In *S. cerevisiae*, Pex11, Pex25 and Pex27 constitute Pex11 family of peroxisomal membrane associated proteins. They have been implicated in peroxisome fission to regulate peroxisome abundance. Deficiency of a Pex11 family member leads to a reduced number of peroxisomes. Moreover, *pex11Δ*, *pex25Δ* cells (but not *pex27Δ*) cells show a growth defect when grown on oleate medium (Rottensteiner et al., 2003; Tam et al., 2003). In cells, peroxisome number is maintained by growth followed by fission of existing peroxisomes. The current model for peroxisome multiplication involves three successive events i) growth ii) elongation iii) constriction followed by fission **(Figure 3.1)** (Huber et al., 2012; Schrader et al., 2012). Pex11 recruits Fis1 and subsequently Dlp1, to the peroxisomal membrane fission site (Kobayashi et

al., 2007). Pex11 has been shown to interact *in vitro* as well as *in vivo* with Dlp1 in humans and with Dnm1 in *H. polymorpha* (Itoyama et al., 2013; Kobayashi et al., 2007; Williams et al., 2015). Though there is no evidence for interaction between *S. cerevisiae* Pex11 and Dnm1. Mechanistic details in recruitment of Vps1 to the peroxisomes are also unknown. Interestingly, *pex27Δ* cells show a significant reduction in number and increase in peroxisome size. Moreover, many of the peroxisomes are elongated (Tower et al., 2011). Thus, peroxisome number and morphology in *pex27Δ* cells resembles that of *vps1Δ* cells albeit not as severe **(Figure 3.2 A)**. However, *pex11Δ* cells show very small reduction in peroxisome number. In *pex25Δ* cells, peroxisome number and size vary from none or one giant to multiple small peroxisomes. In both, *pex11Δ* and *pex25Δ* cells, elongated peroxisomes are not observed (Smith et al., 2002; Tower et al., 2011) **(Figure 3.3)**. Moreover, the role of Pex27 in the maintenance of peroxisome number is not well characterised. Therefore, it was intriguing to know if Pex27 can play a role in Vps1 dependent peroxisome fission. Hence, the aim of this study was to investigate whether Pex27 functions in the Vps1-dependent pathway for peroxisome fission.

Table 3.1 The phenotype of deletion of *DRPs* and *PEX11* family genes in peroxisome replicative multiplication and proliferation.

Replicative multiplication	**Proliferation ***	**Genes**
+++	**−−**	*Sc-dnm1Δ* (Kuravi et al., 2006)
−−−	**−−−**	*Sc-vps1Δ* (Kuravi et al., 2006)
+++	**−−−**	*Sc-pex11Δ* (Tower et al., 2011)
−−	**−−**	*Sc-pex25Δ* (Tower et al., 2011)
−−−	**−−**	*Sc-pex27Δ* (Tower et al., 2011)
−−−	**−−−**	*Hp-dnm1Δ* (Nagotu et al., 2008)
+++	**+++**	*Hp-vps1Δ* (Nagotu et al., 2008)
−−−	**−−−**	*Hp-pex11Δ* (Nagotu et al., 2008)

Sc: *S. cerevisiae*; *Hp*: *H. polymorpha.* * In case of *H. polymorpha*, instead of oleate, methanol is used to induce peroxisome proliferation.

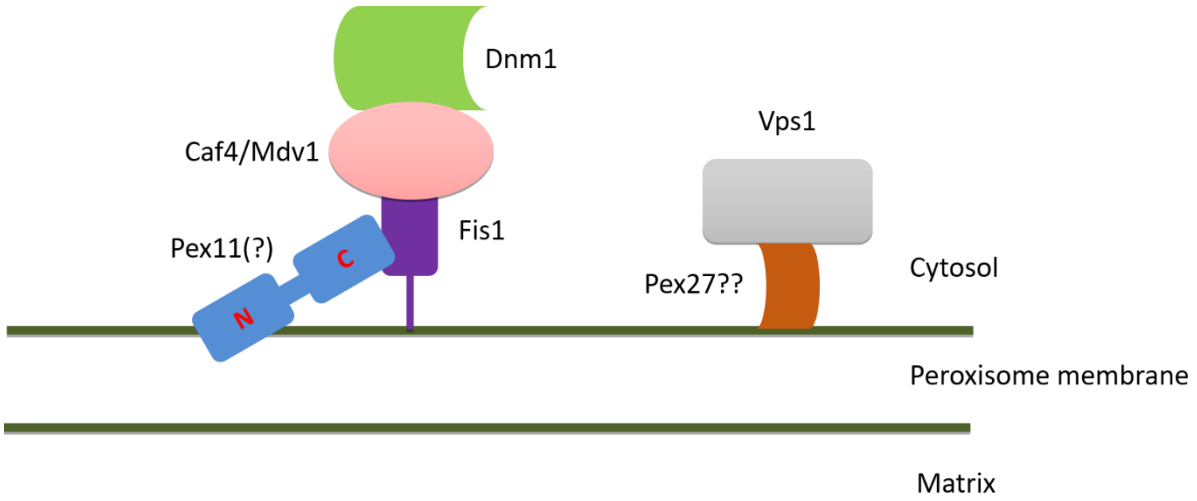

Figure 3.1 Proposed model for peroxisome fission in *S. cerevisiae*. Schematic diagram showing molecular players involved in Dnm1 and Vps1 dependent fission. Fis1 and Mdv1/Caf4 have been shown to be required for Dnm1 recruitment whereas Pex11 role is unclear but may facilitate membrane remodelling and regulate Dnm1 GTPase activity in analogy to HpPex11. The role of Pex27 is unclear but may contribute to Vps1 dependent fission.

3.2 *dnm1Δpex27Δ* and *dnm1Δvps1Δ* have similar peroxisome number and morphology

In *dnm1Δvps1Δ* cells peroxisomes do not divide hence in most cells one frequently elongated peroxisome is observed. These peroxisomes are maintained upon cell division through division during cytokinesis (see chapter 4). We hypothesized that Pex27 is involved in Vps1-dependent peroxisome fission. This hypothesis predicts that the phenotype in *pex27Δ* cells is stronger if Dnm1 dependent fission is blocked. To test this hypothesis peroxisome number and morphology in *dnm1Δpex27Δ* and *dnm1Δvps1Δ* cells were compared. Indeed, many *dnm1Δpex27Δ* cells have one elongated peroxisome positioned at the bud neck as typical to *dnm1Δvps1Δ* cells **(Figure 3.2 B)**. As expected, in *dnm1Δpex11Δ* cells multiple small peroxisomes were observed **(Figure 3.3)**. This suggests that it is Pex27 and not Pex11 is involved in Vps1 dependent peroxisome fission.

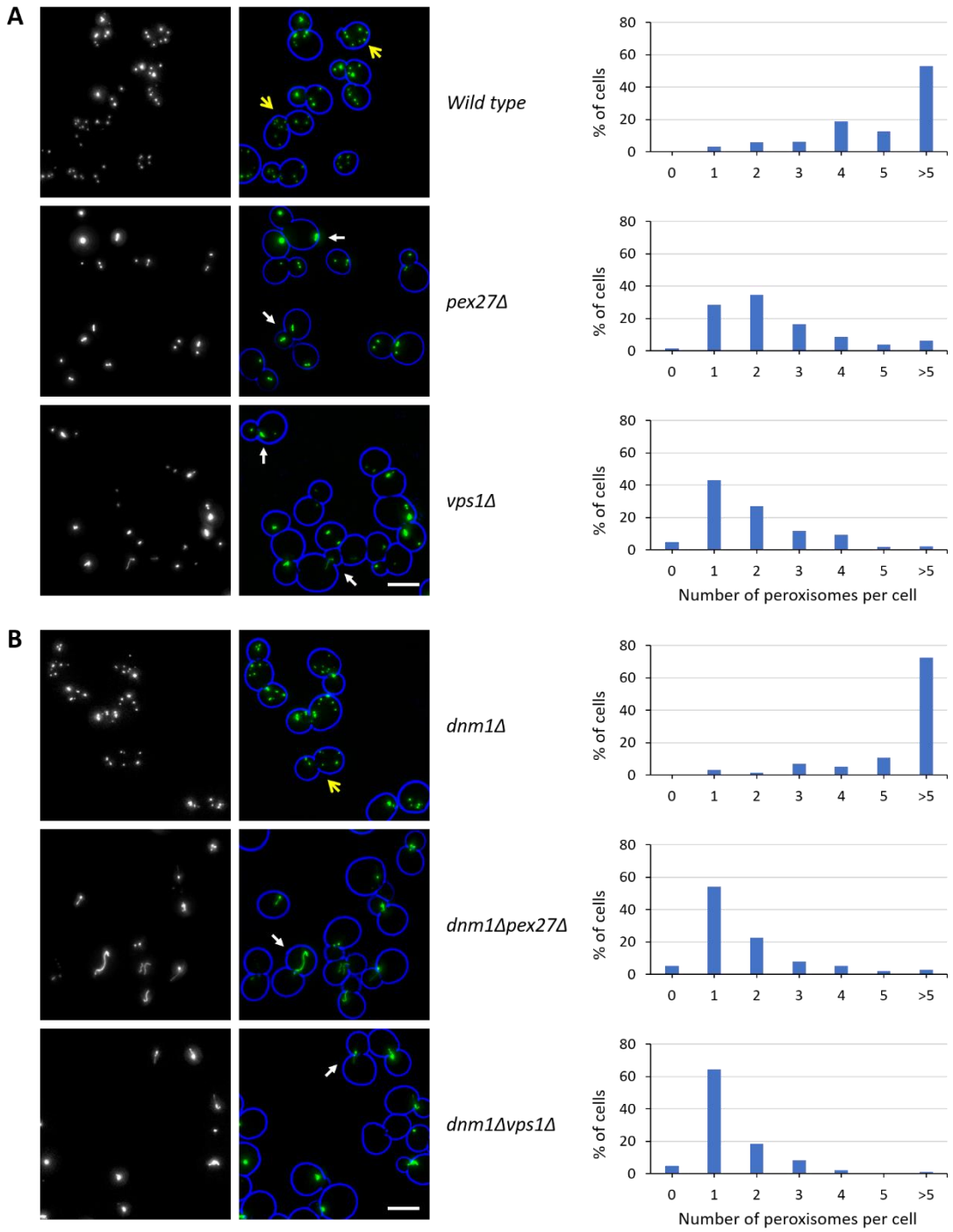

Figure 3.2 *dnm1Δpex27Δ* cells phenocopy *dnm1Δvps1Δ* cells. Cells expressing mNG-PTS1 were grown to log phase and imaged with an epifluorescence microscope. Fluorescence images were collected as 0.5µm stacks and the stacks assessed to be in focus were merged into one plane processed further in Adobe photoshop. Brightfield image from one plane was added to blue channel in photoshop and processed to highlight only the circumference of the cell. Deletion of *PEX27* and *VPS1* in wild type and *dnm1Δ* cells causes reduction in peroxisome number and increase in size. For quantification, a minimum of 130 cells were scored per strain. A yellow arrow indicates a cell with multiple small peroxisomes and a white solid arrow a cell with less and elongated peroxisomes. Scale bar is 5µm. All the subsequent microscopy images were processed in a similar manner unless stated otherwise in the figure legend.

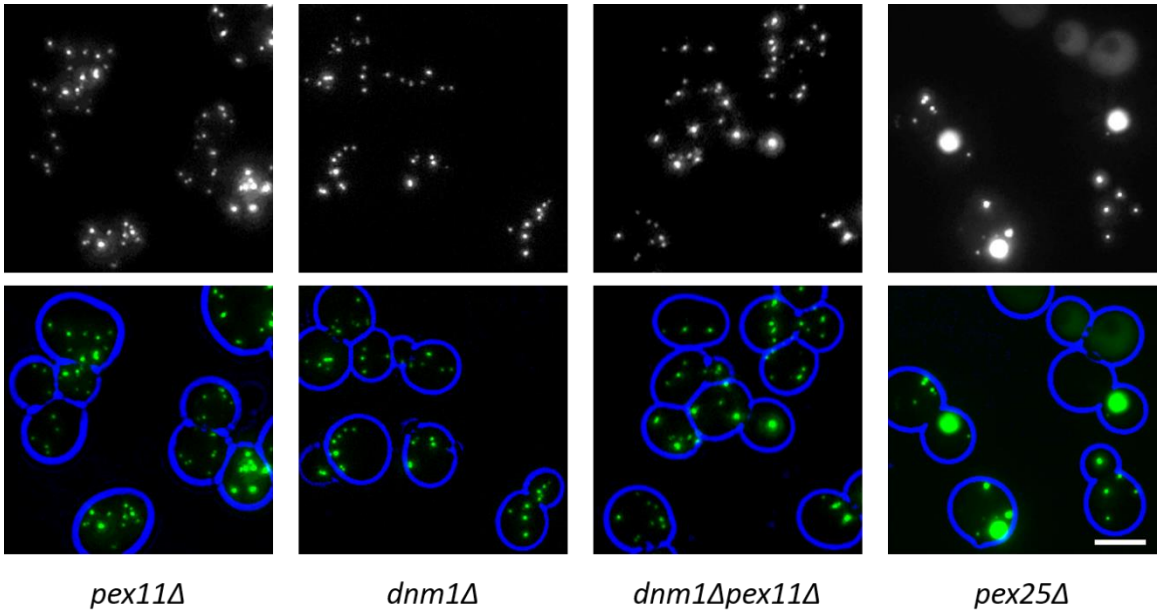

Figure 3.3 The phenotype of *pex11Δ* and *pex25Δ* cells does not resemble that of *vps1Δ* cells. mNG-PTS1 expressing *pex11Δ*, *dnm1Δ*, *dnm1Δpex11Δ* and *pex25Δ* cells were grown to log phase analysed by epifluorescence microscopy. Scale bar is 5µm.

3.3 Pex27 is required for peroxisome fission

Vps1 and Dnm1 are required for fission of existing peroxisomes (Motley and Hettema, 2007). To test whether Pex27 is required for fission a mating assay was performed that test the ability of Vps1 to divide peroxisomes. For this, *pex3Δ* (MatA) cells expressing HcRed-PTS1 were mated with *dnm1Δvps1Δ* (Matα) cells expressing mNG-PTS1. In *pex3Δ* cells peroxisomal matrix proteins are cytosolic and the most membrane proteins are not stable (Hettema et al., 2000), but Vps1 and Dnm1 are present. Most of the *dnm1Δvps1Δ* cells have one elongated peroxisome. Upon mating, Vps1 from the *pex3Δ* partner cell diffuses into the *dnm1Δvps1Δ* partner and rapidly induces the fission of the pre-existing peroxisome (Motley and Hettema, 2007). Mated cells have a typical morphology, moreover peroxisomes in these cells are labelled with both mNG and HcRed and thus are easily identifiable. In all mated cells multiple small peroxisomes were observed before the zygote was formed and this was Vps1 dependent **(Figure 3.4 A, B)**. In contrast, when *dnm1Δvps1Δ* cells lacking *PEX27* were used as mating partner, in mated cells peroxisome number was low and the peroxisomes were still elongated, even after the zygote was formed **(Figure 3.4 C)**. This result showed that Pex27 is required for rapid peroxisome fission.

A *dnm1Δvps1Δ* (mNG-PTS1) X *pex3Δ* (Red-PTS1)

B *dnm1Δvps1Δ* (mNG-PTS1) X *pex3Δvps1Δ* (Red-PTS1)*

C *dnm1Δvps1Δpex27Δ* (mNG-PTS1) X *pex3Δ* (Red-PTS1)

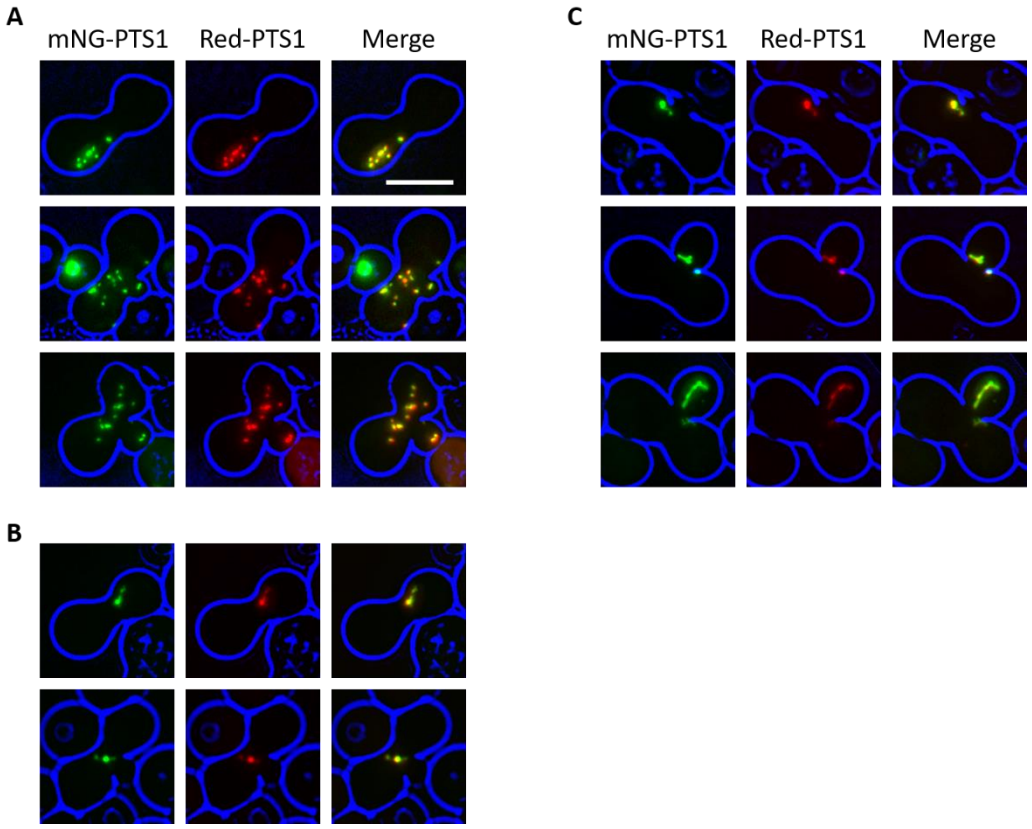

Figure 3.4 Pex27 is required for peroxisome fission. *dnm1Δvps1Δ* and *dnm1Δvps1Δpex27Δ* cells expressing mNG-PTS1 were mated with HcRed-PTS1 expressing *pex3Δ* cells. During mating, cytoplasmic mixing occurs after cell fusion and hence HcRed-PTS1 is imported into mNG-labelled peroxisomes, which in presence of Pex27 are divided into multiple small peroxisomes (A). The peroxisome fission is severely affected in *dnm1Δvps1Δ* cells lacking *PEX27* (B). Scale bar is 5µm. * In *pex3Δvps1Δ* cells, instead of HcRed-PTS1 mKate2-PTS1 was expressed to label peroxisomes.

3.4 Pex27 is required for Vps1 function in peroxisome multiplication

As Pex27 appears to contribute to peroxisome fission to a similar extent as Vps1, and independent to Dnm1, Vps1 and Pex27 may act in same pathway. To test this hypothesis, we tested whether Pex27 is required for Vps1 function specifically and not for Dnm1 dependent fission. First, *VPS1* and *DNM1* were overexpressed in cells lacking *PEX27*. Whereas, *DNM1* overexpression induces peroxisome fission, *VPS1* overexpression does not. A clearer effect is observed in *pex27Δ* cells where *DNM1* is also deleted **(Figure 3.5 A, B)**. On the other hand, *VPS1* overexpression does restore peroxisome number in a *vps1Δpex11Δ* cells to near wild type. Surprisingly, *DNM1* overexpression also rescued this mutant phenotype, suggesting that

Pex11 is not required for Dnm1 dependent fission upon overexpression of *DNM1* **(Figure 3.5 C)**. We conclude that Vps1 requires Pex27 to induce peroxisome fission. Neither Pex11 nor Pex27 are essential for Dnm1 dependent peroxisome fission.

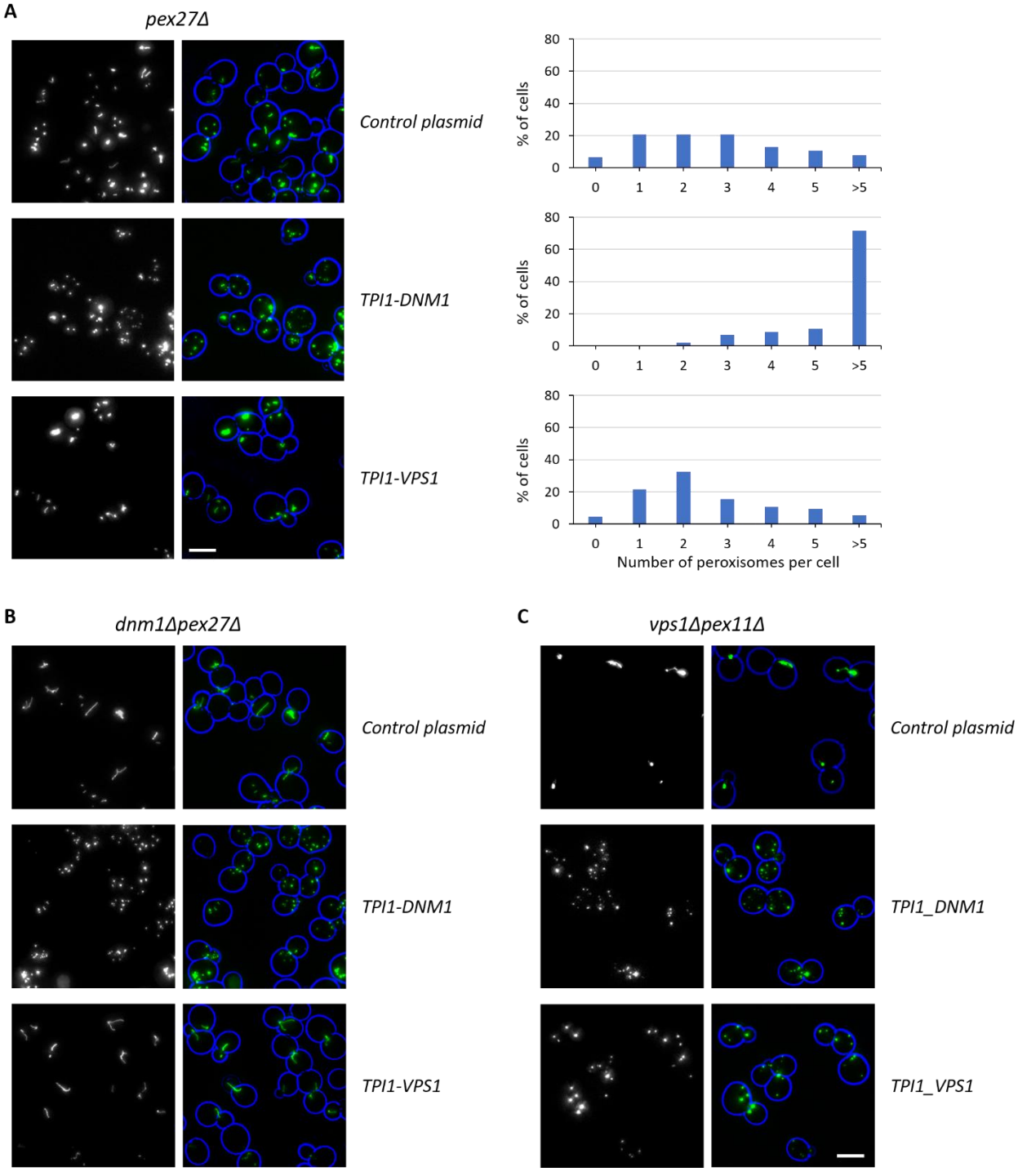

Figure 3.5 Pex27 is required for Vps1 dependent peroxisome fission. Dnm1 and Vps1 were constitutively expressed under control of the *TPI1* promoter along with mNG-PTS1 in *pex27Δ* (A), *dnm1Δpex27Δ* (B) and *vps1Δpex11Δ* (C) cells. Log phase cells were imaged with an epifluorescence microscope. Scale bar is 5µm. In (A) more than 125 cells were analysed per strain.

3.5 Vps1 is essential for Pex27 dependent peroxisome fission

To further characterise peroxisome fission, *PEX27* was overexpressed in *dnm1Δpex27Δ* cells and *vps1Δpex11Δ* cells. Here, overexpression of *PEX27* induced formation of lots of tiny peroxisomes in *dnm1Δpex27Δ* cells but not in *vps1Δpex11Δ* cells **(Figure 3.6)**. This suggests that Vps1 is essential for Pex27 function in peroxisome number maintenance. Furthermore, Pex27 cannot promote Dnm1 dependent fission. In addition, it was also observed that upon *PEX27* overexpression the matrix protein marker was slightly mis-localised to the cytosol in both *dnm1Δpex27Δ* and *vps1Δpex11Δ* cells. This could happen if excess of Pex27 directly affects matrix protein import or excessive fission decrease the efficiency of import. To test this *PEX27* was overexpressed into *dnm1Δvps1Δ* carrying Pex11-mNG and Red-PTS1 as membrane and matrix protein markers respectively. Again, Red-PTS1 was mis-localised to cytosol (arrows) whereas Pex11-mNG was still present in elongated peroxisomal structures as expected **(Figure 3.7)**. This result showed that Pex27 overexpression causes a defect in peroxisome matrix protein import by an unknown mechanism.

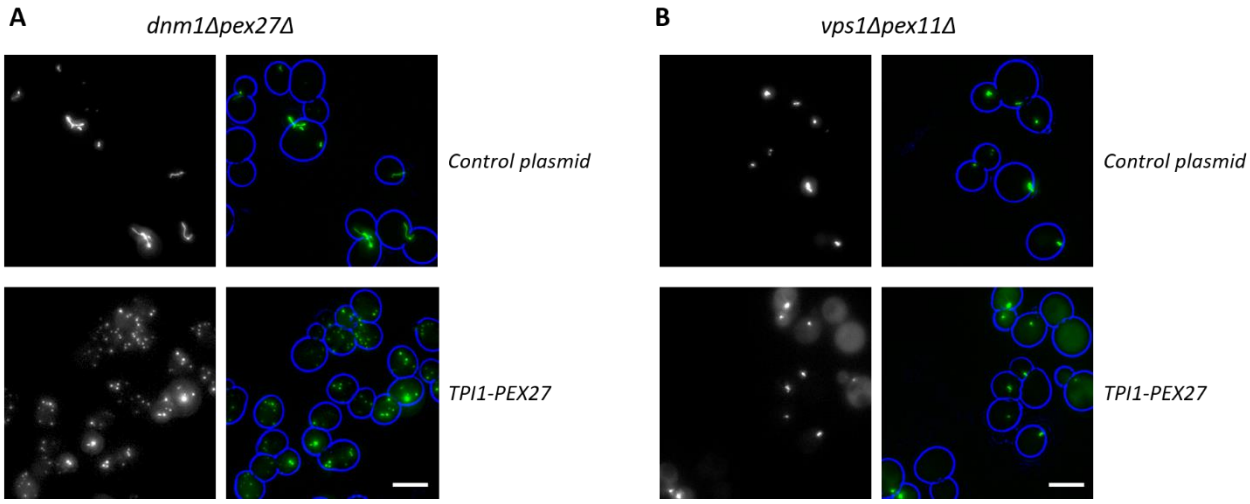

Figure 3.6 Pex27 requires Vps1 for its role in peroxisome multiplication. Untagged Pex27 was expressed constitutively under control of the *TPI1* promoter in (A) *dnm1Δpex27Δ* (B) *vps1Δpex11Δ* cells. Peroxisomes were visualised by expressing mNG-PTS1 marker. Scale bar is 5μm.

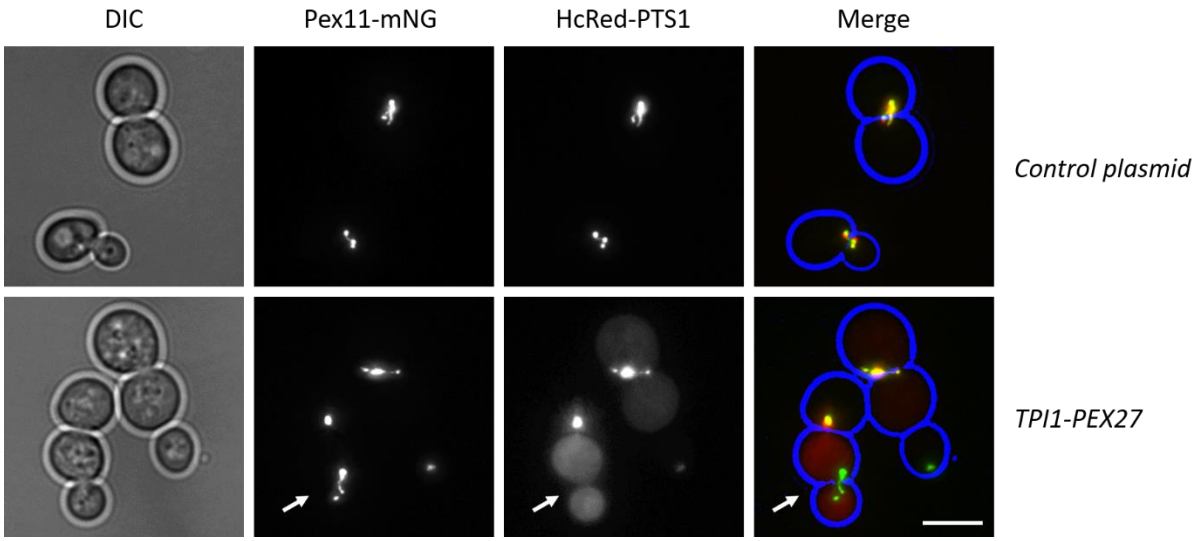

Figure 3.7 *PEX27* overexpression causes mis-localisation of matrix protein marker. *dnm1Δvps1Δ* cells expressing Pex11-mNG were transformed with HcRed-PTS1 marker along with either control plasmid or *TPI1-PEX27*. Cells were grown to log phase and imaged. Scale bar is 5µm.

3.6 Pex27-mNG localizes to the constricted sites in *dnm1Δvps1Δ*

In *vps1Δ* and *dnm1Δvps1Δ* cells peroxisome look like beads on a string that is the peroxisomal membrane is constricted at several sites but remains as one continuous elongated structure (Hoepfner et al., 2001; Knoblach and Rachubinski, 2015a; Kuravi et al., 2006). These constriction sites are potential fission sites. Similar morphology has been also reported for mitochondria in mammalian cells when siRNA mediated *DYN2* knock down was induced. Moreover, it was also proposed that mitochondrial tubules are initially constricted by ER and actin so that Drp1 can assemble on it. Drp1 further constricts the membrane to mediate Dyn2 assembly and Dyn2 induces the final fission step (Lee et al., 2016). Therefore, to analyse the role of Pex27 in Vps1 dependent peroxisome fission we decided to localize Pex27 in *vps1Δ* and *dnm1Δvps1Δ* cells. Hence, Pex27 and Pex11 were tagged independently in the genome with mNeonGreen (mNG) at the C-terminus by means of mNG-HIS3 integration cassette. The obtained strains were transformed with a plasmid directing the expression of HcRed-PTS1. The cells were grown to log phase and imaged by epifluorescence microscope. It was observed that Pex11-mNG co-localises with Red-PTS1 in both *vps1Δ* and *dnm1Δvps1Δ* cells. In contrast, although Pex27-mNG labelled the same structures as the peroxisomal marker, Pex27-mNG was seen in discrete punctate pattern that did not completely overlap with Red-PTS1 **(Figure 3.8)**.

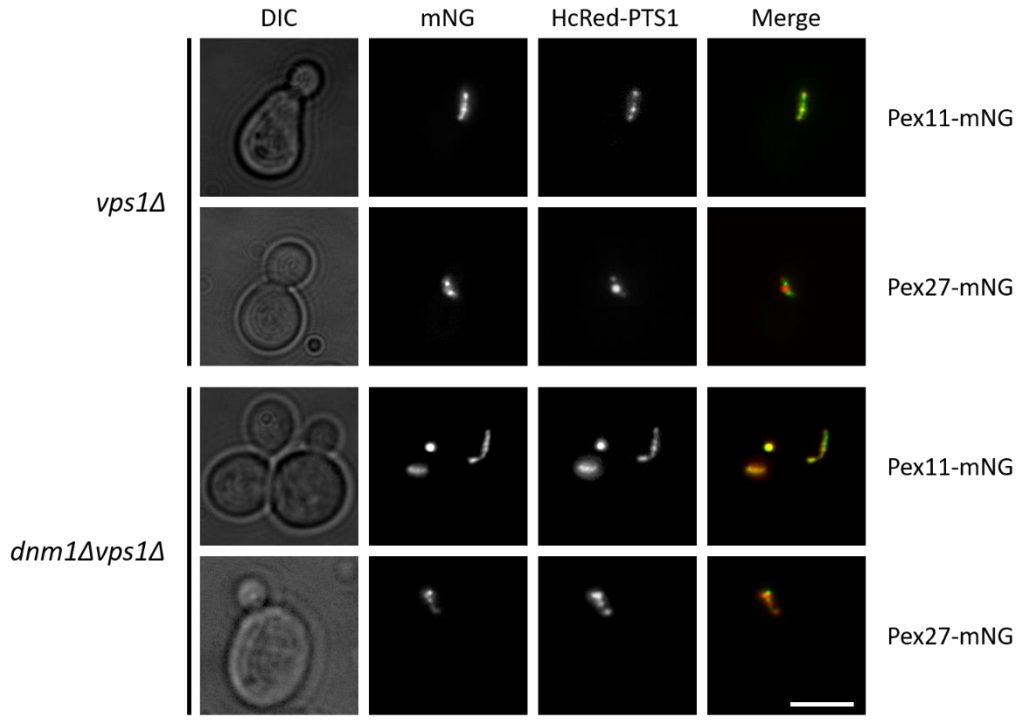

Figure 3.8 Pex11-mNG and Pex27-mNG localisation in *vps1Δ* and *dnm1Δvps1Δ* cells. *vps1Δ* and *dnm1Δvps1Δ* strains were genetically modified to express either Pex11-mNG or Pex27-mNG. The modified strains were transformed with HcRed-PTS1 marker. Cells were grown to log phase and imaged with an epifluorescence microscope. Scale bar is 5µm.

To determine a more detailed distribution of Pex27-mNG, super-resolution imaging is required. For this, we used Structured Illumination Microscopy (SIM) in *dnm1Δvps1Δ* cells. Interestingly Pex27-mNG and Red-PTS1 were clearly seen in a distinct punctate pattern but were juxtaposed and there was very minimal overlap between the signals. On the contrary, Pex11-mNG labelled the peroxisomal membrane evenly. Furthermore, in contrast to Pex27-mNG, Pex11-mNG did not seem to concentrate at construction sites **(Figure 3.9 A)**. This result lead us to hypothesize that Pex27 can act as a part of the Vps1 recruiting complex or constricts the membrane to a certain size so that Vps1 can act on it. We next asked whether the constriction sites are still present in *dnm1Δpex27Δ* peroxisomes. To address this question *dnm1Δpex27Δ* cells expressing Pex11-mNG were analysed. As expected an elongated peroxisome was observed in many cells and interestingly the constricted sites were also present **(Figure 3.9 B)**. In addition, it was not clear if there is difference in the size of peroxisome constrictions in *dnm1Δpex27Δ* and *dnm1Δvps1Δ* cells. Here, it can be concluded that Pex27-mNG is present at the constricted sites on the peroxisomes. These sites are potential fission sites where Dnm1 and Vps1 can act.

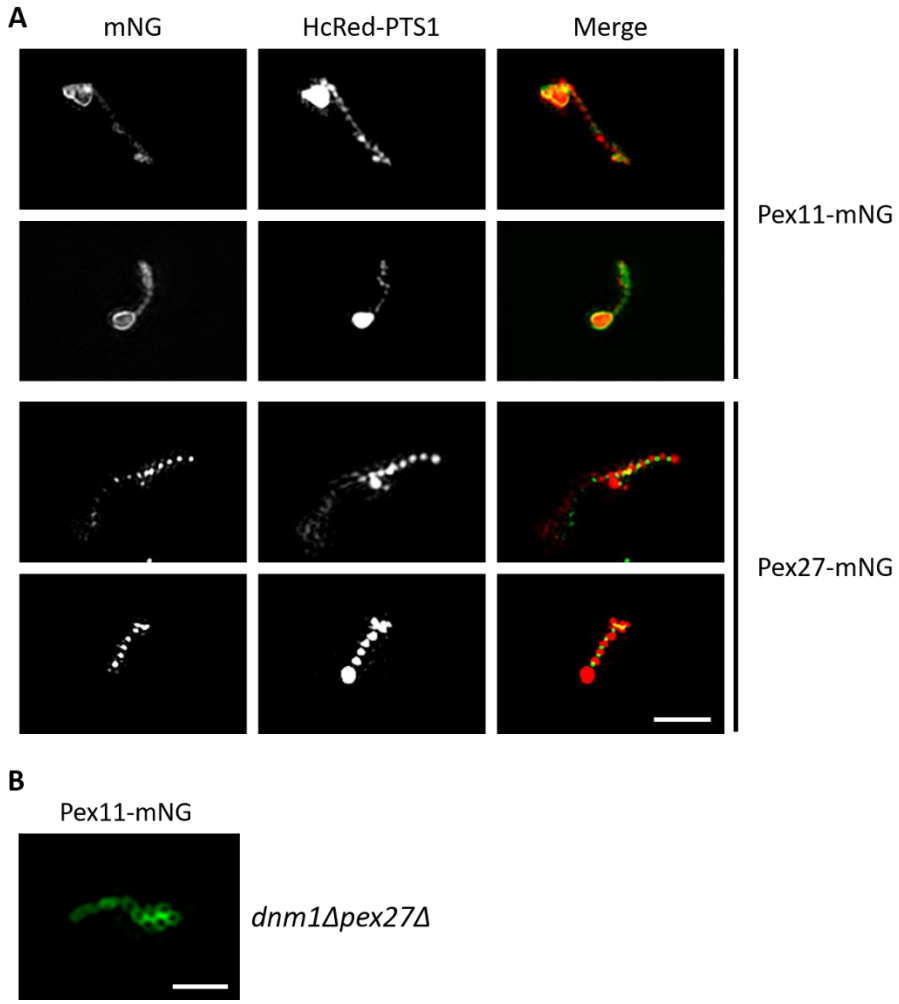

Figure 3.9 Pex27-mNG localises to the potential fission sites in *dnm1Δvps1Δ* cells. SIM microscopy was performed on log phase *dnm1Δvps1Δ* cells expressing either Pex11-mNG or Pex27-mNG. HcRed-PTS1 marker was expressed to label peroxisomal matrix (A). Scale bar is 2µm. (B) Peroxisome morphology was analysed in *dnm1Δpex27Δ* cells. Scale bar is 1µm.

3.7 Pex27 interacts with Vps1 *in vivo*

Vps1 controls peroxisome size and number and Pex27 mediates this function in peroxisome maintenance. We next asked if Pex27 can interact with Vps1 *in vivo*. Vps1-GFP and GFP-PTS1 were expressed in a C-terminally TAP tagged Pex27 strain. Immuno-precipitation (IP) was performed using GFP-nanobody beads (GFP-Trap, Chromo Tek). Pex27-TAP was more concentrated in the Vps1-GFP pulldown than in GFP-PTS1 and control pull downs. Moreover, Vps1-GFP did not specifically bind to another TAP tagged PMP, Pex22 **(Figure 3.10)**. We conclude that Pex27 interacts with Vps1 *in vivo*. As expected, endogenous Vps1 also co-immunoprecipitated with Vps1-GFP **(Figure 3.10)**.

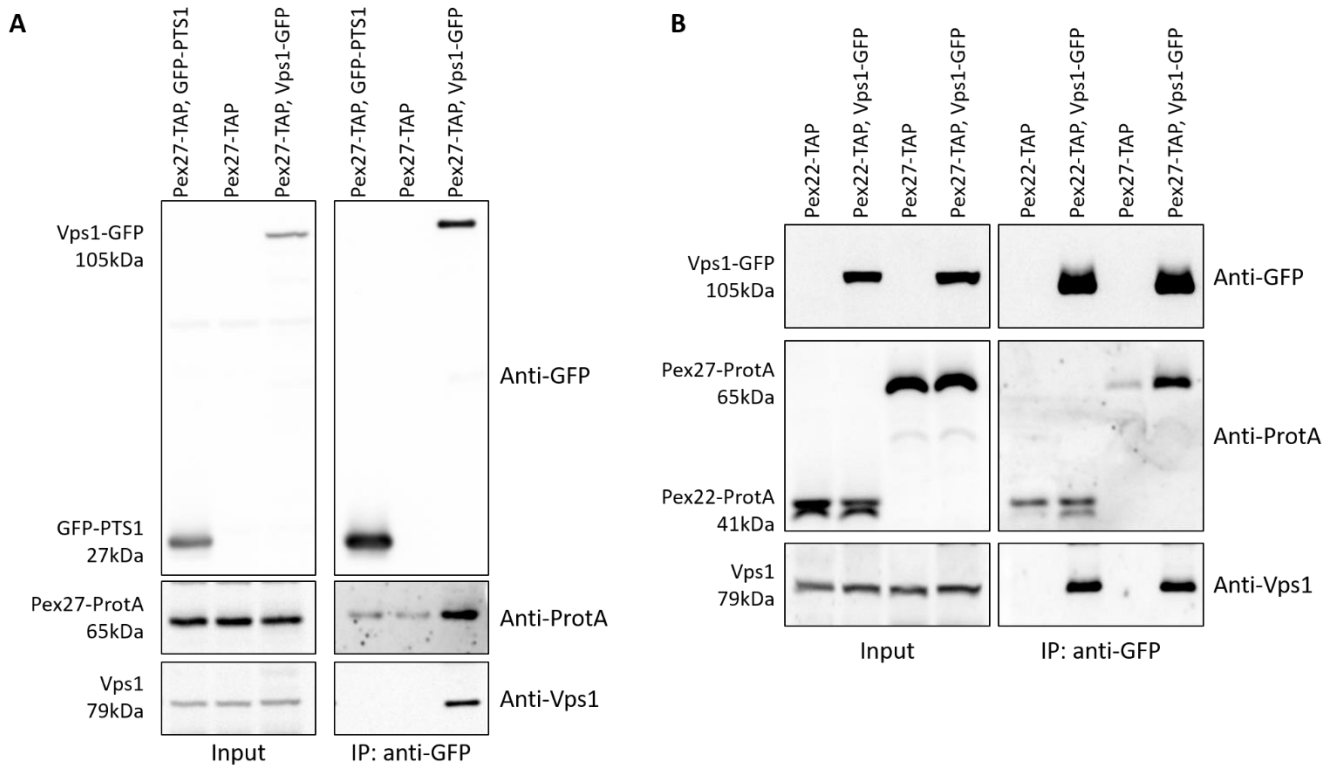

Figure 3.10 Co-immunoprecipitation (Co-IP) for Pex27 and Vps1 interaction. Vps1-GFP was immunoprecipitated using GFP-nanobody beads and the IP samples were analysed by immunoblotting using antibodies against GFP, TAP and Vps1. (A) Pex27-TAP preferentially interacts with Vps1-GFP over GFP-PTS1. (B) Vps1 interacts with Pex27-TAP more efficiently than with Pex22-TAP. Vps1-GFP interacts with endogenous Vps1 (Input:Co-IP::1:12.5). The Co-IP anti-ProtA blots were exposed longer than the Input blots.

3.8 Discussion

Peroxisome duplication involves three crucial steps including 1) peroxisomal growth, 2) elongation and constriction followed by 3) fission. Pex11 family proteins are implicated in peroxisome elongation followed by recruitment of dynamin GTPases, Dnm1 (Huber et al., 2012; Schrader et al., 2012). The peroxisome phenotype of *pex27Δ* strongly resembles that of *vps1Δ* (Hoepfner et al., 2001; Tower et al., 2011). We showed that Pex27 and Vps1 act in the same genetic pathway and Pex27 is required for Vps1 dependent peroxisome fission. Moreover, Pex11 is not essential for Vps1 function. Furthermore, the presence of Pex11 and Pex25 is not sufficient to induce peroxisome fission in *dnm1Δpex27Δ* cells upon *VPS1* overexpression. In addition, neither Pex11 nor Pex27 are essential for Dnm1 dependent peroxisome multiplication. Moreover, *PEX27* overexpression did not promote Dnm1 activity in *vps1Δpex11Δ* cells also suggesting Vps1 is essential for Pex27 function in peroxisome number maintenance. The localisation studies revealed that Pex27 is concentrated in a

subdomain of peroxisomes. These domains are the narrow constrictions between bulbous parts of peroxisomes in *vps1Δ* and *dnm1Δvps1Δ* cells and these are potential fission sites. In contrast Pex11 labels the whole peroxisomal membrane. Moreover, peroxisomes undergo constriction even in *dnm1Δpex27Δ* cells. Furthermore, *in vivo* binding assay showed that Pex27 interacts with Vps1. Here, we conclude that Pex27 is required for Vps1 but not Dnm1 dependent peroxisome fission. We propose that Pex27 is either a recruitment factor for Vps1 at the peroxisome membrane fission sites or a regulator of Vps1 activator at these sites **(Figure 3.12)**.

Surprisingly, Pex11 upon overexpression causes formation of multiple small peroxisomes in both *dnm1Δpex27Δ* and *vps1Δpex11Δ* but the elongated structures are concomitantly present in many cells. This is possible if either Pex11 can recruit both the Dnm1 and Vps1 but inefficiently or overexpression of Pex11 induces *de novo* peroxisome formation or excessive elongated intermediate formation. To test this Pex11 was overexpressed in *dnm1Δvps1Δ* cells. Surprisingly, in *dnm1Δvps1Δ* cells as similar phenotype was observed **(Figure 3.11)**. Hence, this indicates that this phenotype is not necessarily associated with Dnm1 and Vps1 dependent fission process. However, Pex27 overexpression does not give rise to multiple peroxisomes in the absence of Dnm1 and Vps1.

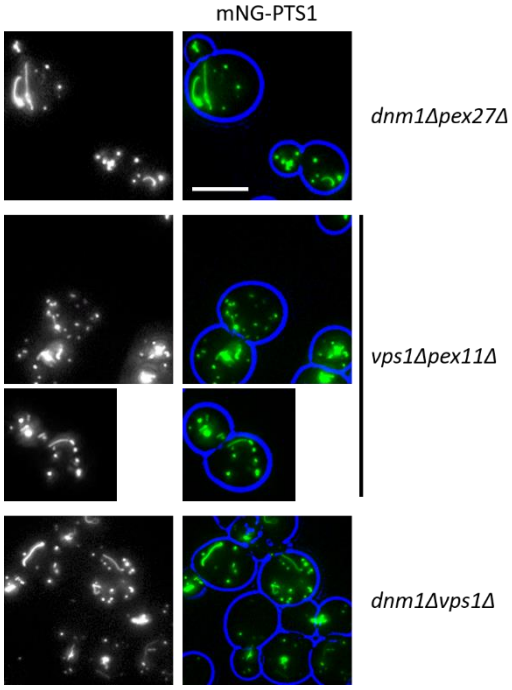

Figure 3.11 Overexpression of *PEX11* leads to formation of multiple peroxisomes. *PEX11* was expressed constitutively under control of the *TPI1* promoter in (A) *dnm1Δpex27Δ* (B) *vps1Δpex11Δ* and (C) *dnm1Δvps1Δ* cells. Peroxisomes were visualised by expressing mNG-PTS1 marker. Scale bar is 5μm.

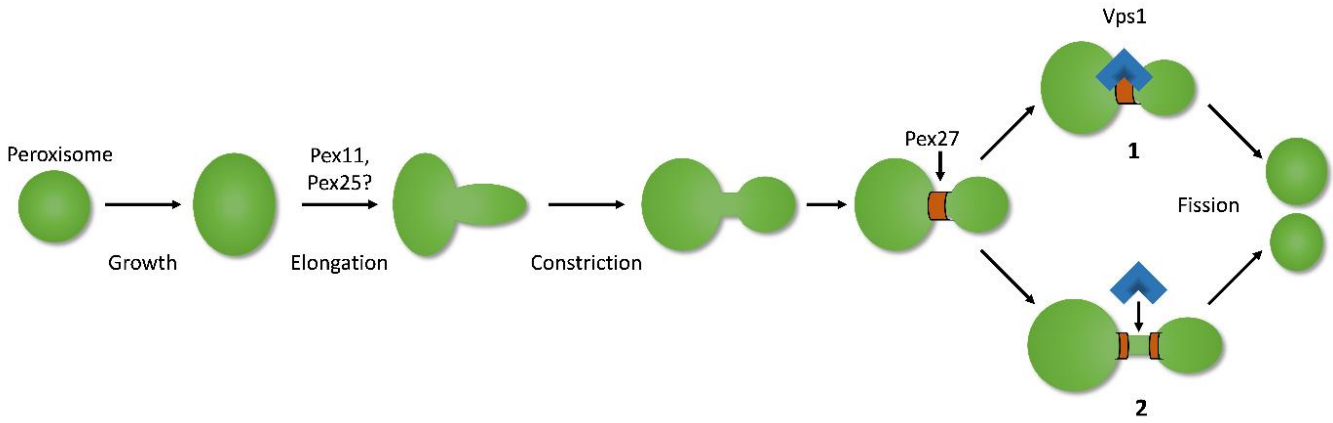

Figure 3.12 Model showing Pex27 involvement in peroxisome fission process. Pex27 is localised to the fission site and interacts with Vps1. Here, it can either directly recruit or regulate Vps1 activity (1) or can modulate membrane further so that Vps1 can act on it (2).

Vps1 plays vital role in peroxisome fission but the dynamics of Vps1 recruitment and activity at the peroxisomal membrane have been elusive. One of the reasons is that peroxisomes divide once per cell cycle (once per ~2h). Moreover, the average number of peroxisomes per cell when grown on medium containing glucose is 8-10 (Tower et al., 2011). Thus, the number of events is very low to capture Vps1 on peroxisomes. However, Vps1 is observed at the plasma membrane during endocytosis. Vps1 has been implicated to maintain Rvs167 at the endocytic membrane. Here, Rvs167 is an amphiphysin protein required for vesicle scission during endocytosis. The lifetime of Vps1 at the cell cortex is around 8.7sec and the order of events during endocytosis is well characterised (Smaczynska-de et al., 2010). Because of this, one can predict where Vps1 will next appear at the cortex. This makes it possible to capture Vps1 at the site of endocytosis. In analogy, Vps1 may be recruited to the peroxisomal fission sites for only a few seconds explaining the difficulty of showing Vps1 associated with peroxisomes. Taken together, it is intriguing to identify mutants (in Pex27 or otherwise) that will affect not only Vps1 function in peroxisome multiplication but will also help to localise Vps1 to the peroxisomal membrane. This well further help to understand in detail the cascade of events involved in peroxisome fission.

Chapter 4 Identification of novel factors required for peroxisome maintenance in yeast

4.1 Introduction

In dividing yeast cells, peroxisomes multiply by growth and division before they segregate with high fidelity between mother and daughter cell. The balance between transport to the bud and retention in the mother determines equal segregation (Hoepfner et al., 2001). Retention is mediated via the peroxisomal membrane associated protein Inp1. The peroxisomal membrane protein, Inp2, recruits the classV unconventional myosin Myo2 to facilitate transport of peroxisomes along actin cables to the bud (Fagarasanu et al., 2006; Fagarasanu et al., 2005; Hoepfner et al., 2001). The DRPs Vps1 and Dnm1 mediate peroxisome fission in *S. cerevisiae*. Hence, in *dnm1Δvps1Δ* cells one enlarged and elongated peroxisome is observed frequently anchored via Inp1 on the mother side of the bud neck and pulled into the bud by Inp2/Myo2 (Hoepfner et al., 2001; Knoblach and Rachubinski, 2015a; Kuravi et al., 2006). Around the time of cytokinesis this elongated peroxisome is split in two and both mother and daughter cell obtain part of this peroxisome. Indeed, when the actin-myosin ring (AMR) is labelled with Myo1-GFP in *dnm1Δvps1Δ* cells, we observed that the peroxisomal structure (labelled with Pex11-mRuby2), is divided within 1-2min after disappearance of the AMR **(Figure 4.1)**. However, segregation via this process is not as efficient as in wild type cells and a low percentage of cells fail to either inherit or retain a peroxisome. Cells that do not inherit or retain peroxisomes form multiple small peroxisomes *de novo* (Motley and Hettema, 2007). In *dnm1Δvps1Δ* cells, these small peroxisomes grow with time and reduce in number with every cell division as they are distributed between mother and daughter (Motley et al., 2015). How peroxisome segregation is regulated and how cells decide when to grow peroxisomes or form them *de novo* is unclear.

The **aim** of this chapter was to identify novel factors that either

1) influence peroxisome segregation or
2) affect whether cells multiply peroxisomes by growth and division or *de novo* formation.

Since *dnm1Δvps1Δ* cells inherently show a weak peroxisome inheritance defect we used this genetic background to identify factors that modulate peroxisome segregation. Since *de novo* formation can be easily detected in this strain by the presence of multiple small peroxisomes instead of a single large peroxisome, the same screen will identify factors that modulate *de novo* formation. We used an automated platform to generate a genome-wide mutant library.

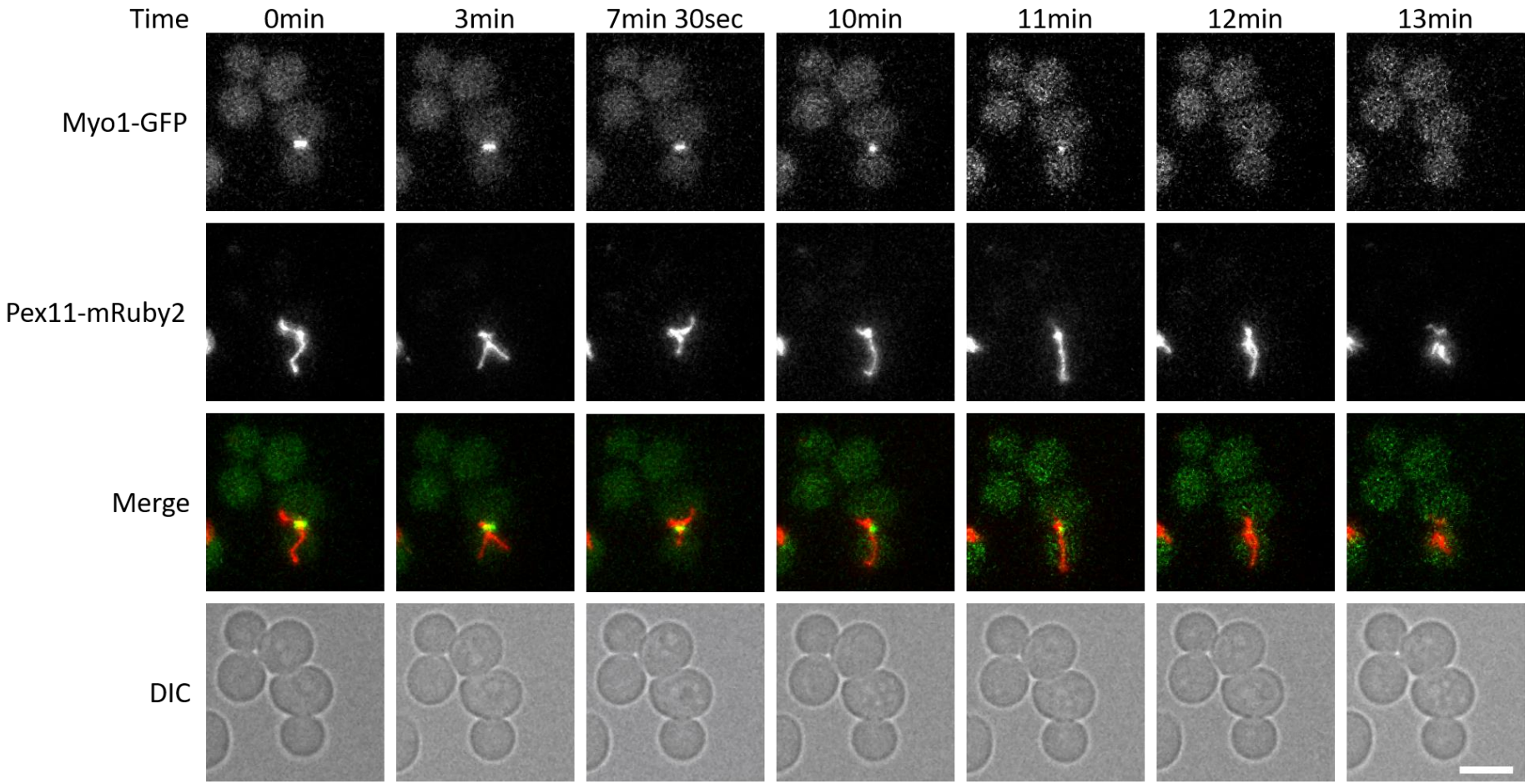

Figure 4.1 Peroxisomes divide during cytokinesis in *dnm1Δvps1Δ* cells. Time lapse images were taken of cell expressing Myo1-GFP and Pex11-mRuby2. Myo1-GFP is localised to the mother bud neck and is a cytokinetic ring contraction marker. Scale bar is 5μm.

This library was screened by microscopy image analysis for peroxisome number per cell and morphology.

Systematic genetic screens are vital tools to address fundamental questions in biology. These screens have pioneered many cellular pathways and have discerned functions of myriad of genes. In *S. cerevisiae*, for many of the screens several yeast libraries are made. Synthetic Genetic Array (SGA) methodology has been an efficient technique to make these libraries(Cohen and Schuldiner, 2011; Tong et al., 2001). SGA based screens are not limited to the budding yeast only but have been developed for the fission yeast *Schizosaccharomyces pombe* and in the bacteria as well (*E. coli*) (Butland et al., 2008; Roguev et al., 2007; Tong et al., 2001; Typas et al., 2008). To create a library using SGA, a haploid query strain carrying an appropriate genetic modification is constructed and crossed with one of the available yeast haploid mutant libraries. Then the diploids are selected before they are induced to go through meiosis and form haploid spores. Then the haploid cells with desired genetic modifications are selected. This new library of mutants can be used for screening. By means of the SWAp-Tag (SWAT) method one precursor library can be further modified to generate multiple new libraries (Yofe et al., 2016).

4.2 High content microscopy screen and analysis

Using SGA methodology, the *dnm1Δvps1Δ* strain expressing cytosolic mCherry and the peroxisomal marker mNG-PTS1 was crossed with the single gene deletion and DAmP libraries (Breslow et al., 2008; Giaever et al., 2002) to obtain the triple gene mutant library. The mutant strains were grown to log phase in selective minimal media in 384 well plates and were imaged using an automated fluorescence microscopy set up (Cohen and Schuldiner, 2011). For each sample, images were taken from three different fields in the well. I generated the library and performed the automated microscopy screening in the laboratory of Maya Schuldiner (Weizmann Institute of Science, Rehovot, Israel) **(Figure 4.2)**.

Before carrying out a detailed analysis of the data, it was crucial to confirm that the mutant library was constructed properly. The antibiotic based haploid selection during the SGA procedure is such a that there should be no growth on the plate in the positions of *dnm1Δ* and *vps1Δ* strains. Indeed, there was no colony growth at those positions. Furthermore, the peroxisome matrix protein import machinery mutants were tested and, as expected, cytosolic labelling of the mNG-PTS1 marker was observed in these mutants **(Figure 4.3)**. Subsequently, images of each generated strain (~18000 in total) were visually inspected. The qualitative data

was subsequently analysed according to four different criteria; i) the number of peroxisomes, ii) mNG-PTS1 marker import, iii) positioning of the peroxisome in the cell and iv) morphology.

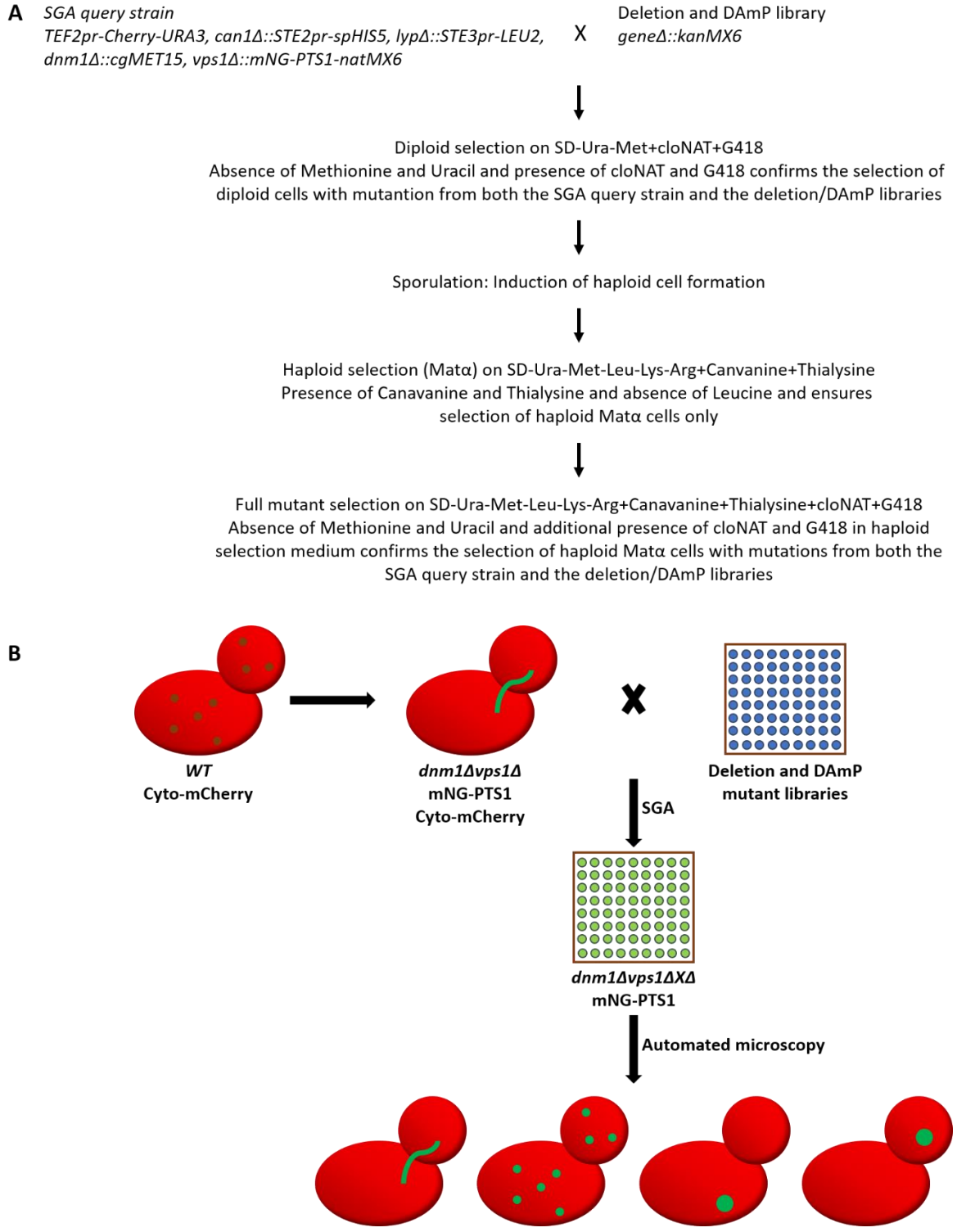

Figure 4.2 Schematic representation of the SGA screen. (A) The query strain was crossed with single gene deletion and DAmP libraries to generate triple mutant library using SGA methodology. (B) The mutants were further imaged and analysed for different phenotypes. The steps in the SGA screen are elaborated in Chapter 2, **Figure 2.3**.

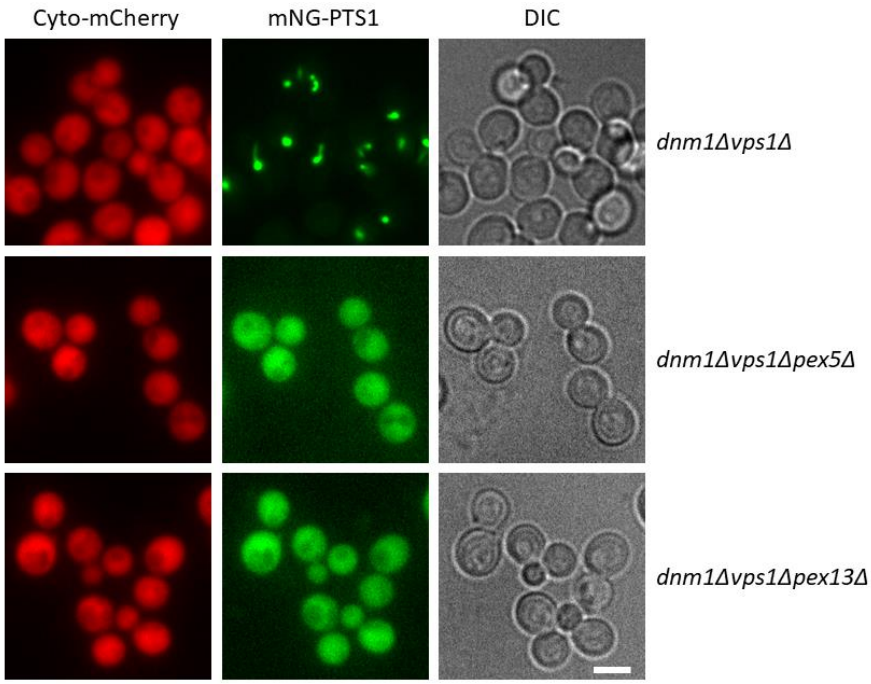

Figure 4.3 Primary check before analysing the complete library. Triple mutants generated by SGA defective in matrix protein import were tested to validate the mutant library construction. Scale bar is 5μm.

4.3 Identification of novel factors involved in peroxisome maintenance

The SGA screen analysis revealed 154 mutants with phenotypes that were aberrant in one or more of the 4 criteria mentioned above. There were 130 mutants that displayed multiple peroxisomes. Surprisingly many of these were chromosome segregation mutants. Hence there was a possibility of mis-segregation of the *VPS1* gene at meiosis (sporulation) step during mutant library construction. Therefore, to identify false positives, mutants containing multiple peroxisomes were tested for the presence of Vps1 by immunoblotting. Indeed, in most of the strains, Vps1 was expressed. The eight mutants that contain multiple peroxisomes per cell and did not express Vps1 are tabulated in **(Table 4.1)**. These mutants all contained a *DNM1* gene deletion as confirmed by PCR **(Figure 4.4)**. Seventeen mutants mis-localised mNG-PTS1 to the cytosol. Out of these 17, 15 are well established peroxisome biogenesis (*pex*) mutants. The remaining two, *YJL211C* and *YGL152C* are dubious open reading frames that partially overlap with *PEX2* and *PEX14*, respectively. This further corroborated the assumption that these are not genuine hits. Finally, there were eight mutants in which some cells in the population lacked peroxisomes. A variable number of peroxisomes per cell is generally observed in mutants that are defective in peroxisome inheritance such as in *inp1Δ* and *inp2Δ* cells. *PEX25* and *PEX27*, previously reported genes that are required for peroxisome maintenance, were also part of this list **(Table 4.2)**.

Table 4.1 The list of genes that affect peroxisome number.

ORF	Gene name	Gene Description
YDR102C	-	Uncharacterised
YAR014C	***BUD14***	BUD site selection
YKL075C	-	Uncharacterised
YOR193W	***PEX27***	PEroXisome related
YCR045C	***RRT12***	Regulator of rDNA Transcription
YCL026C-B	***HBN1***	Homologous to Bacterial Nitroreductases
YER116C	***SLX8***	Synthetic Lethal of unknown (X) function
*YJL077W-B**	-	Uncharacterised

* Does not give reproducible phenotype

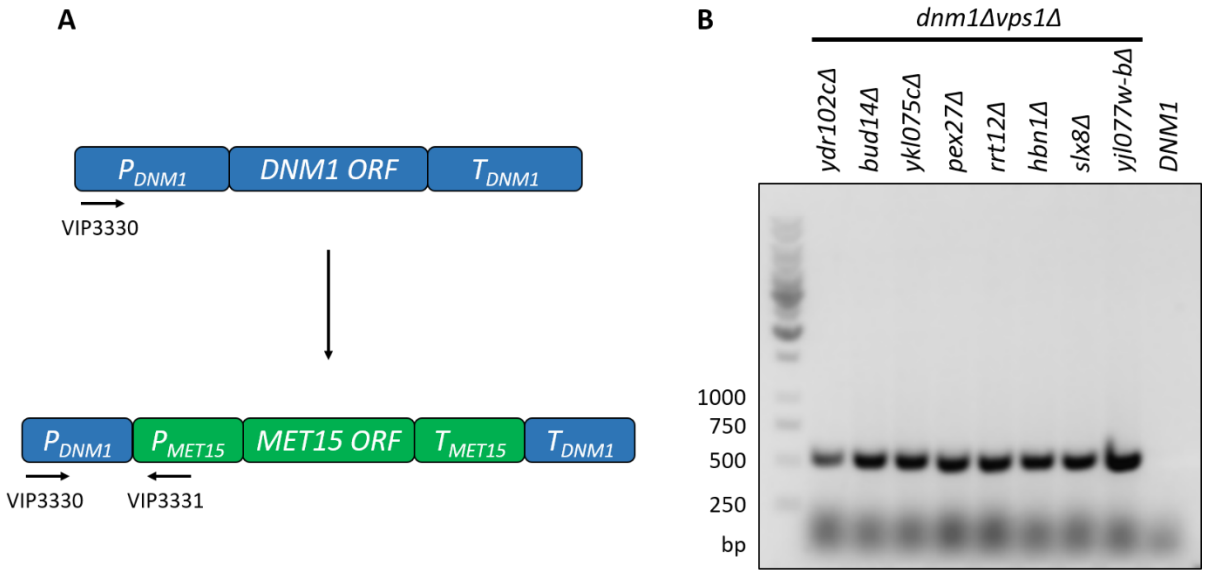

Figure 4.4 *DNM1* deletion check PCR. (A) *DNM1* gene deletion was carried out using *MET15* cassette. (B) The strains with multiple peroxisomes were tested by PCR using VIP3330 and VIP3331 primers to confirm *DNM1* gene deletion. Expected PCR band size is ~570bp. P_X and T_X indicate promoter and terminator of gene X.

All the potential segregation mutants were grown to log phase and analysed again by microscopy to confirm the phenotypes. Of these eight only *KIN4* along with the four genes mentioned above showed a robust phenotype when deleted in the *dnm1Δvps1Δ* genetic background as had been observed in the genome wide screen data analysis. *INP1* and *INP2* are well described genes for their role in peroxisome retention in the mother and transport to the bud, respectively. *dnm1Δvps1Δpex25Δ* cell populations showed a mixed phenotype, with cells showing a defect in segregation and others in matrix protein import. This phenotype was also

observed when *PEX25* was first identified and not much has been reported since then about its functional role. Most of the *dnmΔvpsΔpex27Δ* cells contained either one elongated peroxisome as seen in *dnm1Δvps1Δ* or multiple small ones. *PEX27* is one of the least characterised *PEX* genes. Pex27 is partial redundant with Pex11 and Pex25 and hence complicates the analysis and interpretation of the phenotype of *dnmΔvpsΔpex27Δ* cells. In an independent study, Pex27 has been found to be required for Vps1 dependent peroxisome fission (Chapter 3). Thus, Pex27 is a multifunctional protein and has been studied separately to characterise its role in peroxisome maintenance. *dnm1Δvps1Δkin4Δ* cells showed a consistent phenotype where the distribution between mother and daughter cell is affected with more peroxisomes present in the mother than in the bud as observed in *dnm1Δvps1Δinp2Δ* cells. Frequently large buds were observed that lacked a peroxisome and the number of elongated peroxisomes traversing the bud neck was strongly reduced **(Figure 4.5, Figure 4.7)**. Quantitative analysis showed that in *dnm1Δvps1Δkin4Δ* cells, the variation in peroxisome number is larger than in *dnm1Δvps1Δ* cells and is comparable to that observed in *dnm1Δvps1Δinp1Δ* and *dnm1Δvps1Δinp2Δ* cells **(Figure 4.6)**. These results suggest a role for Kin4 in peroxisome distribution. Kin4 is an established spindle position checkpoint (SPoC) kinase. An accurate spindle alignment is a prerequisite for faithful nuclear inheritance during mitosis. There are not many protein kinases reported to be involved in peroxisome maintenance. In fact, *KIN4* itself has not been previously reported to be involved in either peroxisome or another organelle distribution. The robust peroxisome distribution phenotype and its direct involvement in spindle pole body segregation makes *KIN4* an interesting candidate to explore further.

Table 4.2 The list of genes that affect peroxisome inheritance.

ORF	Gene name	Gene Description
YHR028C	***DAP2***	Dipeptidyl AminoPeptidase
YMR163C	***INP2***	INheritance of Peroxisomes
YMR204C	***INP1***	INheritance of Peroxisomes
YNL064C	***YDJ1***	Yeast dnaJ
YNL307C	***MCK1***	Meiosis and Centromere regulatory Kinase
YOR193W	***PEX27****	PEroXisome related
YOR233W	***KIN4***	KINase
YPL112C	***PEX25***	PEroXisome related

* *PEX27* is also a part of the list of genes that affected peroxisome number **(Table 4.1)**.

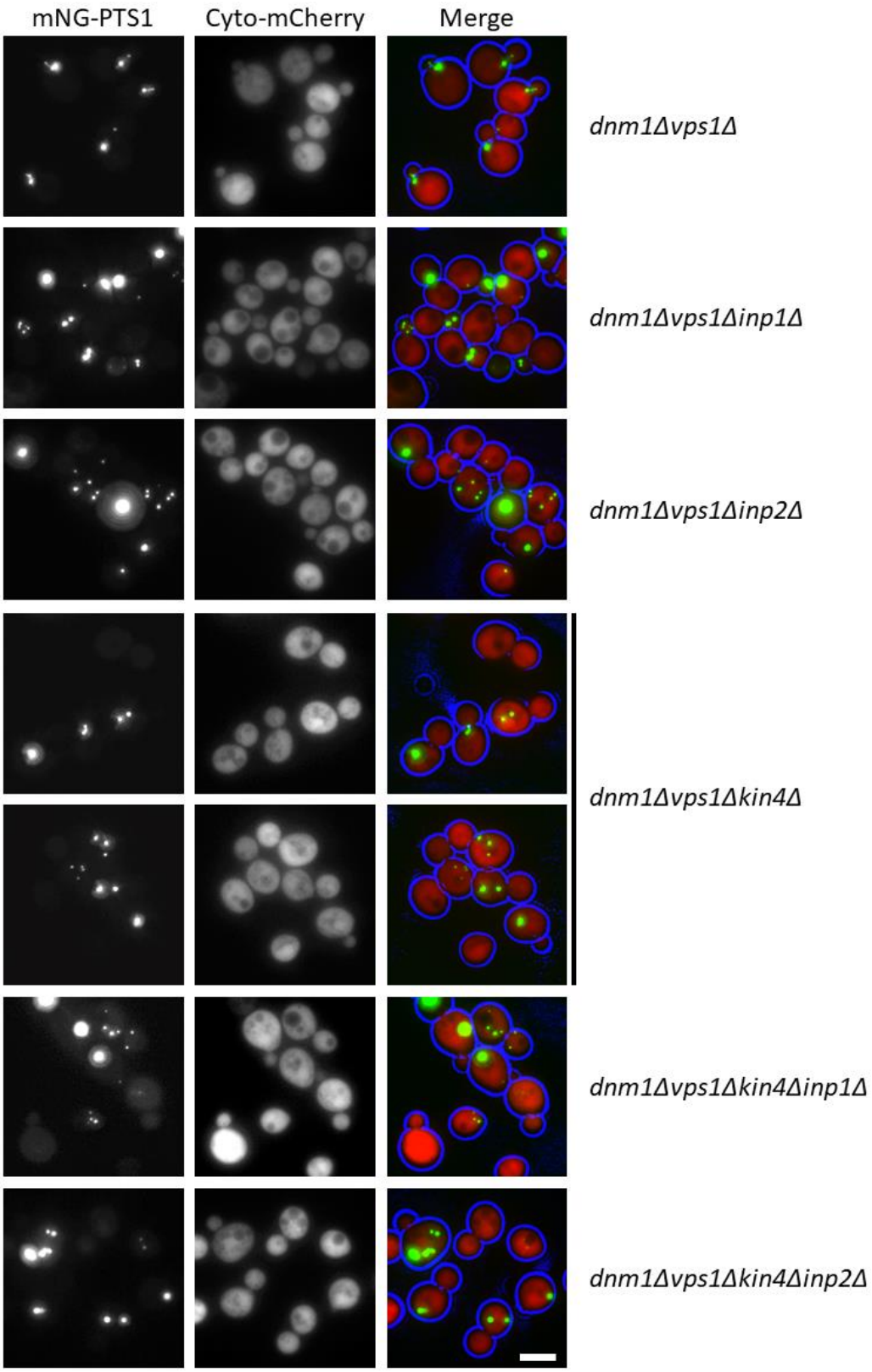

Figure 4.5 Kin4 contributes to the peroxisome transport to the bud. Peroxisome transport is defective in *dnm1Δvps1Δkin4Δ* cells and this is confirmed by additional deletion of *INP1* and *INP2* genes into *dnm1Δvps1Δkin4Δ*. The mutant strains were grown to log phase and were imaged by epifluorescence microscopy. Scale bar is 5μm.

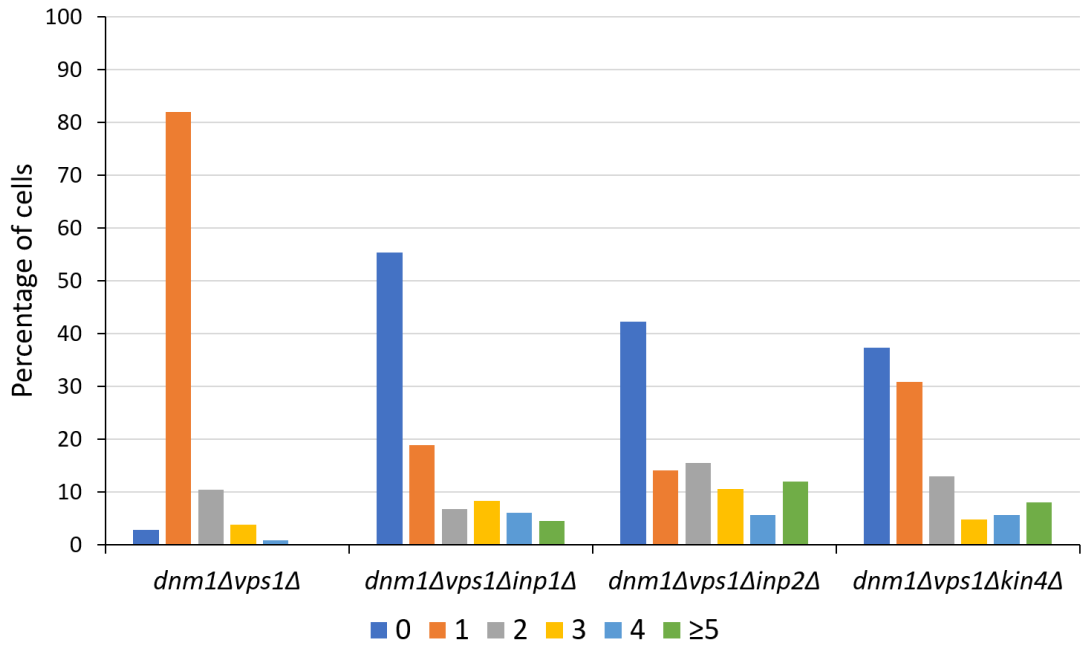

Figure 4.6 Peroxisome number distribution plot for mutant strains. Peroxisome number per cell was counted in different mutant backgrounds. The mutant strains were grown to log phase and were imaged by epifluorescence microscopy. More than 100 cells were analysed per strain.

4.4 Kin4 contributes to peroxisome transport to the bud

To understand the role of Kin4 in peroxisome distribution we reasoned that the lack of a peroxisome in daughter *dnm1Δvps1Δkin4Δ* cells can be a consequence of either excessive retention by Inp1 or a defect in Inp2-dependent forward transport to the bud. To resolve this, the *INP1* and *INP2* genes were knocked out independently in *dnm1Δvps1Δkin4Δ* cells and these strains were analysed by microscopy. In *dnm1Δvps1Δinp1Δ* cells almost all peroxisomes ended up in the bud. This is in line with previous observations that Inp1 is most probably, the only anchor to hold peroxisomes back in the mother (Fagarasanu et al., 2005). Interestingly, in *dnm1Δvps1Δkin4Δinp1Δ* cells very few peroxisomes entered the bud. Furthermore, there was no significant difference in the distribution of peroxisomes in *dnm1Δvps1Δkin4Δinp2Δ* cells compared to *dnm1Δvps1Δinp2Δ* cells **(Figure 4.5, Figure 4.6)**. This suggests that Kin4 is involved in transport of peroxisomes to the bud rather than a negative regulator of peroxisome retention in the mother. To gain more insight into the role of Kin4, *kin4Δ* cells were analysed and it was observed that there was a considerable defect in peroxisome inheritance, but this was not as severe as in *inp2Δ* cells where in most budding cells the buds are devoid of peroxisomes **(Figure 4.8)**.

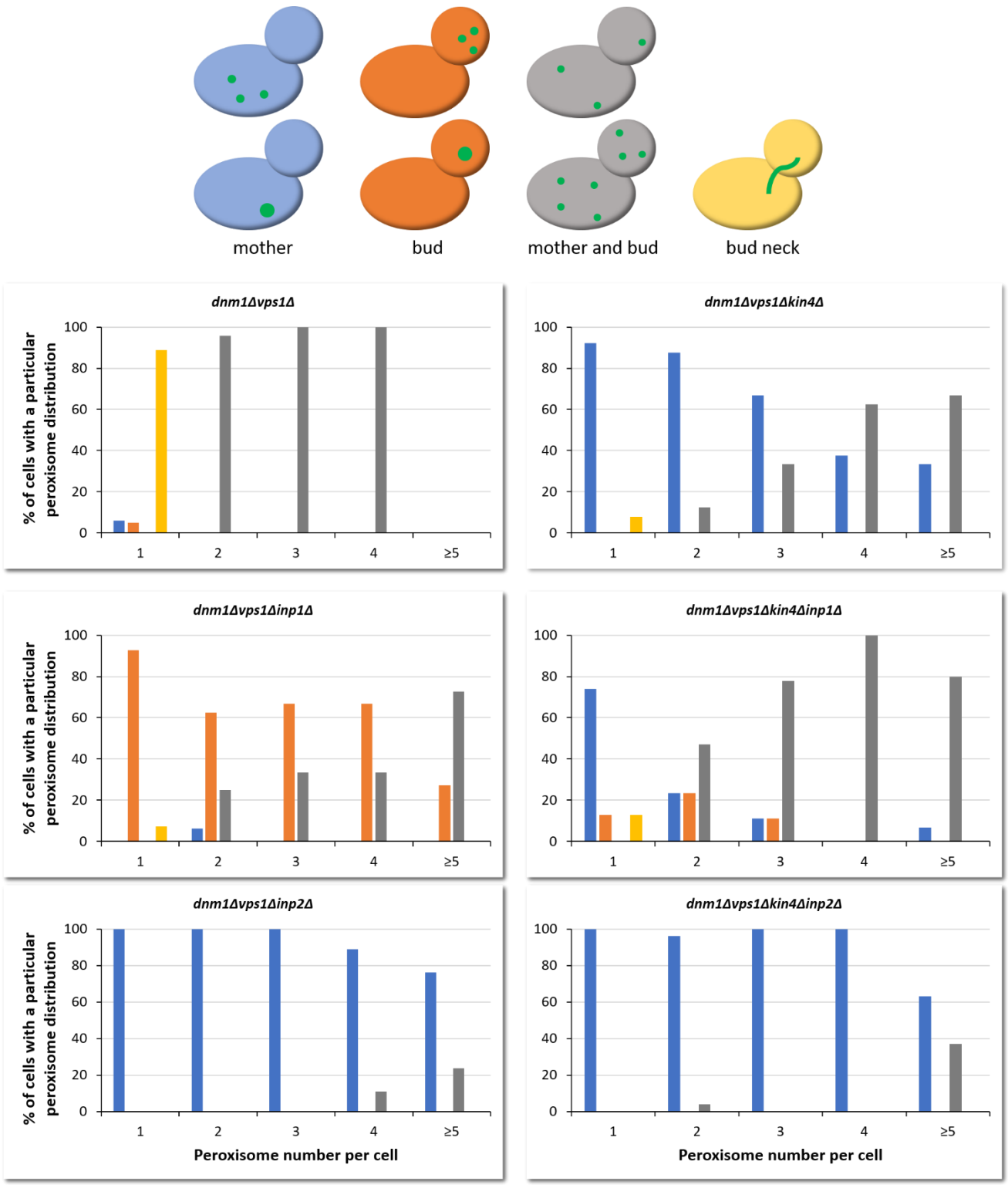

Figure 4.7 Kin4 contributes to the peroxisome transport to the bud. The peroxisome distribution in different mutants was quantified. Colour coded bars in the plots represent the distributions indicated in the top panel of the figure. The mutant strains were grown to log phase and were imaged by epifluorescence microscopy. Minimum 77 budding cells with peroxisomes were analysed for each mutant type. For some of the mutants this represents a fraction of a cell population **(Figure 4.6)**.

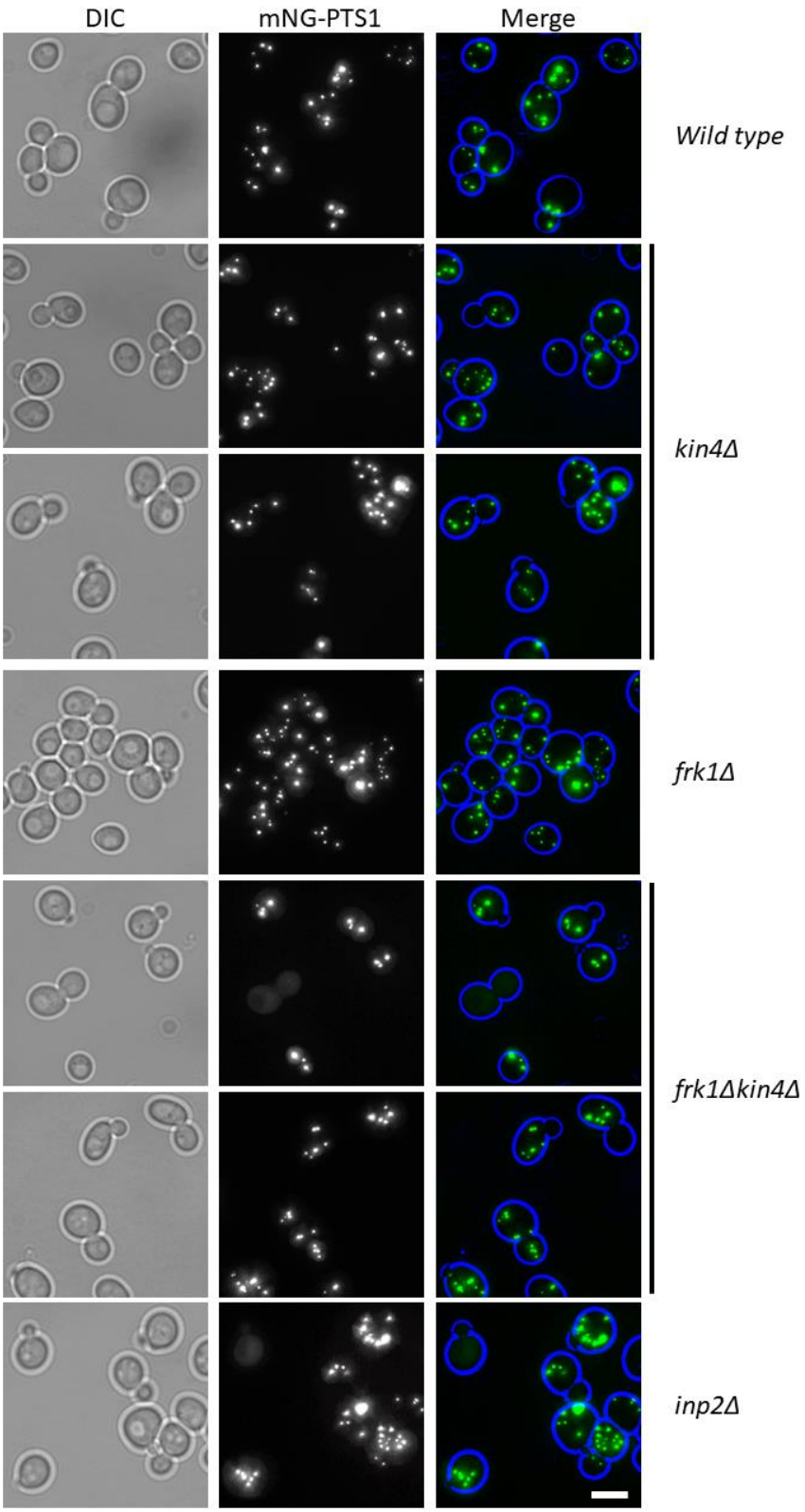

Figure 4.8 *frkΔ1kin4Δ* cells fail to deliver efficiently peroxisomes to the bud. The peroxisomal matrix protein marker, mNG-PTS1 was expressed to label the peroxisomes. Log phase cells were imaged using an epifluorescence microscope. Scale bar is 5μm.

In a Saccharomyces Genome Database (SGD) search, it was found that Frk1 is a Kin4 paralog. Kin4 and Frk1 share 43.6% identity and 57.7% similarity at amino acid sequence level. Deletion of *KIN4* in *frk1Δ* cells resulted in a strong defect in peroxisome inheritance resembling that of *inp2Δ* cells. Though *frk1Δ* cells did not show any defect in peroxisome segregation **(Figure 4.8, Figure 4.9)**. In *inp1Δ* most of the peroxisomes are transported to the bud leaving mother cells empty. This leads to cells without peroxisomes (~35%). A block in forward transport in *inp1Δ* cells by deletion of *INP2* leads to partial suppression of the distribution defect, with many more cells containing peroxisomes. To further test the role of Kin4 and Frk1 in peroxisome transport to the bud, cells containing peroxisomes were counted in *inp1Δ* and *frk1Δkin4Δinp1Δ*. In *inp1Δ* 38.15% cells were without peroxisomes whereas in *frk1Δkin4Δinp1Δ* only 14.93% cells were without peroxisomes **(Figure 4.10)**. This demonstrates that the additional deletion of *FRK1* and *KIN4* in *inp1Δ* cells causes a defect in peroxisome transport to the bud and thus leads to redistribution of peroxisomes between mother and the bud. Deletion of *FRK1* in *dnm1Δvps1Δkin4Δ* exacerbated the inheritance defect. Moreover, peroxisome distribution in *dnm1Δvps1Δfrk1Δ* cells was not drastically different from that in *dnm1Δvps1Δ* cells and thus explains the absence *FRK1* among the hits from the SGA screen **(Figure 4.11)**. These results suggest that there is redundancy between Kin4 and Frk1 function in peroxisome transport, where Kin4 plays a major role over Frk1.

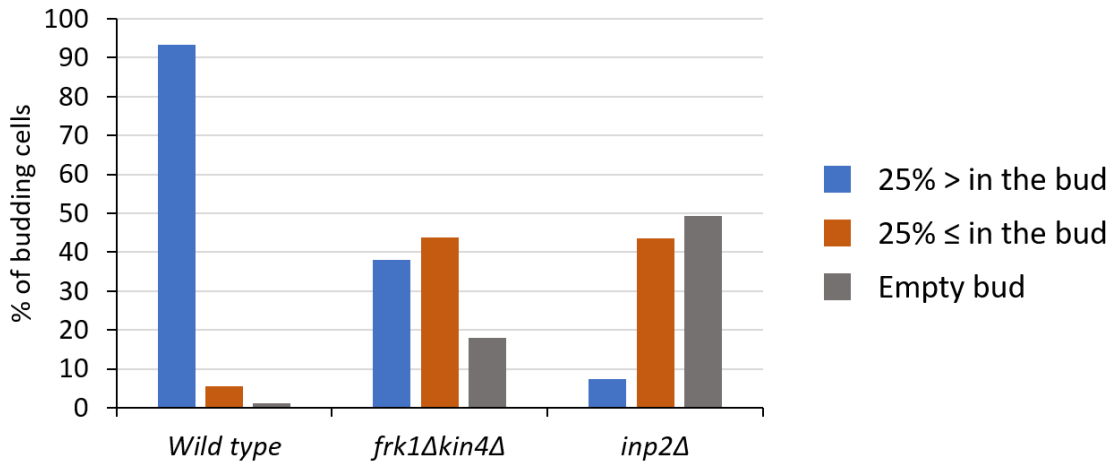

Figure 4.9 Peroxisome transport to the bud is strongly affected in *frk1Δkin4Δ* cells. mNG-PTS1 expressing wild type, *frk1Δkin4Δ* and *inp2Δ* cells were grown to log phase and imaged by epifluorescence microscopy. A minimum of 85 medium to large budded cells were analysed for presence of peroxisomes in the bud.

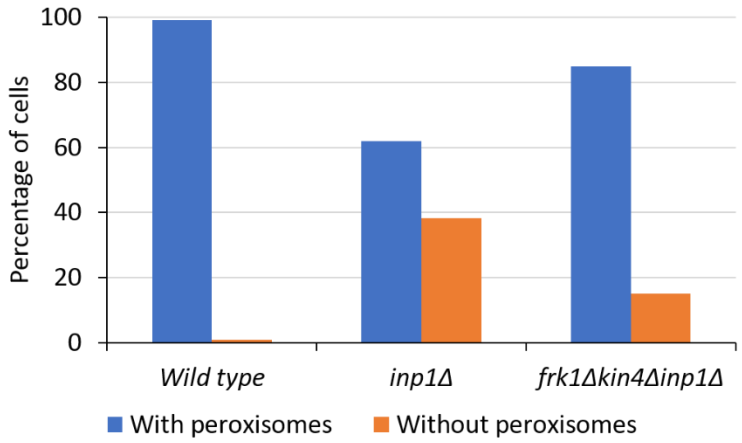

Figure 4.10 *KIN4* and *FRK1* deletion alleviates retention defect in *inp1Δ* cells. Cells expressing mNG-PTS1 were analysed for the presence of peroxisomes. The mutant strains were grown to log phase and were imaged by epifluorescence microscopy. More than 120 cells were scored per strain.

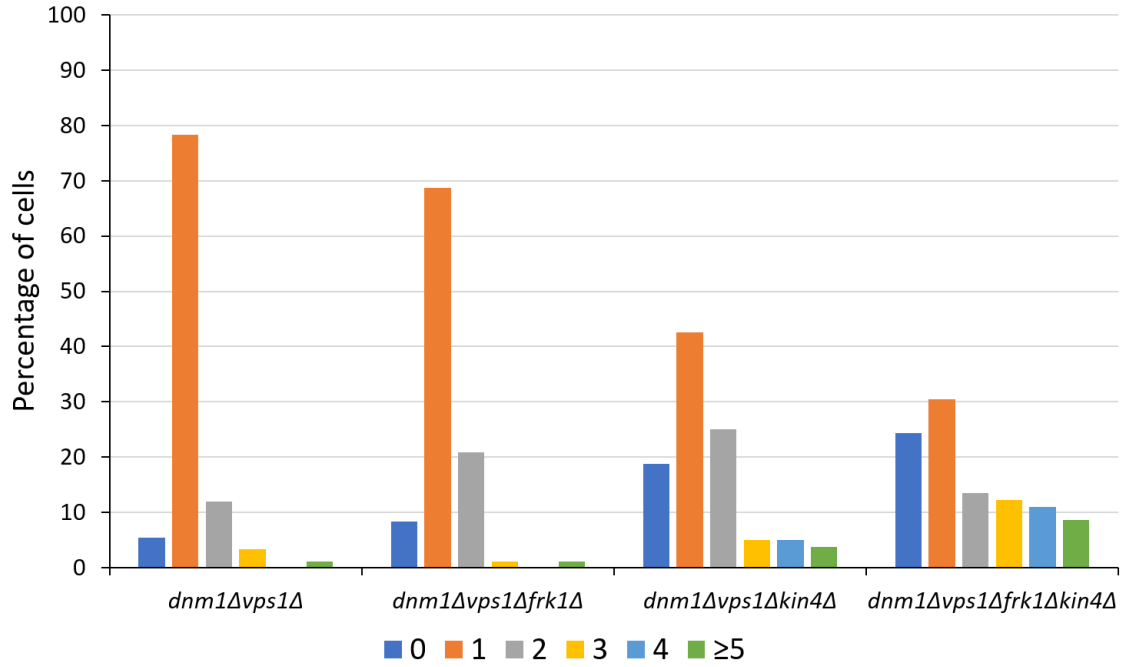

Figure 4.11 *FRK1* deletion exacerbates the peroxisome inheritance defect in *dnm1Δvps1Δkin4Δ* cells. Peroxisome number per cell in the mutant strains was quantified. Log phase cells were imaged and a minimum of 80 budding cells were scored for each mutant strain. The mutant strains were grown to log phase and were imaged by epifluorescence microscopy.

4.5 Frk1 is a potential SPoC kinase as Kin4

Kin4 and Frk1 are members of the serine/threonine protein kinase family. Kin4, Snf1 and Hsl1 kinases are positively regulated by Elm1 kinase by phosphorylation of a threonine residue in the kinase activation loop (Caydasi et al., 2010b; Moore et al., 2010). The activation loop motif is strongly conserved in all the three kinases and interestingly it is also present in Frk1 **(Figure 4.12 A)**. Overexpression of *KIN4* is toxic to the cells since Kin4 is negative regulator of MEN and therefore cells do not exit from mitosis. Kin4 acts via Bfa1, a part of the bipartite GAP complex Bub2/Bfa1 for Tem1 GTPase; the activator of MEN. Phosphorylation by Elm1 at Thr209 is required for Kin4 activity in the SPoC. Hence, deletion of either *BFA1* or *ELM1* suppresses the lethal effect of *KIN4* overexpression. On the other hand, Frk1 has not been previously implicated in SPoC. Hence, we tested whether overexpression of *FRK1* is toxic. *FRK1* was expressed in the wild type, *bfa1Δ* and *elm1Δ* cells under control of the strong inducible *GAL1/10* promoter. The transformants were grown in raffinose containing minimal medium before shifting to galactose medium which induces expression. Indeed, wild type cells expressing *FRK1* showed very little growth on galactose medium and were perfectly fine on glucose medium. Moreover, *bfa1Δ* and *elm1Δ* cells expressing *FRK1* did not show such growth defect **(Figure 4.12 B, C)**. This clearly indicates that Frk1 can act like Kin4 in SPoC. The homology with Kin4 at the amino acid sequence and functional level strongly hints towards Frk1 being a potential SPoC kinase as Kin4. Hence it can be concluded that Frk1 is paralog of Kin4 at both the protein level and functional level.

A

SNF1 206 NFLK**TSCGSP**N**YA**A**PE** 221
HSL1 269 KLLK**TSCGSP**H**YA**S**PE** 284
KIN4 205 ELMK**TSCGSP**C**YA**A**PE** 220
FRK1 205 ELMK**TSCGSP**C**YA**A**PE** 220

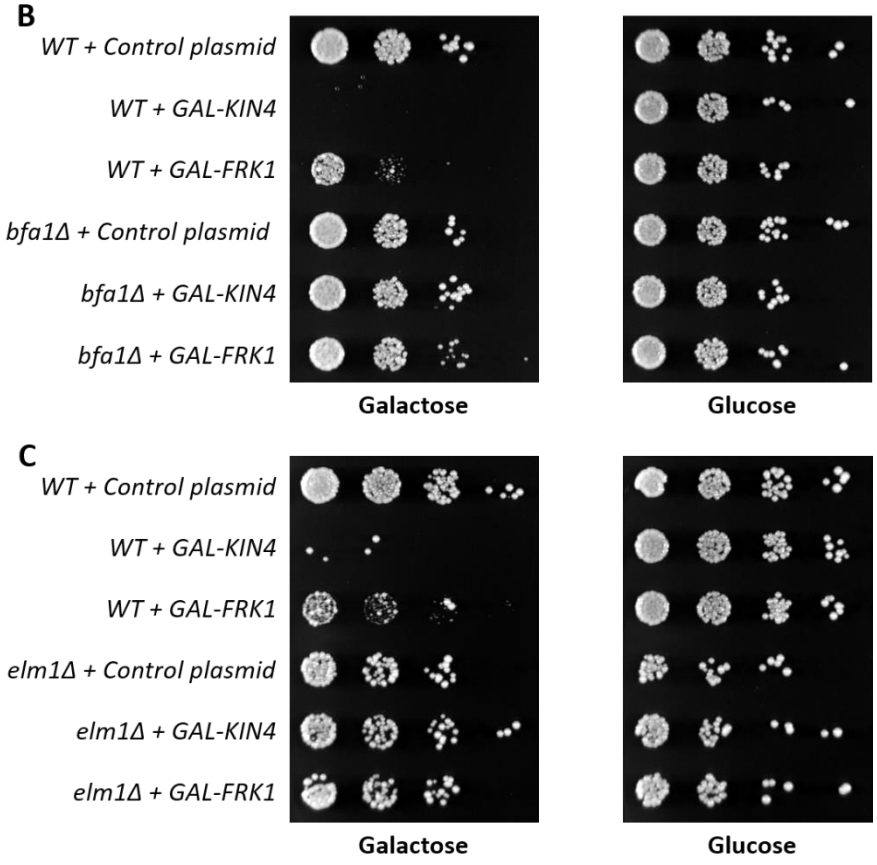

Figure 4.12 Frk1 is a potential SPoC kinase as Kin4. (A) Sequence alignment for kinase activation loop motifs where conserved residues are highlighted. (B-C) As *GAL1-KIN4*, induced *GAL1-FRK1* overexpression is toxic to the cells. However, *bfa1Δ* and *elm1Δ* rescue the toxicity arising from overexpression. Serial dilutions of cells were spotted on YM media containing either galactose or glucose.

4.6 Inheritance defect in *frk1Δkin4Δ* is independent of SPoC

Both Frk1 and Kin4 play a role in the SPoC and in peroxisome inheritance. So, we asked if both SPoC activation and peroxisome inheritance affect each other. Therefore, GFP-Tub1 was expressed in wild type, *frk1Δkin4Δ* and *kar9Δ* cells and the orientation of the mitotic spindle was analysed. Wild type and *frk1Δkin4Δ* cells showed similar spindle pole body alignment unlike *kar9Δ* cells, where in many cells the mitotic spindle was misaligned. Moreover, *kar9Δ*

cells are not affected in peroxisome inheritance **(Figure 4.13 A)**. The SPoC is activated only when the mitotic spindle is not aligned parallel to the cell polarity axis during early anaphase. We conclude that the peroxisome inheritance defect observed in *frk1Δkin4Δ* cells is not a consequence of spindle misalignment and subsequent SPoC activation. In addition, overexpression of *KIN4* in *inp2Δ* is lethal as observed in wild type cells, indicating that peroxisome inheritance is not required for SPoC activation **(Figure 4.13 B)**. Since neither *bfa1Δ* nor *bub2Δ* cells nor *dnm1Δvps1Δbfa1Δ* and *dnm1Δvps1Δbub2Δ* cells fail to transport peroxisomes to the bud, Kin4 and Frk1 do not signal through the SPoC pathway to mediate peroxisome inheritance **(Figure 4.14 A, B)**. Moreover, transport of peroxisomes is initiated in G1 phase, which is much earlier in the cell cycle than SPoC signalling. All the above confirmed that the function of Kin4 in peroxisome transport is independent of its role in SPoC. We also conclude that SPoC activation and peroxisome inheritance do not affect each other.

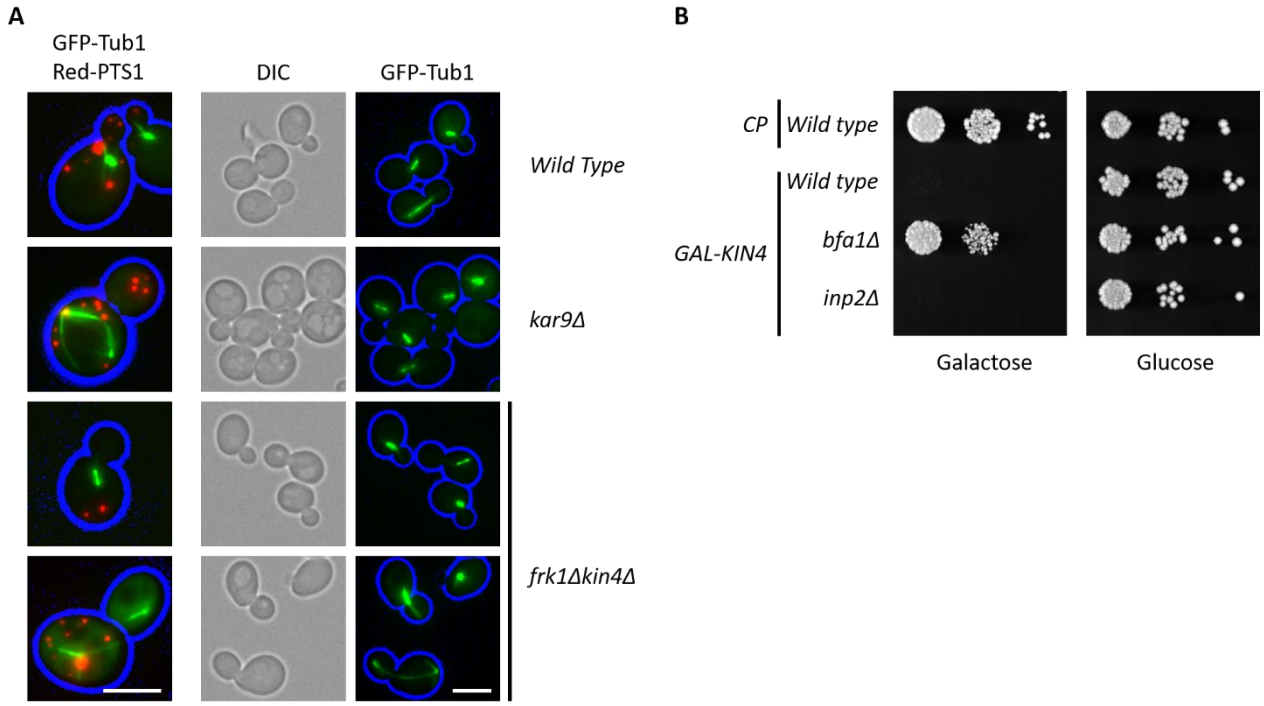

Figure 4.13 Kin4 dependent SPoC activation and inheritance of peroxisomes are independent processes. (A) Mitotic spindle alignment in *frk1Δkin4Δ* cells is unaffected. Cells expressing GFP-Tub1 or/and mKate2-PTS1 were grown to log phase and imaged. Scale bar is 5μm. (B) Peroxisome inheritance is not required for SPoC activation. Serial dilutions of cells were spotted on YM media containing either galactose or glucose.

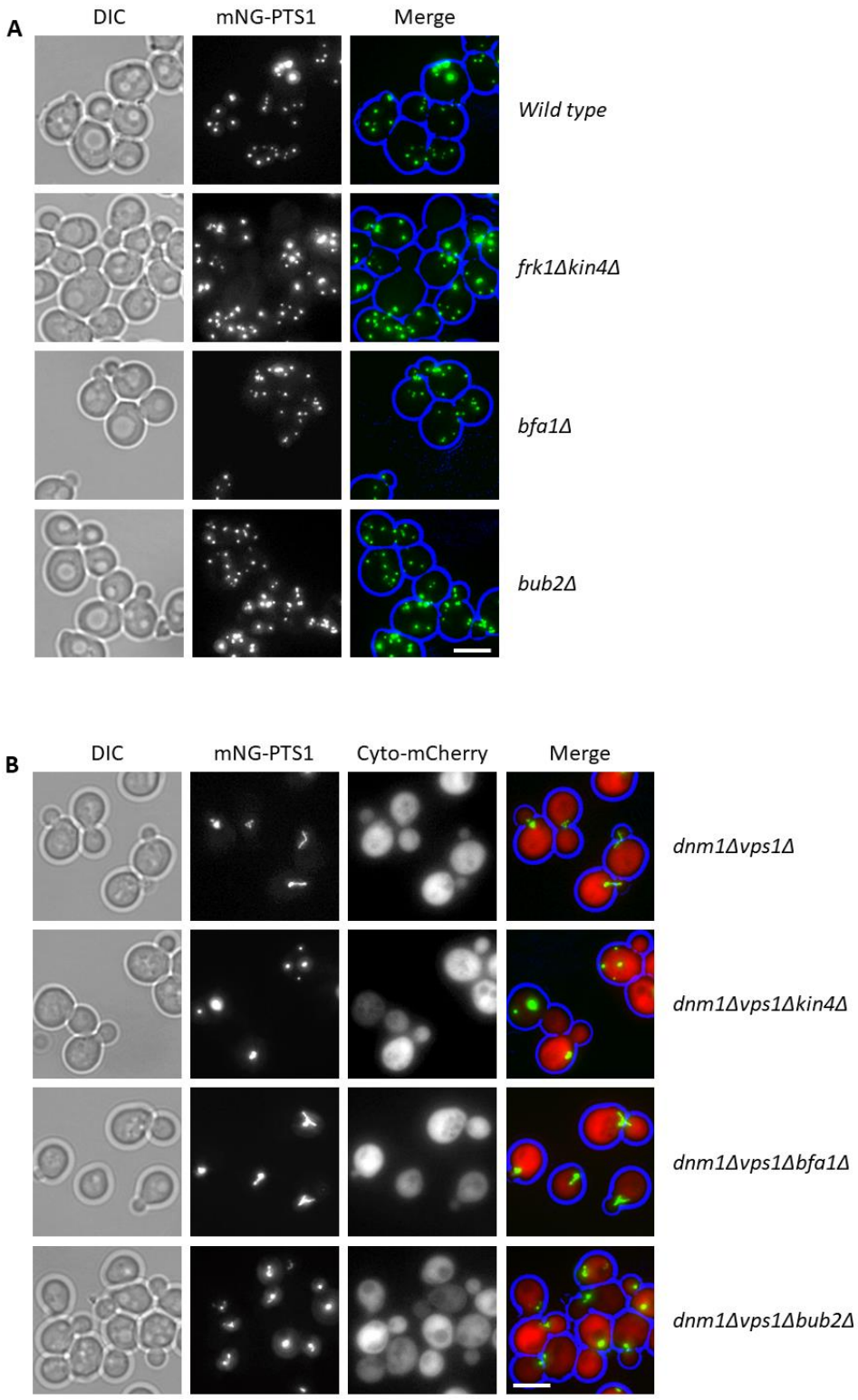

Figure 4.14 SPoC components Bfa1 and Bub2 are not required for peroxisome inheritance. The cells were grown to log phase and imaged with an epifluorescence microscopy. (A) Peroxisome inheritance is not affected in *bfa1Δ* and *bub2Δ* cells as in *frk1Δkin4Δ* cells. (B) Moreover, *dnm1Δvps1Δbfa1Δ* and *dnm1Δvps1Δbub2Δ* cells have one elongated peroxisome per cell as observed in *dnm1Δvps1Δ* cells. Scale bar is 5µm.

4.7 Inheritance of other Myo2 cargoes in *frk1Δkin4Δ* cells

The unconventional ClassV myosin Myo2 plays a vital role in the transport of most of the yeast organelles including peroxisomes. Hence, we analysed the distribution of other Myo2 dependent cargoes in *frk1Δkin4Δ* cells. The inheritance of late-Golgi, lipid bodies, mitochondria and vacuoles were tested in wild type and *frk1Δkin4Δ* cells. It was observed that the distribution of late Golgi elements, lipid droplets and mitochondria was not affected in *frk1Δkin4Δ* compared to in wild type cells **(Figure 4.15)**. However, there was a strong vacuole inheritance defect in *frk1Δkin4Δ* cells and the phenotype resembled that of the vacuole inheritance mutant *vac17Δ* **(Figure 4.16)**. Subsequently, inheritance of vacuoles was tested in *frk1Δ* and *kin4Δ* cells. Neither of the single gene deletions showed a strong defect in vacuole transport suggesting that Kin4 and Frk1 are redundant for this process **(Figure 4.16)**. Moreover, we also conclude that Kin4 and Frk1 are required for vacuole and peroxisome transport and not for a variety of other organelles.

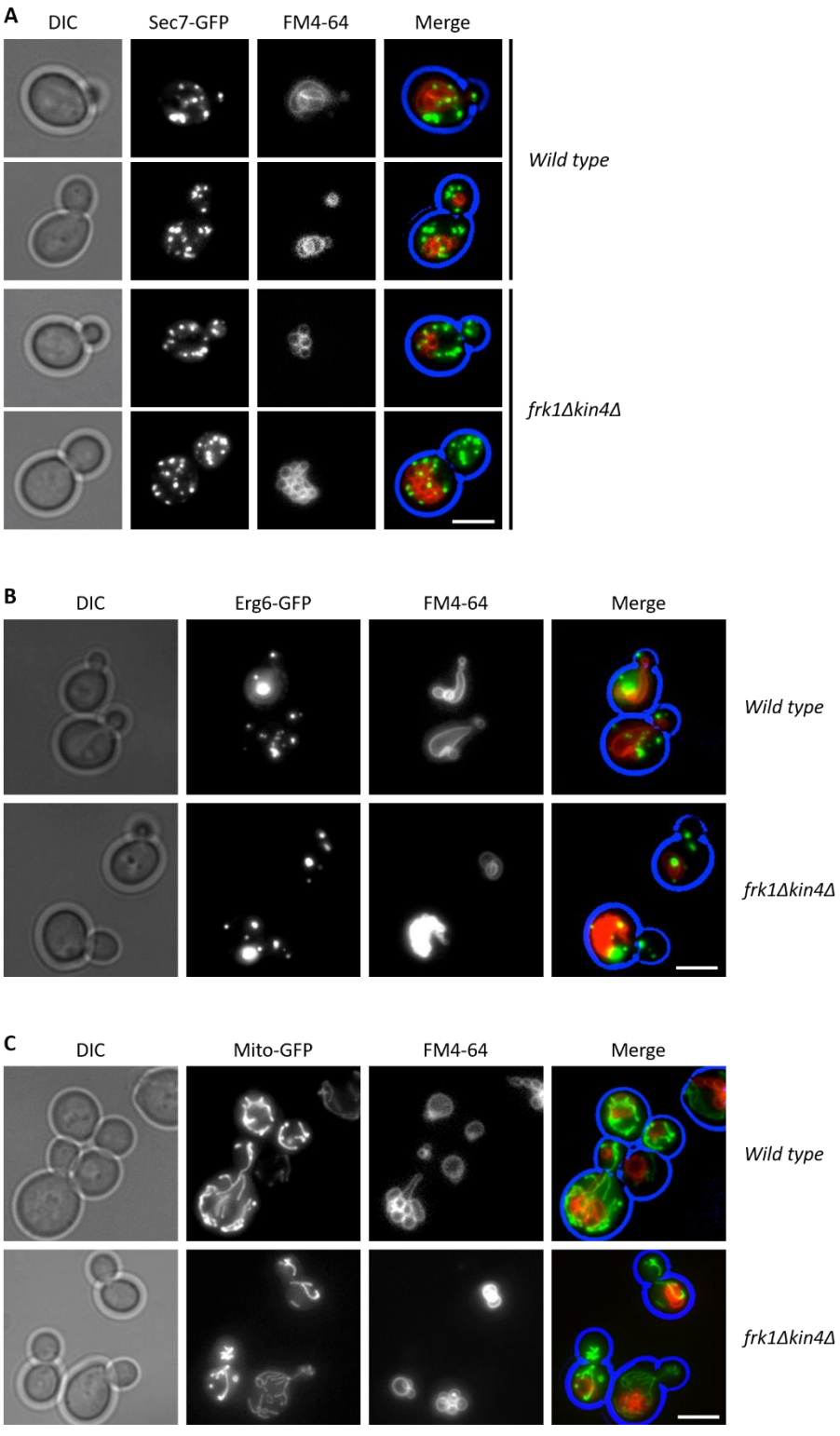

Figure 4.15 Inheritance of late Golgi elements, lipid bodies and mitochondria are not affected notably in *frk1Δkin4Δ* cells. The log phase cells were stained with FM4-64 and imaged where Golgi elements (A), lipid droplets (B) and mitochondria (C) are labelled with Sec7-GFP, Erg6-GFP and Mito-GFP markers respectively. Scale bar is 5µm.

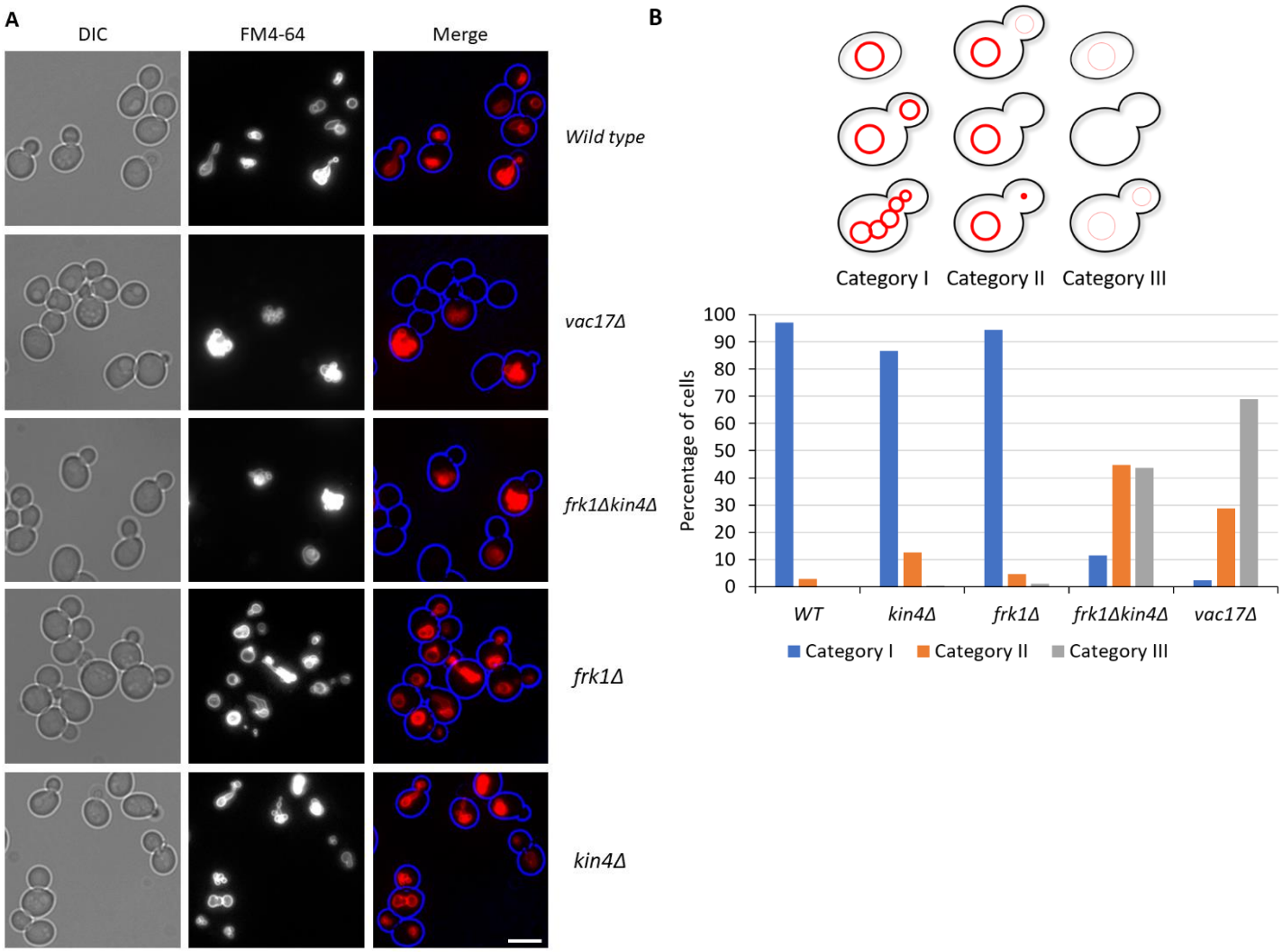

Figure 4.16 Vacuole inheritance is strongly affected in *frk1Δkin4Δ* cells. The cells were grown to log phase and incubated with FM4-64 for an hour to stain the vacuoles. Subsequently, the cells were washed thrice and incubated with fresh medium for 4-5h before imaging. (A) *frk1Δkin4Δ* cells are deficient in vacuole inheritance resembling *vac17Δ* cells. Scale bar is 5µm. (B) A minimum of 170 cells were scored to analyse the defect in vacuole inheritance.

4.8 *De novo* peroxisome and vacuole formation in *frk1Δkin4Δ* cells

In previous studies it has been shown that the cells lacking either peroxisomes or vacuoles due to defect in inheritance can form them *de novo* (Jin and Weisman, 2015; Motley and Hettema, 2007). Since peroxisome and vacuole inheritance is affected in *frk1Δkin4Δ* cells the *de novo* formation of both the organelles was tested in wild type and *frk1Δkin4Δ* cells. To test peroxisome *de novo* formation constitutive mKate2-PTS1 and galactose inducible mNG-PTS1 markers were expressed in wild type and *frk1Δkin4Δ* cells. In cells mNG-PTS1 expression was induced by growing cells into galactose containing medium for 2.5h and then shifted the cells to glucose medium for 2h to shut down the expression. Then the cells were seeded under the agarose pad in mini-dishes and grown for an additional 6-8h at 30°C to allow colony formation. Subsequently, the cells were imaged using epifluorescence microscopy. The peroxisomes in wild type colony cells were labelled with both mKate2 and mNG. This suggests proper peroxisomes' fission and segregation during cell division in line with previous observations (Motley and Hettema, 2007). In contrast, only one or two cells of the *frk1Δkin4Δ* colony contained peroxisomes that were labelled with both mKate2 and mNG and most cells contained multiple mKate2-only labelled peroxisomes. This clearly showed that the parent cell; with mNG peroxisomes, from which the colony was derived failed to pass on its peroxisomes during cell division **(Figure 4.17 A)**. Vacuole inheritance and formation was studied in a similar fashion where Vph1-GFP was used as constitutive marker and FM4-64 dye was used to pulse label the vacuoles. Wild type and *frk1Δkin4Δ* cells expressing Vph1-GFP were incubated with FM4-64 at 30°C for an hour and washed thrice before shifted to fresh medium without FM4-64. The cells were grown for 4-5h at 30°C and imaged. Like peroxisomes, vacuoles in wild type cells were labelled with both FM4-64 and Vph1-GFP whereas in many *frk1Δkin4Δ* cells vacuoles were labelled with only Vph1-GFP and not with FM4-64. In some cells, mother cell vacuoles were labelled with both Vph1-GFP and FM4-64 and in contrast vacuoles in bud were labelled only with Vph1-GFP. This showed that the vacuole segregation is clearly affected in *frk1Δkin4Δ* cells, but cells do not undergo division until bud forms *de novo* vacuoles **(Figure 4.17 B)**. This observation is in line with *de novo* vacuole formation in *vac17Δ* cells reported previously (Jin and Weisman, 2015). We conclude that *frk1Δkin4Δ* cells that fail to inherit either peroxisomes or vacuoles due to defect in inheritance can form them *de novo*.

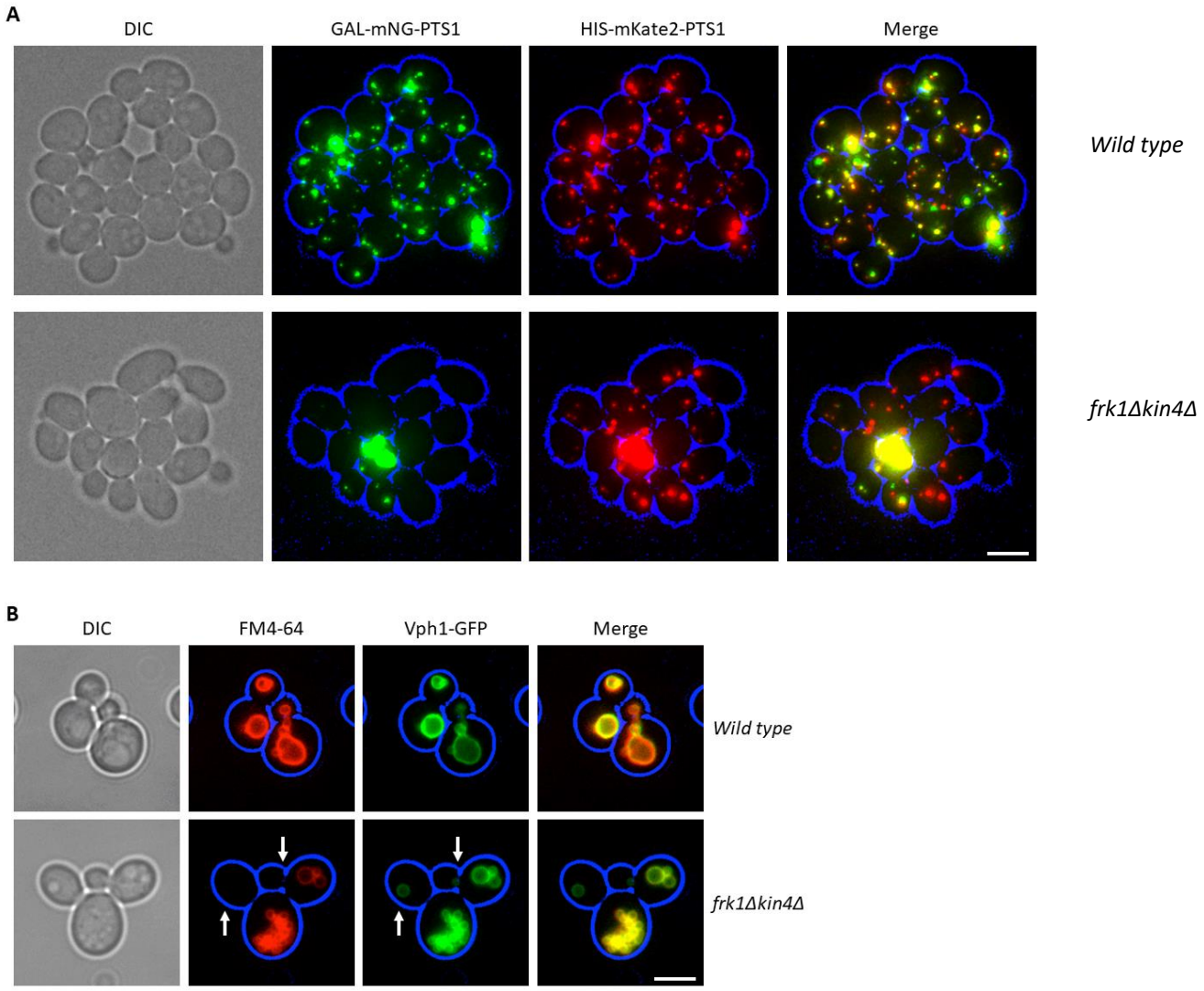

Figure 4.17 *frk1Δkin4Δ* cells lacking peroxisomes or vacuoles form them *de novo*. (A) Wild type and *frk1Δkin4Δ* cells constitutively expressing mKate2-PTS1 and conditionally expressing mNG-PTS1 were grown for 2.5h on galactose medium and chased for 2h on glucose medium. Cells were then seeded thinly under a glucose-containing agarose pad in an imaging µ-dish (Ibidi) and allowed to grow for 6-8h before imaging, so that single budding cells can give rise to a colony. If any peroxisomes are formed *de novo* after the shutdown of mNG-PTS1 expression, these peroxisomes will be labeled with mKate2-PTS1 only. In wild type cells all peroxisomes are labelled with red and green indicating that peroxisomes are actively dividing and segregating. In contrast, in the *frk1Δkin4Δ* colony there are some cells with red peroxisomes that lack any mNG signal. These peroxisomes have been formed *de novo*. (B) Cells constitutively expressing Vph1-GFP, a vacuole membrane protein marker, were incubated with FM4-64 (red) for an hour to stain the vacuoles (pulse) subsequently, the cells were chased in fresh medium for 4-5h before imaging. In wild type cells the vacuoles were stained with both Vph1-GFP and FM4-64 indicating they have been inherited. In *frk1Δkin4Δ* cells very little to no FM4-64 labelled vacuoles were observed in the bud however all of them were labelled with Vph1-GFP. These vacuoles were formed *de novo* (arrows). Scale bar is 5µm.

4.9 Actin cytoskeleton is in place in *frk1Δkin4Δ* cells

The ClassV myosin motors use actin cables as tracks to transport organelles to the emerging bud. Defects in actin cable formation (or polymerisation) severely disrupts the transport of organelles. Therefore, intact interaction between actin cytoskeleton and the myosin motors is indispensable for organelle movement (Bretscher, 2003). The defect in transport of some organelles but not all in *frk1Δkin4Δ* cells indicates that the interaction of Myo2 with actin cytoskeleton is not significantly affected. To visualise the distribution of the actin cytoskeleton, life-act (Riedl et al., 2008) was expressed in wild type and *frk1Δkin4Δ* cells. Indeed, the actin cable patterns were similar, and the cables did converge at the bud tip and bud neck as expected in both wild type and *frk1Δkin4Δ* cells **(Figure 4.18)**.

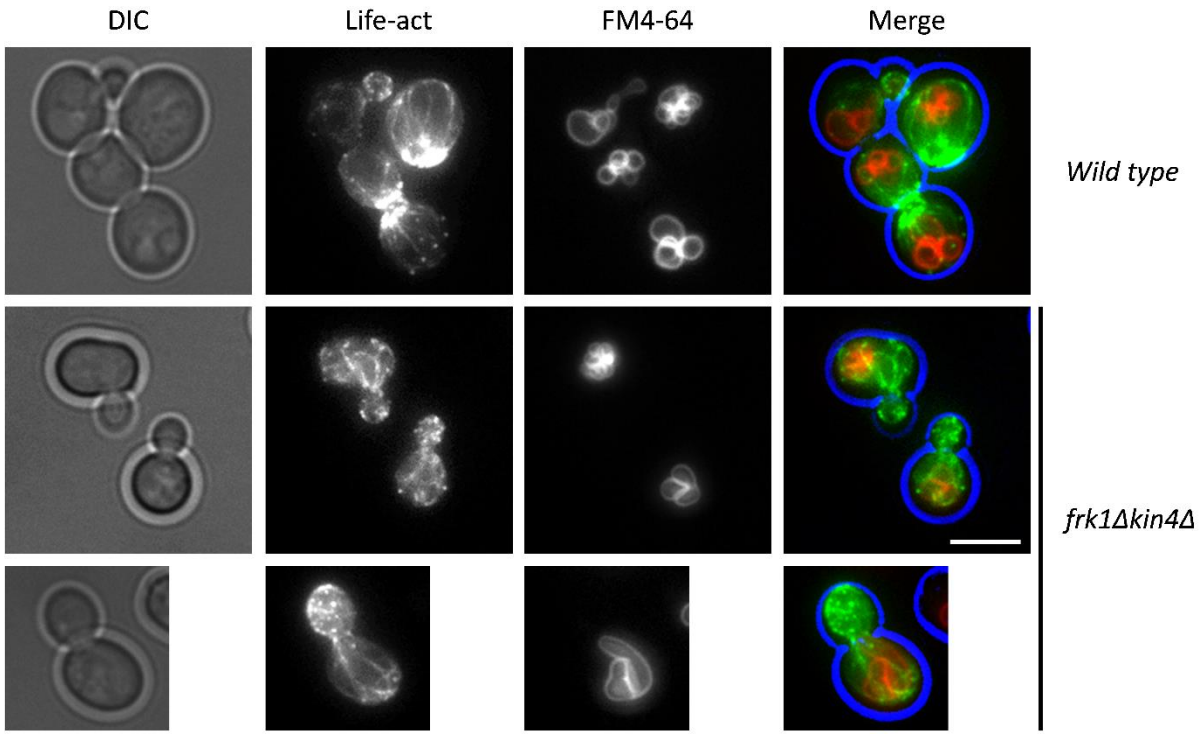

Figure 4.18 Actin cytoskeleton is not affected notably in *frk1Δkin4Δ* cells. Log phase cells expressing Life-act were imaged with an epifluorescence microscopy. Vacuoles were visualised by FM4-64 staining. Scale bar is 5μm.

4.10 Inp2 and Vac17 protein levels are down in *frk1Δkin4Δ* cells

The inheritance defects for peroxisomes and vacuoles in *frk1Δkin4Δ* cells resemble the defect observed in mutants lacking Inp2 and Vac17, respectively. Hence, Inp2 and Vac17 protein levels in *frk1Δkin4Δ* cells were compared to those in wild type cells. To test protein levels both Inp2-ProtA and Vac17-ProtA were expressed under control of their endogenous promoters in wild type and *frk1Δkin4Δ* cells. Interestingly, western blot analysis revealed that both Inp2 and Vac17 protein levels were much lower in *frk1Δkin4Δ* than in wild type cells. In contrast, Myo2-3xHA levels were comparable in wild type and *frk1Δkin4Δ* cells **(Figure 4.19)**. This suggests that the inheritance defect most probably is a direct consequence of lowered Myo2 receptor protein levels.

4.11 Discussion

We sought to understand how peroxisome inheritance is regulated and to identify factor(s) required for this process. For this we used SGA methodology based high throughput screens in *S. cerevisiae*. It is an effective genetic method to systematically approach a scientific question. The high throughput screen was performed in *dnm1Δvps1Δ* cells to generate a triple gene deletion library and followed by microscopy imaging analysis. Several novel mutants were identified along with known factors that affected either peroxisome number or inheritance. Among the inheritance mutants, *dnm1Δvps1Δkin4Δ* showed a robust phenotype where peroxisomes are observed more in the mother cell than in the bud compared to *dnm1Δvps1Δ* cells. Detailed analysis revealed that it is forward transport to the bud that is affected rather than excessive retention in the mother.

Kin4 is an established SPoC kinase. Kin4 shares significant sequence similarity and identity with Frk1. Like in case of *KIN4*, overexpression of *FRK1* is toxic to the cells and the toxicity can be rescued by further deletion of either *BFA1* or *ELM1*. Thus, Frk1 is therefore a potential second SPoC kinase in addition to Kin4. Peroxisome transport to *kin4Δ* daughter cells is not as severely affected as in *inp2Δ* daughter cells. But, additional deletion of *FRK1* in *kin4Δ* exacerbated the peroxisome transport to the bud and the subsequent phenotype was like that observed in *inp2Δ* cells. This suggests that Frk1 also contributes to the peroxisome maintenance. The homology at amino acid sequence and functional level confirmed that Frk1 is a functional paralog of Kin4.

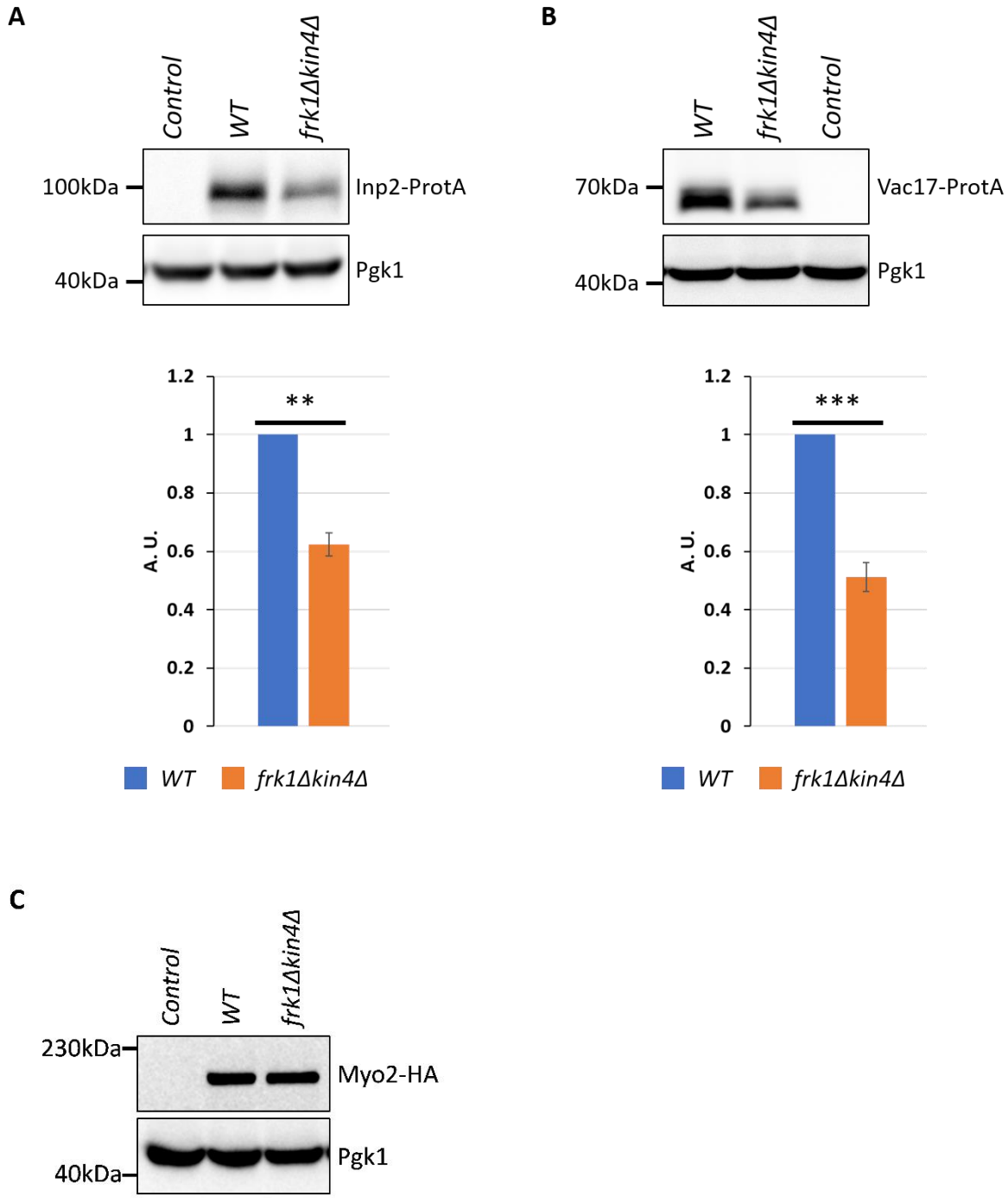

Figure 4.19 Kin4 and Frk1 are required to maintain protein level of Myo2 receptors. (A, B) Inp2-ProtA, Vac17-ProtA were expressed in wild type and *frk1Δkin4Δ* cells. TCA lysates were analysed by western blot. Values for Inp2-ProtA and Vac17-ProtA bands were normalised against unsaturated Pgk1 bands (Not shown) and were plotted. Normalised ProtA signals in wild type cells were set to 1 A. U. where A. U. is arbitrary units. (C) Myo2 was tagged with 3xHA in genome. TCA extraction followed by western blot analysis was performed on modified wild type and *frk1Δkin4Δ* strains. Error bars indicate SEM (Standard Error Mean). N=3. ** p-value < 0.01; *** p-value <0.001; two tailed Student's t-test.

The defect in peroxisome transport is independent of SPoC because spindle orientation is unaffected in *frk1Δkin4Δ* cells. In addition, peroxisome inheritance was not affected in *bfa1Δ* and *bub2*Δ cells. Myo2-dependent transport of other cargoes revealed that vacuole inheritance is also severely affected in *frk1Δkin4Δ* cells. Furthermore, *frk1Δkin4Δ* cells devoid of peroxisomes and vacuoles form them *de novo* as has been reported previously in *inp2Δ* and *vac17Δ,* respectively (Jin and Weisman, 2015; Motley and Hettema, 2007). The defects in peroxisome and vacuole inheritance are not a consequence of pleiotropic effects of the loss of Kin4 and Frk1 since the distribution of mitochondria, Golgi bodies and lipid droplets are unaffected. This is in line with the observation that cells appear to organise their actin cytoskeleton properly and grow in a polarised fashion. Inp2 and Vac17 protein levels are lower in *frk1Δkin4Δ* cells than in wild type cells whereas Myo2 levels are unaffected. This suggests that the defect in peroxisome and vacuole inheritance in *frk1Δkin4Δ* cells can be a direct consequence of reduced stability of Inp2 and Vac17, respectively. Interestingly, both Inp2 and Vac17 protein levels have been shown to fluctuate during cell cycle (Fagarasanu et al., 2006; Tang et al., 2003). Therefore, we hypothesized that Kin4 and Frk1 contribute to the Inp2 and Vac17 protein stability during the cell cycle. The spatial and temporal regulation of vacuole inheritance including Vac17 is studied in much more detail compared to that of any other organelle. At this point it was more important to unravel underlying mechanism through which Kin4 and Frk1 contribute to the organelle transport. Therefore, further functional characterisation of Kin4 and Frk1 was carried out in the context of vacuole transport.

Chapter 5 Functional characterisation of Kin4 and Frk1 in vacuole inheritance

5.1 Introduction

There are three major events involved in organelle transport in *S. cerevisiae*. The first is the assembly of a transport complex consisting of the myosin motor and its organelle receptor. The second step is organelle transport along actin cables to the bud. The third is the termination process which includes organelle release from myosin motors and proper positioning in the bud **(Figure 5.1)**. Transport needs to be coordinated with the cell cycle hence transport is under both temporal and spatial control. In the case of the vacuole, Cdk1-dependent direct phosphorylation of both Vac17 and Myo2 stimulates the assembly of the vacuole transport complex at G1 (Legesse-Miller et al., 2006; Peng and Weisman, 2008). Spatial regulation is mediated by degradation of Vac17 when the vacuole enters the bud. Phosphorylation of Vac17-Thr240 by an unknown kinase in the mother cell recruits Dma1, an E3-ubiquitin ligase, to the above complex. Once the vacuole reaches the bud Cla4 and Ste20 trigger the termination process. Cla4 and Ste20 are PAK kinases and are mainly localised to the bud cortex. Cla4 phosphorylates Vac17 at Ser222 residue and this leads to Dma1-dependent ubiquitination of Vac17 and subsequently degradation by the proteasome. Vac17 Ser222 and Thr240 are present in a PEST motif (204-250aa) (Tang et al., 2003). PEST motifs are sequences that target proteins for rapid degradation and they are generally rich in proline, glutamic acid, serine and threonine amino acid residues (Rechsteiner and Rogers, 1996). Vac17 S222A, T240A and PESTΔ mutants are defective in spatially regulated Vac17 breakdown. In cells expressing these Vac17 mutants, the vacuole positions inappropriately in the bud as it remains attached to Myo2 till late in the cell cycle and follows Myo2 to the mother bud neck. Moreover, the recruitment and activity of Dma1 and Cla4 have been suggested to be restricted to the bud (Yau et al., 2014; Yau et al., 2017). Overexpression of Cla4 and Ste20 causes excessive degradation of Vac17 thereby leading to a defect in vacuole inheritance. But this defect can be rescued by expressing Vac17 without PEST sequence (Bartholomew and Hardy, 2009). This result showed that Cla4 and Ste20 can diffuse into mother upon overexpression. The current model of spatial and temporal regulation of vacuole transport is depicted in **(Figure 5.1)**.

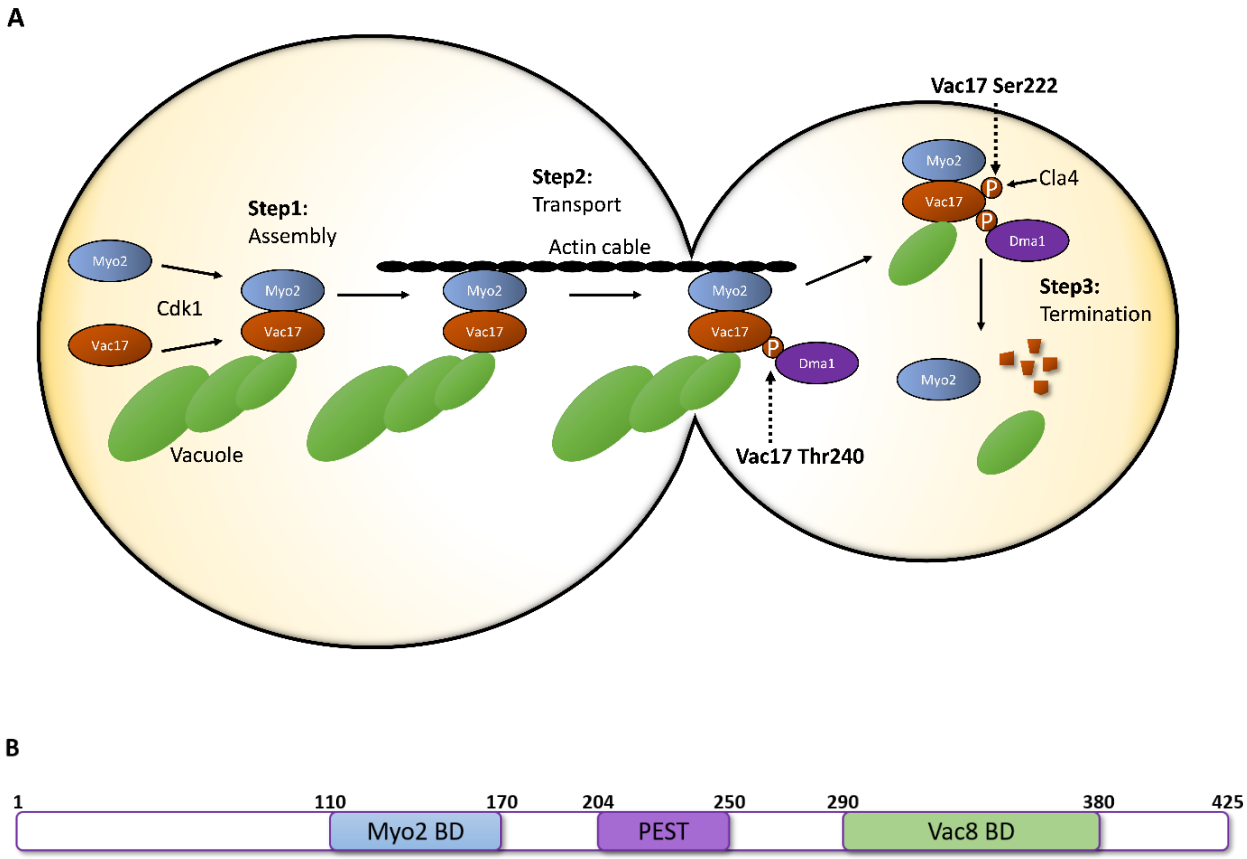

Figure 5.1 Schematic representation for spatial and temporal regulation of vacuole transport in *S. cerevisiae*. (A) Model showing three important steps in vacuole transport to the bud and molecular players involved in it. (B) A diagram with various domains in Vac17 (Yau et al., 2014; Yau et al., 2017). BD is binding domain.

This model however, does not include a role for Kin4 and Frk1 in vacuole transport to the bud. Kin4 and Frk1 are serine/threonine kinases. Kin4 is mainly localised to the mother cell cortex (D'Aquino et al., 2005; Pereira and Schiebel, 2005). According to SGD, Frk1-GFP localises to the cytoplasm. There are two independent reports that link Kin4 and Frk1 to the vacuole. In the first report, overexpression of *FRK1* under control of the *GAL* promoter showed enlarged vacuoles compared to the control strain (Arlt et al., 2011). And in second report, Kin4 was identified as an interactor of Ycf1, an ABC transporter that is required for vacuole fusion (Paumi et al., 2007). Both studies involved genome wide screens and neither revealed any mechanistic involvement of Frk1 and Kin4 in vacuole maintenance. In this study we found that vacuole transport to the bud is severely affected in *frk1Δkin4Δ* cells and Vac17 protein levels are also down in these cells. All the above compelled us to hypothesize that Kin4 and Frk1 prevent premature degradation of Vac17 in the mother by Cla4. We sought to test this hypothesis and determine the molecular mechanism through which Kin4 and Frk1 act.

5.2 Vac17 interacts with Myo2 in *frk1Δkin4Δ* cells

To gain more insight into the role of Kin4 in Vac17 regulation it was crucial to understand whether Vac17 can interact with Myo2 in *frk1Δkin4Δ* cells. It has been reported that Myo2 mutants that cannot efficiently interact with Vac17 not only show a defect in vacuole inheritance but also show an increased level of Vac17 in the cell (Eves et al., 2012; Ishikawa et al., 2003; Tang et al., 2003). In contrast, in *frk1Δkin4Δ* cells, the level of Vac17 is decreased. Moreover, in co-immunoprecipitation experiments, we found that Vac17 still forms a complex with Myo2 in *frk1Δkin4Δ* cells **(Figure 5.2)**. Furthermore, time lapse imaging revealed that segregation structures were formed in *frk1Δkin4Δ* cells, but that the cells fail to maintain them **(Figure 5.2, Figure 5.3)**. Occasionally, some transport of vacuolar membranes is observed. Taken together, we conclude that the initial Myo2-Vac17 complex formation occurs independent of Kin4 and Frk1 but that these kinases are required for a subsequent step in the inheritance process.

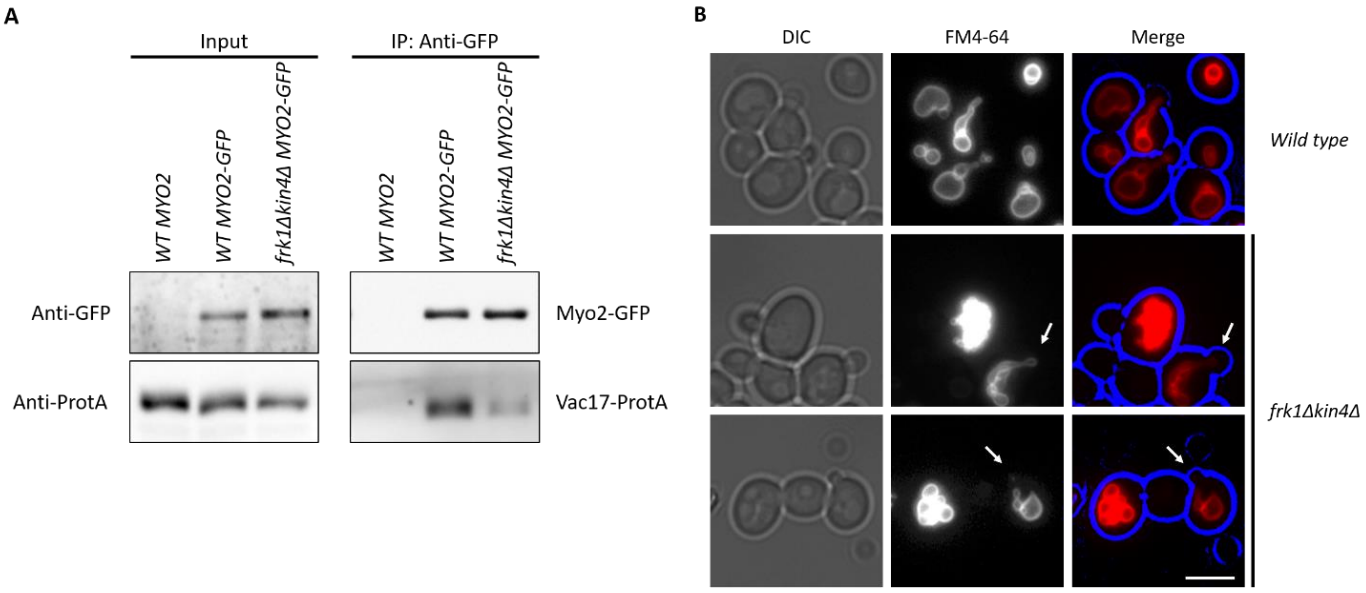

Figure 5.2 The Myo2-Vac17 complex assembles in *frk1Δkin4Δ* cells. (A) Vac17 and Myo2 interaction were analysed by co-immunoprecipitation where Myo2 was tagged with GFP in the genome and Vac17-ProtA was expressed from a plasmid under control of its own promoter. (B) Vacuole segregation structures were observed in some *frk1Δkin4Δ* cells, mainly in small budded cells (arrows). Scale bar is 5µm.

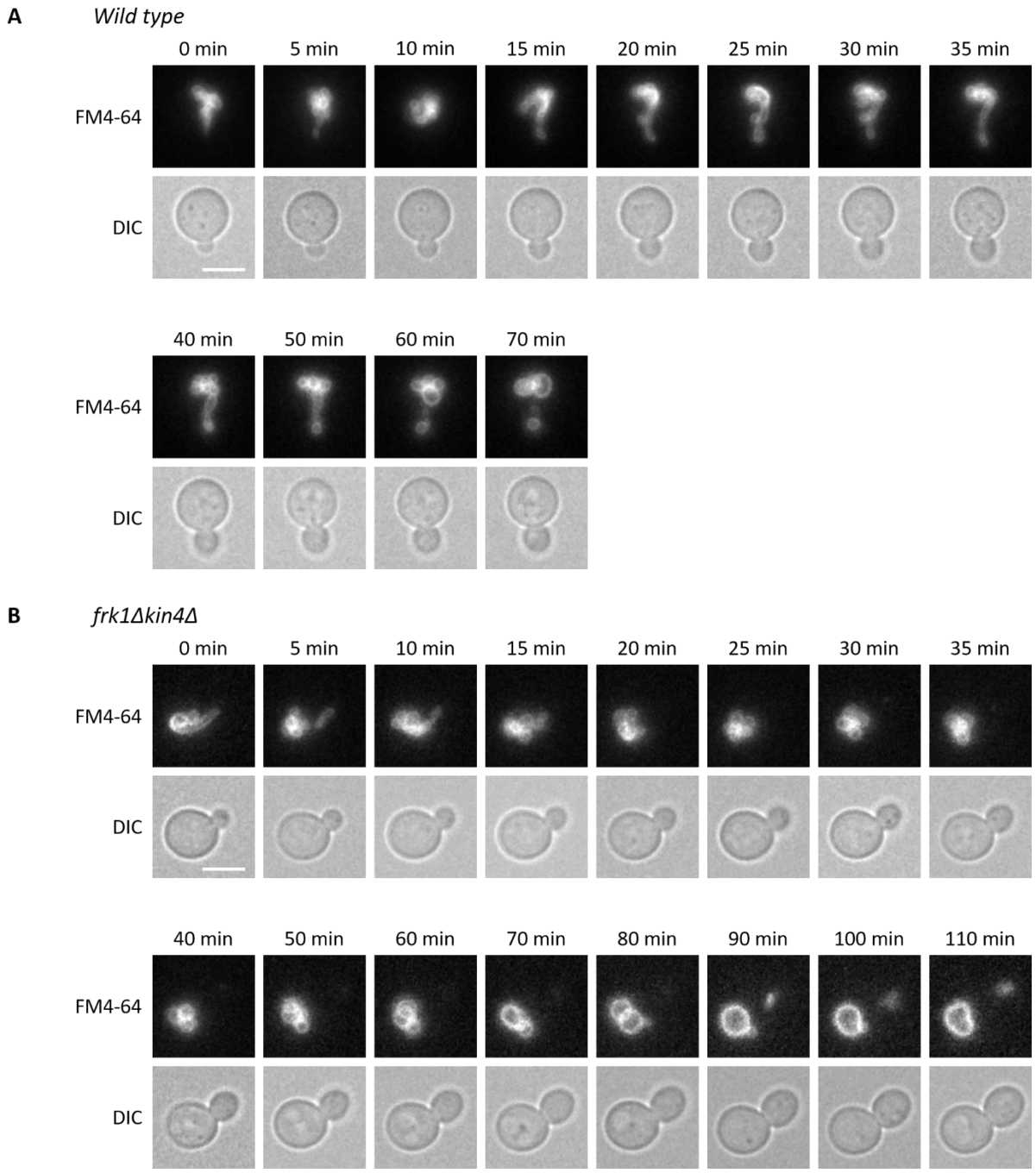

Figure 5.3 Time lapse analysis for vacuole movement. Time lapse images of FM4-64 pulse chased wild type (A) and *frk1Δkin4Δ* (B) cells were taken at 5min interval. Kin4 and Frk1 are not required for segregation structure formation but for maintenance of these structures. Only a small fraction of the vacuole is passed on from mother to daughter between 80 and 90min of this image series (B). Scale bar is 5μm.

5.3 Kinase activity is required for regulation of vacuole inheritance and Vac17 protein level

Kin4 and Frk1 both have a conserved c-AMP kinase domain at the N-terminus of the protein. Elm1 phosphorylates Kin4 at Thr209 residue in the activation loop of the kinase domain. This phosphorylation is crucial for Kin4 activity in the SPoC. Interestingly, SPoC occurs at early anaphase but Thr209 residue phosphorylation is observed throughout the cell cycle (Caydasi et al., 2010b; Moore et al., 2010). It was intriguing to check whether Kin4 kinase activity is required for the vacuole inheritance. To test this, wild type *KIN4-GFP* and the *T209A* mutant were expressed in *frk1Δkin4Δ* cells. Vacuole inheritance was restored by wild type Kin4-GFP but not by the T209A mutant. Though there was no significance difference in the localisation of Kin4-GFP at the mother cell cortex and at the bud neck late in the cell cycle. The activation loop of Kin4 and Frk1 are identical in amino acid sequence including Thr209 residue. Moreover, as shown previously **(Chapter 4, Figure 4.12)**, toxicity caused by *FRK1* overexpression can be rescued by deletion of *ELM1* gene. This tempted us to hypothesize that Frk1 is also a potential substrate for Elm1. Therefore, Frk1-GFP was also tested in this assay. Indeed, wild type Frk1-GFP restored vacuole inheritance in contrast to the T209A mutant **(Figure 5.4 A)**. Kin4-GFP and Frk1-GFP along with their T209A mutants were tested by western blot using anti-GFP antibody. Kin4-GFP band migrated slower than the T209A mutant on the gel as reported previously (Caydasi et al., 2010b; Moore et al., 2010). Interestingly, the Frk1-GFP bands showed a similar pattern in that the wild type protein band migrated slower than the T209A mutant **(Figure 5.4 B)**. As described in Chapter 4, Vac17-ProtA levels were down in *frk1Δkin4Δ* cells compared to wild type cells. Vac17 protein amounts were restored back to almost wild type levels in *frk1Δkin4Δ* cells expressing Kin4 or Frk1-GFP in contrast to in cells expressing the T209A kinase versions **(Figure 5.5 A, B)**. Moreover, Vac17-ProtA migrates slower in *frk1Δkin4Δ* cells compared to wild type cells and a similar pattern was observed upon re-introduction of Kin4 and Frk1 T209A mutant copies **(**Figure 5.5 **A)**.

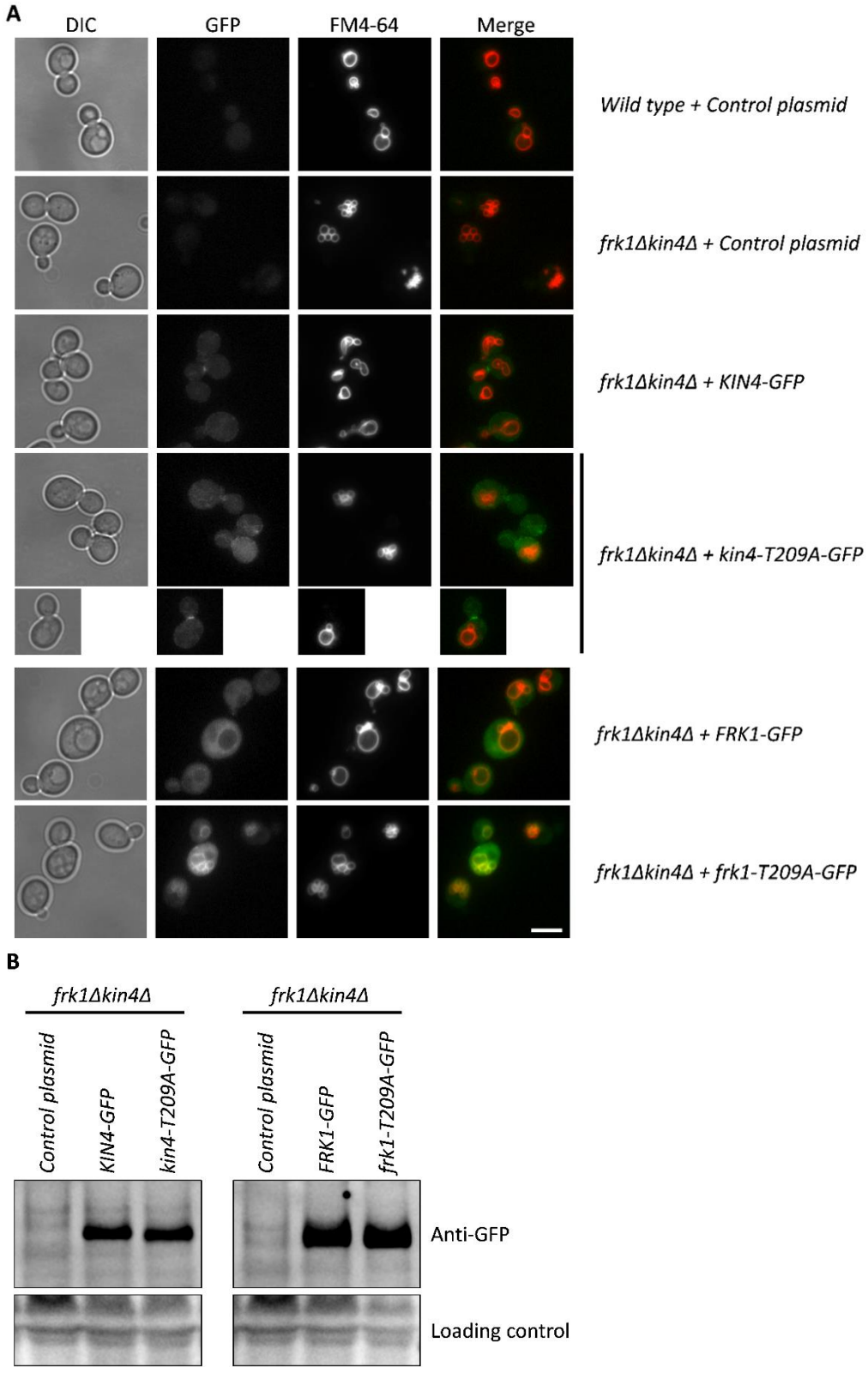

Figure 5.4 Kin4 and Frk1 catalytic activity is required for vacuole inheritance. (A) Kin4 and Frk1-GFP but not Kin4-T209A and Frk1-T209A-GFP restore vacuole inheritance in frk1kin4 cells to the normal level. Scale bar is 5μm. (B) Expression of Kin4-GFP and Frk1-GFP (WT and T209A mutant) were analysed by western blot using anti-GFP antibody.

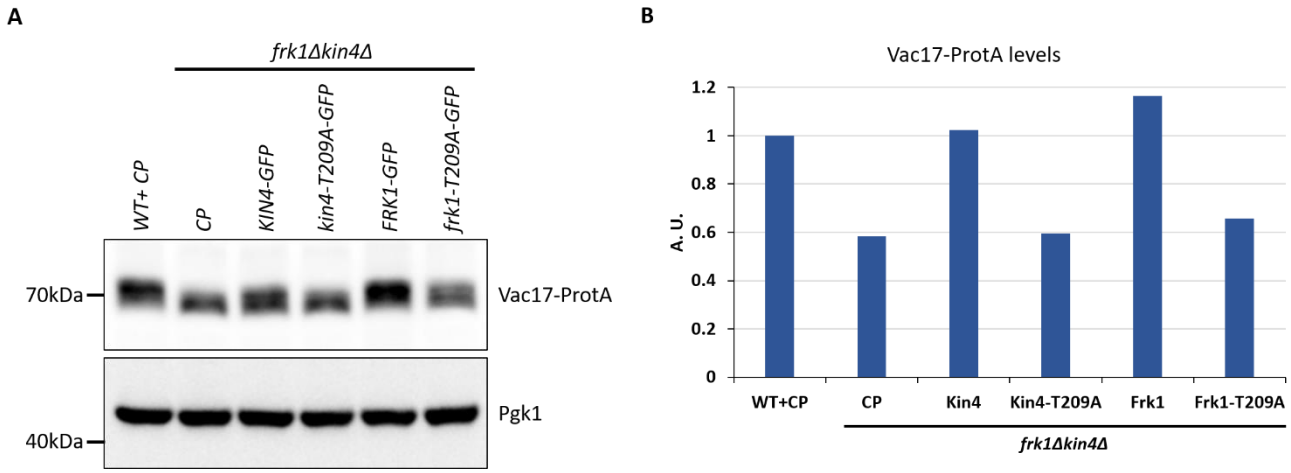

Figure 5.5 Vac17-ProtA levels are regulated by Kin4 and Frk1 kinase activity. (A) Vac17-ProtA was analysed by immunoblotting by anti-ProtA and anti-Pgk1 antibodies. (B) The samples were loaded 2 times and WT+CP band intensity value was set to 1 A.U. and other bands' values were normalised accordingly. A.U. is arbitrary units. CP is control plasmid.

Furthermore, since Elm1 is required for activation of Kin4 by phosphorylating Kin4 at Thr209, vacuole inheritance was analysed in *elm1Δ* cells. Indeed, many *elm1Δ* cells are defective in vacuole inheritance compared to wild type cells **(Figure 5.6)**. Again, as in *frk1Δkin4Δ* cells, in *elm1Δ* cells the level of Vac17 is decreased and Vac17 migrates differently in SDS-PAGE compared to in wild type cells, suggesting Vac17 phosphorylation is affected by the *elm1* mutation. The inheritance defect in *elm1Δ* cells is more pronounced than in *kin4Δ* cells and resembles more *frk1Δkin4Δ* cells. Combined, all these observations strongly suggest that Elm1 activates both Kin4 and Frk1 by phosphorylation of Thr209 in the activation loop and that this is required for the vacuole inheritance.

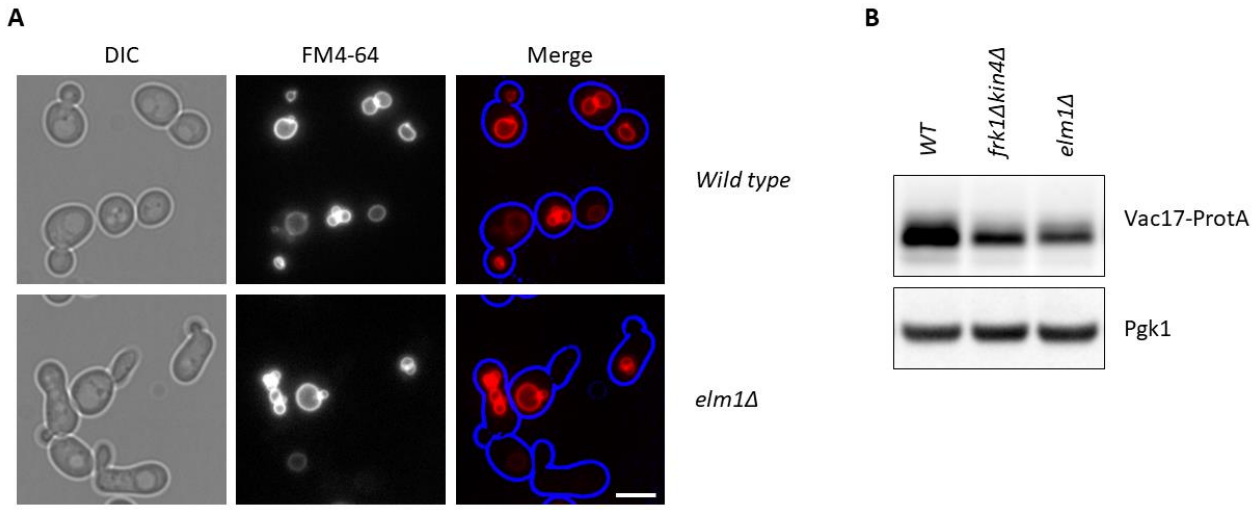

Figure 5.6 *elm1Δ* cells are defective in vacuole inheritance. Vacuole inheritance (A) and Vac17 protein levels (B) were analysed by fluorescence microscopy and immunoblotting respectively. Scale bar is 5µm.

5.4 Stabilization of Vac17 rescues the inheritance defect in *frk1Δkin4Δ* cells

We next asked if the defect in vacuole inheritance in *frk1Δkin4Δ* cells is a consequence of reduced Vac17 levels. The controlled breakdown of Vac17 requires the activity of the two redundant ubiquitin ligases Dma1 and Dma2. *DMA1* was knocked out in *frk1Δkin4Δ* and Vac17-ProtA levels and vacuole inheritance were analysed in *frk1Δkin4Δdma1Δ* cells. It was observed that the additional deletion of *DMA1* in *frk1Δkin4Δ* cells rescued the inheritance defect almost to the wild type level. Western blot analysis revealed that Vac17 protein levels in *frk1Δkin4Δdma1Δ* are restored to similar levels as in wild type cells **(Figure 5.7)**. This clearly indicated that the vacuole inheritance defect in *frk1Δkin4Δ* is a consequence of reduced levels of Vac17.

In addition, we analysed the effect of Vac17 mutants defective in Dma1/2 dependent breakdown on vacuole inheritance in *frk1Δkin4Δ* cells. C-terminally GFP tagged *VAC17*, *VAC17-S222A* and *VAC17-T240A* were expressed in *frk1Δkin4Δvac17Δ* cells and vacuole inheritance was analysed. As expected, *frk1Δkin4Δvac17Δ* cells expressing Vac17-GFP showed a severe defect in vacuole inheritance. But interestingly, Vac17-S222A-GFP and Vac17-T240A-GFP both restored the vacuole inheritance to the normal level in *frk1Δkin4Δvac17Δ* cells and the inappropriate positioning of the vacuoles in the bud was also observed. Moreover, Vac17-ProtA levels of S222A and T240A mutants were not affected by the absence of *FRK1* and *KIN4* **(Figure 5.8)** This demonstrated that Vac17 stable mutants

rescued the defect in vacuole inheritance in *frk1Δkin4Δ* cells and suggest that Kin4 and Frk1 act upstream of the Dma1/2 dependent breakdown of Vac17.

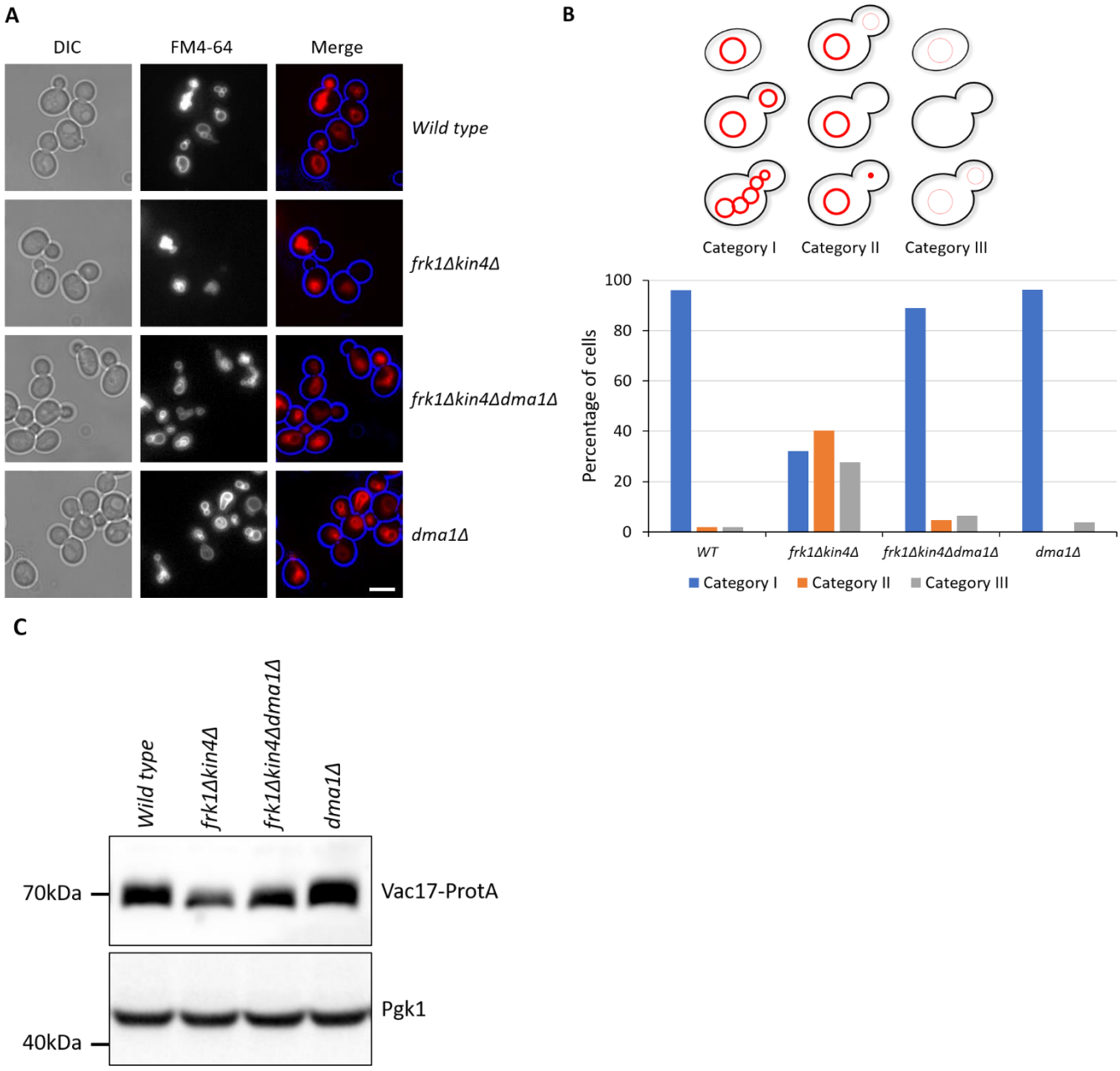

Figure 5.7 In the absence of *DMA1*, Kin4 and Frk1 are almost dispensable for vacuole inheritance. Vacuole inheritance (A, B) and Vac17 protein level (C) were analysed in wild type, *frk1Δkin4Δ*, *frk1Δkin4Δdma1Δ* and *dma1Δ*. Scale bar is 5µm. A minimum of 100 cells were analysed for quantification in (B).

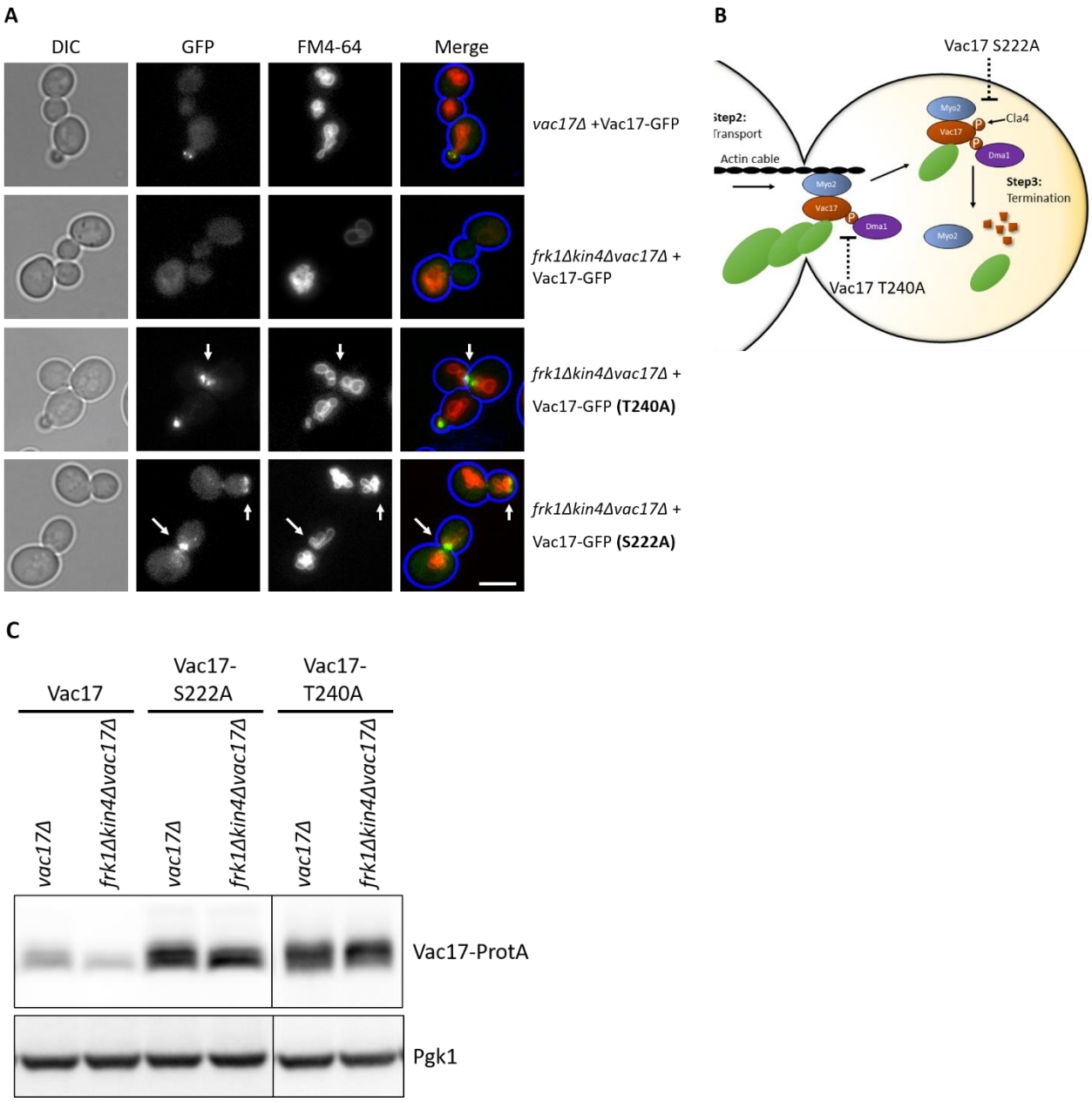

Figure 5.8 Vac17-T240A and S222A mutants restored vacuole inheritance in *frk1Δkin4Δ* cells. (A) Vac17 mutants resistant to Dma1 dependent breakdown not only rescue vacuole inheritance but also lead to inappropriate positioning of the vacuole in the bud (arrows) in *frk1Δkin4Δvac17Δ* cells. Scale bar is 5µm. (B) Model showing steps affected by Vac17 T240A and S222A mutants. (C) The levels of ProteinA tagged Vac17, Vac17-S222A and Vac17-T240A in *vac17Δ* and *frk1Δkin4Δvac17Δ* cells were analysed by immunoblotting.

5.5 Kin4 and Frk1 prevent premature Vac17 breakdown in the mother

Dma1 has been reported to associate with Vac17 already before it is activated by Cla4 in the bud. We hypothesised that in *frk1Δkin4Δ* cells, Dma1 is already active in the mother thereby degrading Vac17 before vacuoles have reached the bud. To test this, we analysed Vac17-ProtA levels in cells that fail to transport vacuoles to the bud but still recruit Vac17 to the vacuole (Yau et al., 2014). *myo2-D1297N* cells harbour a mutation in the Myo2 cargo binding domain that specifically affect its interaction with Vac17. This mutant shows increased levels of Vac17 as Dma1/Dma2 dependent degradation is not activated by Cla4/Ste20 in the mother (Eves et al., 2012; Ishikawa et al., 2003). Indeed, in *myo2-D1297N* cells Vac17 levels are upregulated **(Figure 5.9 A)** and are comparable to Vac17-S222A protein levels. Moreover, it has been shown that Vac17-Thr240 phosphorylation is unperturbed in these cells and Dma1 can bind Vac17 (Yau et al., 2014). Interestingly, expression of *myo2-D1297N* in *frk1Δkin4Δ* cells did not lead to increased level of Vac17-ProtA. In fact, there was no clear difference in Vac17 levels between *frk1Δkin4Δ* cells with either *MYO2* or *myo2-D1297N*. Furthermore, *vac17-S222A* was expressed in *frk1Δkin4Δ* cells with *myo2-D1297N* mutant. It was observed that *vac17-S222A* expression restored protein levels in *frk1Δkin4Δ* cells with *myo2-D1297N* to normal level as in wild type cells with *myo2-D1297N* **(Figure 5.9 B)**. These results demonstrated that Kin4 and Frk1 prevent Dma1-dependent premature degradation of Vac17 in mother.

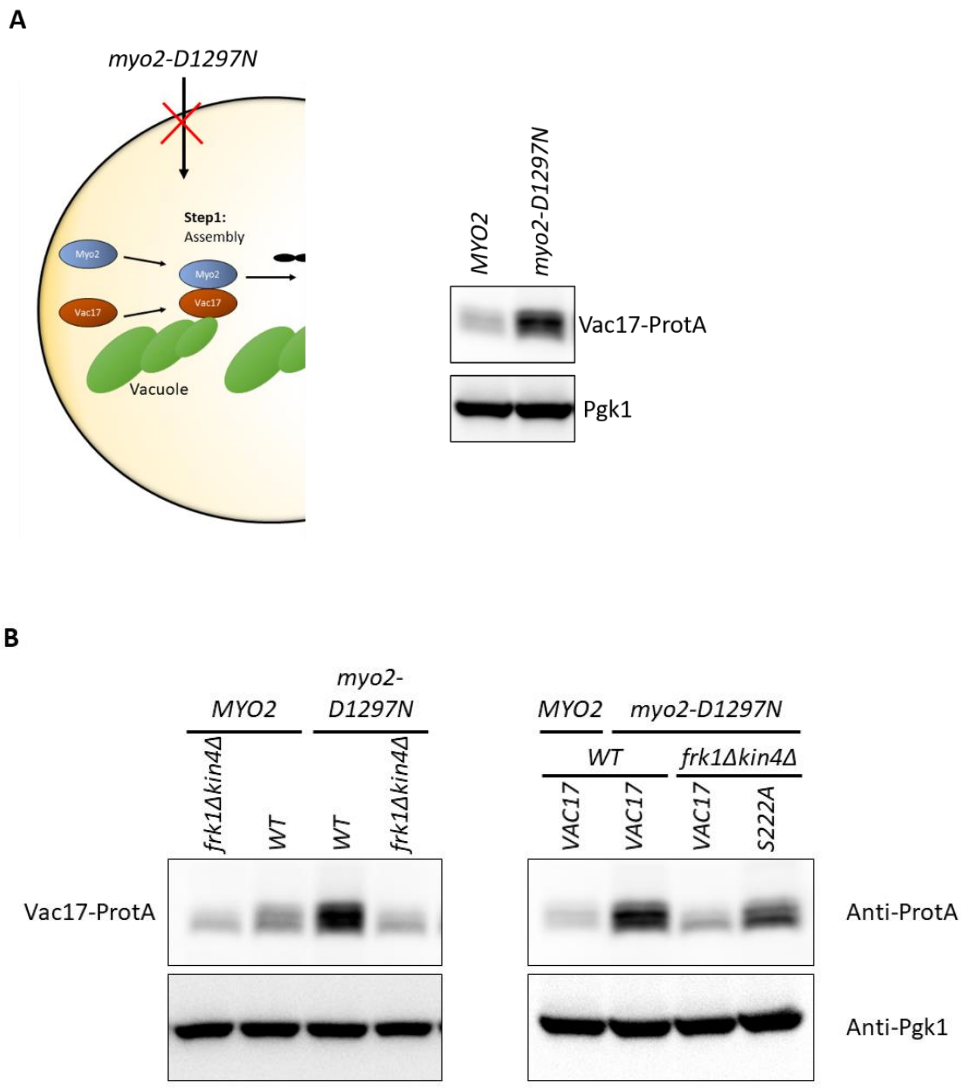

Figure 5.9 Kin4 and Frk1 are required to maintain elevated Vac17 level in Myo2-D129N mutant cells. (A) Model presenting the step affected by Myo2-D1297N mutant which leads to defect in vacuole inheritance and increase in Vac17-ProtA levels. (B) Vac17-ProtA WT and S222A were analysed in *frk1Δkin4Δ* cells expressing Myo2-D1297N mutant. Pgk1 was used as a loading control.

5.6 Overexpression of Kin4 and Frk1 stabilises Vac17

We next asked if Kin4 and Frk1 can regulate Vac17 stability. To test this *VAC17-GFP* was expressed along with either *GAL-KIN4* or *GAL-FRK1* in *bfa1Δ* cells, because *KIN4* and *FRK1* overexpression causes lethality in wild type cells by blocking mitotic exit via Bfa1. The cells were grown overnight in raffinose medium and shifted to galactose medium to induce expression. The induction was carried out for 6h and the cells were imaged with fluorescence microscopy. It was observed that overexpression of either *KIN4* or *FRK1* increased the Vac17-GFP signal compared to the cells expressing control plasmid. Furthermore, Vac17-GFP was localised either at the bud tip or at the bud neck in large budded cells, implying a block in

degradation in the bud. In agreement with this is the observation that in many cells vacuole positioning was inappropriate as observed in *dma1Δdma2Δ* cells. Western blot analysis revealed that Vac17-ProtA levels were elevated in cells overexpressing either *KIN4* or *FRK1* compared to the control cells **(Figure 5.10)**. This demonstrated that Vac17 levels are upregulated by *KIN4* and *FRK1* overexpression. Therefore, it can be concluded that Kin4 and Frk1 are key factors that regulate Vac17 stability in the cell.

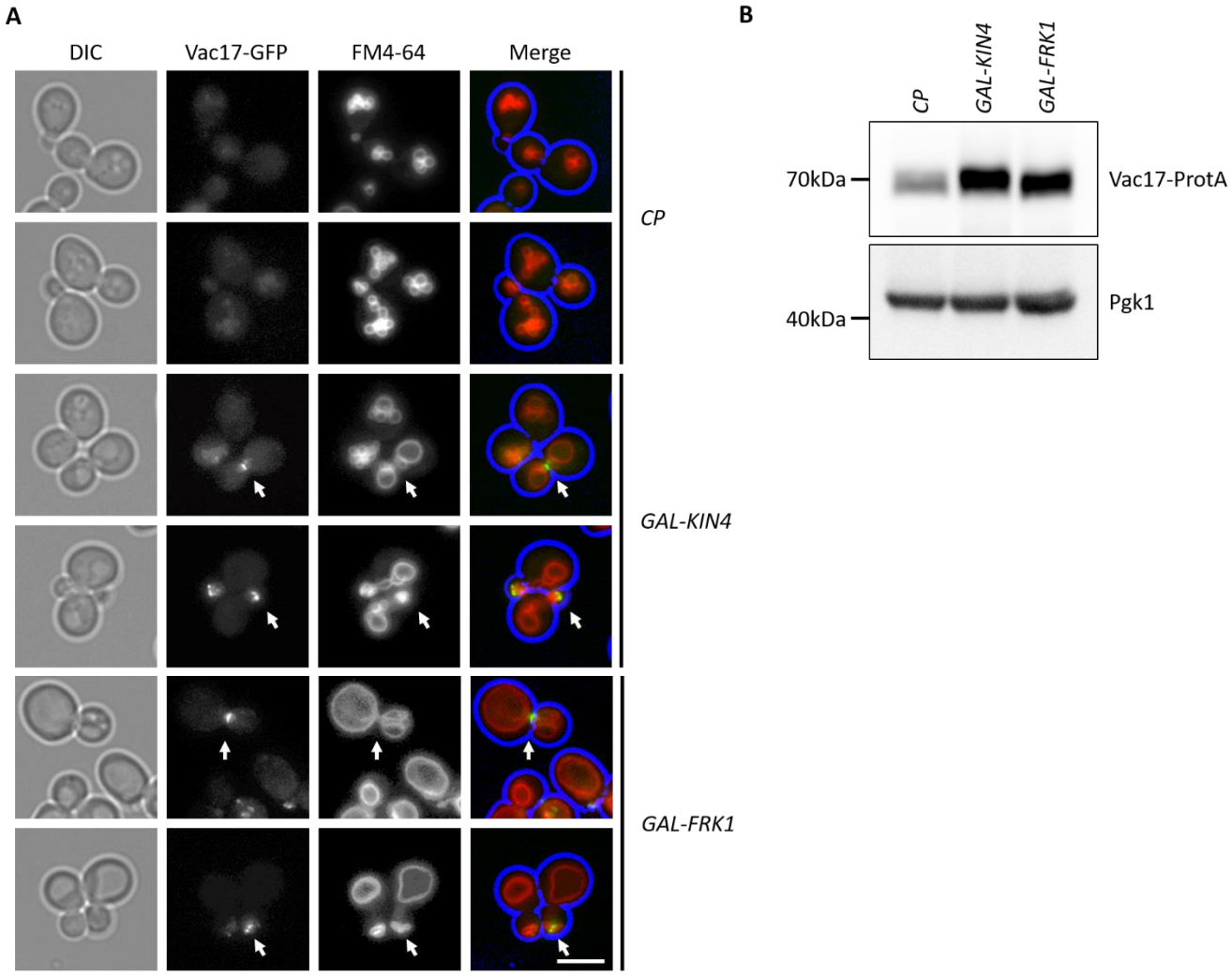

Figure 5.10 Vac17 levels are elevated upon Kin4 and Frk1 overexpression. (A) Induction of *GAL-KIN4* and *GAL-FRK1* in *bfa1Δ* cells resulted in increased level of Vac17-GFP and mispositioning of vacuole (FM4-64) in the bud (arrows). (B) TCA lysates of *bfa1Δ* cells expressing Vac17-ProtA along with either *GAL-KIN4* or *GAL-FRK1* were analysed by immunoblotting using anti-ProtA and anti-Pgk1 antibodies. CP indicates control plasmid.

5.7 Kin4 phosphorylates Vac17 *in vitro*

To unravel underlying mechanism of Kin4 activity in Vac17 maintenance we sought to determine whether Kin4 can phosphorylate Vac17. Vac17 is highly phosphorylated and has been shown to be a direct substrate for Cdc28 and Cla4 kinases (Peng and Weisman, 2008; Yau et al., 2017). The pattern of Vac17 is affected by Kin4 and Frk1 *in vivo* as in *frk1Δkin4Δ* cells Vac17-ProtA migrates differently on SDS-PAGE gel. To test whether Vac17 is a direct target of Kin4, an *in vitro* kinase assay was performed using radio-labelled ^{32}P-γATP. GST-Kin4 and GST-Kin4-T209A were purified from yeast and 6xHis-Vac17 (1-195aa) and (97-355aa) fragments were purified from *E. coli*. GST-Kin4 phosphorylates both Vac17 fragments whereas GST-Kin4-T209A showed strongly reduced activity. Moreover, GST-Kin4 also undergoes auto-phosphorylation. Again, in case of the T209A mutant autophosphorylation was very low **(Figure 5.11)**. These results demonstrated that Kin4 phosphorylates Vac17 *in vitro* and phosphorylation of Kin4 at Thr209 is crucial for its kinase activity.

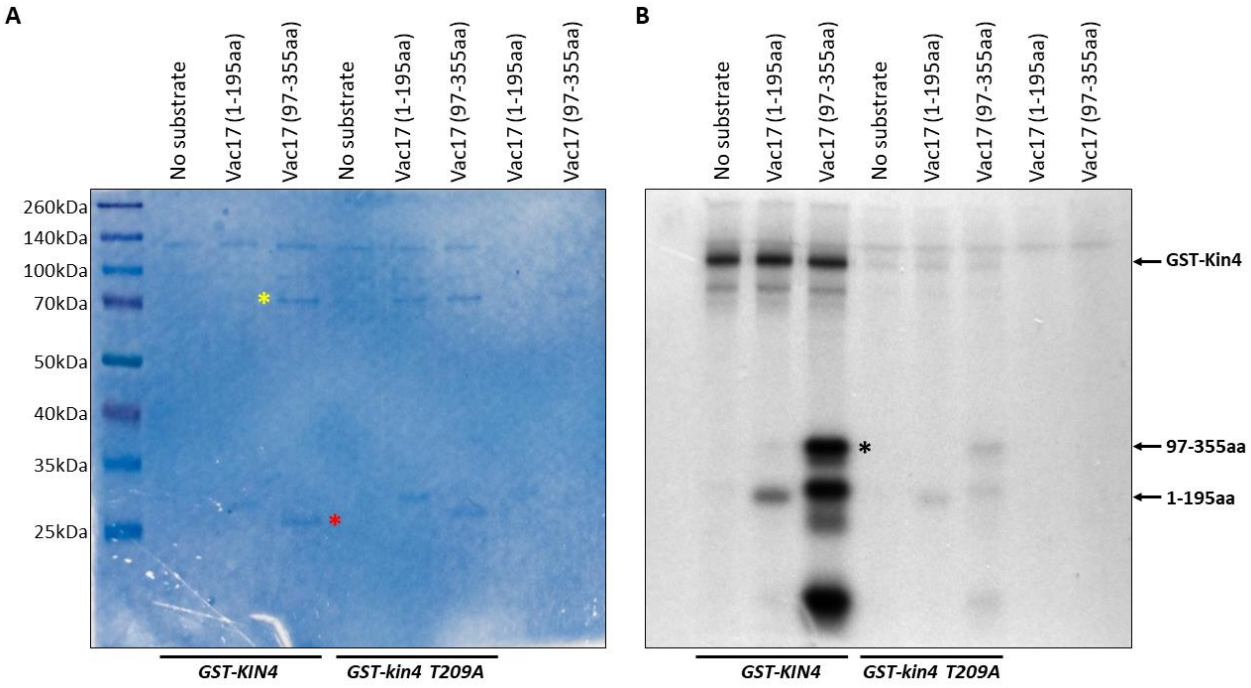

Figure 5.11 Kin4 phosphorylates Vac17 (1-195aa) and (97-355aa) fragments *in vitro*. Kin4-T209A showed strong reduction in phosphorylation Vac17 fragments. *In vitro* kinase assay was performed at 30°C using 32-γ-P labelled ATP and the samples were run on SDS-PAGE gel. The gel was stained with Coomassie stain (A) and the radiolabelled signals were captured by autoradiography on film (B). Yellow asterisk: non-specific band from *E. coli* purification, red asterisk: Vac17 (97-355aa) breakdown product and black asterisk: Vac17 (97-355aa) band at the right size.

5.8 Discussion

In this chapter, we sought to characterise the role of Kin4 and Frk1 in vacuole transport. Our results show that Elm1 dependent phosphorylation of Kin4 at Thr209 residue is critical for its function in vacuole inheritance and thus Kin4 kinase activity is required for both vacuole inheritance and Vac17 stability in the cell. Moreover, Kin4 is partially redundant with Frk1 in this process.

Vacuole transport is a multistep process. It involves the formation of the Vac17-Myo2 transport complex that is required for active transport of vacuolar membranes along actin tracks towards the bud. The presence of a segregation structure is a reflection of this directed movement. Once the vacuoles are delivered, degradation of Vac17 occurs to release the vacuole in the bud. The co-immunoprecipitation experiment showed Vac17 forms a complex with Myo2 in *frk1Δkin4Δ* cells. It was also observed that the segregation structures are formed in *frk1Δkin4Δ* cells but are not maintained. These results indicated that the phenotype observed in *frk1Δkin4Δ* cells is not because of a defect in initiation of transport but rather at a later stage of the process.

The defect in vacuole inheritance in *frk1Δkin4Δ* is rescued by expression of mutants in Vac17 (*VAC17-S222A* and *VAC17-T240A)* that block Dma1-dependent degradation that was presumed to occur in the daughter cell. Moreover, deletion of *DMA1* in *frk1Δkin4Δ* cells restored vacuole inheritance and Vac17 levels. These results suggest that Dma1 is involved in the reduced stability of Vac17 in *frk1Δkin4Δ* cells. This is in line with the observation that in *frk1Δkin4Δ* cells the level of Vac17 S222A or T240A are unaltered compared to in wild type cells. In *frk1Δkin4Δ* cells with Myo2-D1297N mutant Vac17 levels were much lower compared to in wild type cells and expression of *VAC17-S222A* mutant restored Vac17 levels. This demonstrated that Kin4 and Frk1 prevent premature degradation of Vac17 in mother. Furthermore, overexpression of *KIN4* and *FRK1* lead not only to the increased levels of Vac17 but also affected vacuole positioning in the bud. The defect in vacuole positioning is similar to that observed in *dma1Δdma2Δ* cells. These observations corroborated the hypothesis that Kin4 and Frk1 positively regulate Vac17 stability via inhibiting Dma1 dependent premature Vac17 degradation. In addition, we showed that GST-Kin4 phosphorylates Vac17 *in vitro* and phosphorylation of Kin4 at Thr209 is required for its activity. Taken together, we hypothesize that Kin4 and Frk1 phosphorylate Vac17 in the mother and this phosphorylation prevents Dma1 dependent premature Vac17 degradation. However, direct evidence for the above hypothesis is still lacking.

Chapter 6 General discussion

6.1 Introduction

Cells must maintain their organelles to sustain metabolism and viability. Hence, organelle partitioning during cell division is tightly regulated. The budding yeast, *S. cerevisiae* has been studied extensively to uncover the principle mechanisms for organelle maintenance and many of these are conserved to multicellular organisms. In *S. cerevisiae*, peroxisomes are segregated more or less equally between mother and daughter cell by retention of some peroxisomes in the mother and transport of the other to the bud. Retention requires Inp1 and transport to the emerging bud requires the peroxisomal Myosin receptor Inp2. However, very little is known about the regulation of Inp1 and Inp2. Therefore, the main aim of the study was to identify and characterise novel factors that are required for organelle maintenance, primarily for peroxisomes. This was done by using SGA methodology based high throughput microscopy screens which provide an unique platform to approach biological questions in a very systematic manner (Cohen and Schuldiner, 2011). This led to the identification of Kin4 and its paralogue Frk1 as new regulator of organelle inheritance.

The secondary aim of the study was to discern a correlation between Pex27 and Vps1 in fission of peroxisomes. In *S. cerevisiae*, Vps1 is the dynamin related protein that plays a major role in peroxisome multiplication. Initially it was established that Pex27 and Vps1 act in the same pathway. Next, we sought to gain mechanistic insight in their interplay during fission process. In this chapter the role of Kin4 and Frk1 in peroxisome and vacuole transport to the bud is discussed in detail whereas the Pex27 and Vps1 study is analysed in **section 6.6**.

6.2 Identification of novel genes involved in peroxisome maintenance

In budding yeast, retention of organelles in the mother and transport to the emerging bud occur concomitantly. Hence, several mechanisms have evolved to monitor organelle movement during cell growth and division. Peroxisome fission does not occur in *dnm1Δvps1Δ* cells hence they harbour mostly one elongated peroxisome that is retained with one end in the mother and with the other end being pulled into the bud. Upon cytokinesis this single peroxisome is split in two **(Chapter 4, Figure 4.1)**. However, a small percentage (approximately 5-10%) of *dnm1Δvps1Δ* cells fail to position their peroxisome at the bud neck during cytokinesis which leads to a segregation defect in those cells. At the cell population level, there is a weak inheritance defect. This sensitised genetic background was further explored to perform a genome wide high throughput microscopy screen to identify molecular players that have not

been implicated previously in peroxisome maintenance. The screen analysis revealed several mutants along with, *INP1* and *INP2*, that affected either peroxisome inheritance or abundance. Among novel mutants, *KIN4* showed a reproducible strong phenotype and hence was studied further to understand its role in peroxisome maintenance. In *dnm1Δvps1Δkin4Δ* cells peroxisomes frequently fail to be delivered to the daughter cell. This phenotype is due to a defect in forward transport to the bud rather than excessive retention in the mother. A *KIN4* deletion in cells that are proficient in DRP-mediated peroxisome fission, are also affected in peroxisome segregation, with a clear delay of transport of peroxisomes to bud i.e. small buds are frequently found lacking peroxisomes. However, large budded cells frequently do obtain peroxisomes. This may explain why Kin4 had not been identified in previous genetic screens and has not been implicated in organelle transport. However, we showed that Frk1, a Kin4 paralog, also contributes to the peroxisome inheritance. In *frk1Δkin4Δ* cells peroxisome transport to the bud is strongly affected and resembles that of *inp2Δ* cells. Moreover, Frk1 shares significant identity and similarity at the amino acid sequence level with Kin4 therefore we concluded that Frk1 is a Kin4 paralog.

Kin4 is a well characterised SPoC kinase and is required for mitotic spindle alignment maintenance (D'Aquino et al., 2005; Pereira and Schiebel, 2005). However, functional roles of Kin4 in SPoC and in peroxisome inheritance are distinct as the defect in peroxisome transport is not a consequence of Kin4 requirement in SPoC and peroxisome transport is dispensable for Kin4 activity in SPoC. Overexpression of Kin4 is lethal to the cells and we found that overexpression of Frk1 is also inhibits growth. In both cases the toxicity caused due to overexpression can be rescued by deletion of either *BFA1* or *ELM1*. This demonstrated that Frk1 is, in addition to Kin4, a potential SPoC kinase. It would be intriguing to test if Frk1 plays a role in SPoC and thus eventually regulate MEN. This could be tested analysing whether Frk1 is a direct substrate of the kinase Elm1 and whether Frk1 can phosphorylate Bfa1 *in vivo*.

6.3 Kin4 and Frk1 contribute to vacuole transport

We found that inheritance of vacuoles is also strongly affected in *frk1Δkin4Δ* cells and resembled that of *vac17Δ* cells. Delivery of vacuoles to the bud has been characterised in detail hence we focussed our attention to this process as to further understand the role Kin4 and Frk1 in organelle transport. There are three important steps in organelle transport; i) loading of an organelle on a myosin motor, ii) the transport along actin cables and iii) the termination process including release of organelle from motor and proper deposition in the bud. Vac17 is broken down in the bud resulting in release of the vacuole from the motor. Degradation of Vac17 is

spatially regulated and requires i) recruitment of E3 ubiquitin ligases Dma1/2 via phosphorylation of Vac17-Thr240 and ii) Dma1/2 activation via phosphorylation of Vac17-Ser222 by the bud-localised Cla4/Ste20, PAK kinases.

We found that in *frk1Δkin4Δ* cells vacuole segregation structures are formed but are not maintained over long periods as observed in control cells. Furthermore, Myo2-Vac17 complexes form albeit at a lower level. This is because the steady state level of Vac17 is reduced in this mutant. A block in Dma1 dependent Vac17 breakdown, either by *DMA1* deletion or by expressing Vac17 mutants (S222A and T240A) resistant to DMA1-dependent breakdown rescued the inheritance defect in *frk1Δkin4Δ* cells. Therefore, we conclude that the defect in vacuole transport in *frk1Δkin4Δ* cells is due to decreased levels of Vac17. Furthermore, we provided evidence that Vac17 can be broken down in the mother cell in a Dma1/2-dependent manner but that this is prevented by Frk1 and Kin4. Moreover, overexpression of Kin4 and Frk1 not only leads to an increased level of Vac17 but also causes mispositioning of the vacuole in the bud as reported previously for *dma1Δdma2Δ* cells or Vac17 versions that cannot be degraded in the daughter cell (Yau et al., 2014). Taken together these observations clearly demonstrated that Kin4 and Frk1 are negative regulators of Dma1 dependent Vac17 degradation **(Figure 6.1)**.

Next, we showed that Kin4 and Frk1 kinase activity is required for vacuole inheritance and to maintain Vac17 steady state levels. Moreover, the Vac17 phosphorylation pattern is changed in *frk1Δkin4Δ* cells compared to that of in wild type cells. In addition, Kin4 phosphorylates Vac17 *in vitro*. Together we were tempted to hypothesise that Kin4 and Frk1 can phosphorylate Vac17 *in vivo*.

Therefore, we propose that Kin4 and Frk1 stabilise Vac17 most probably via direct phosphorylation of Vac17 which makes it less susceptible to Dma1 dependent degradation. It will be interesting to identify potential phosphosites in Vac17 by means of *in vitro* kinase assay followed by mass spectrometry analysis. Moreover, immunoprecipitated Vac17 from the cells expressing *GAL-KIN4* (or *GAL-FRK1*) can be useful for mass spectrometry analysis to identify changes in Vac17 phosphorylation pattern *in vivo* and novel phosphosites. The identified amino acid residues can then be further tested *in vivo* for their role in vacuole inheritance. In addition, we will need to test whether Dma1 associates and ubiquitinates Vac17 in *frk1Δkin4Δ* cells. Albeit, it is crucial to test whether Kin4 can act directly on Dma1 to prevent Dma1 recruitment to Vac17 or indirectly by negatively regulating Cla4 dependent Vac17 phosphorylation. At this

moment, we favour the hypothesis discussed above, but alternative models cannot be ruled out yet. For instance, the low steady state levels of Vac17 in *frk1Δkin4Δ* cells may be a result of a decrease in Vac17 synthesis and that overexpression of Kin4 or Frk1 induces synthesis. Pulse chase experiments to test this are essential to determine this. Another possibility is that Kin4 and Frk1 do not directly act on Vac17 but regulate Vac17 levels via other factors.

Frk1 has been previously implicated in vacuole fusion since overexpression of Frk1 resulted in enlarged vacuoles (Arlt et al., 2011). In this study we could reproduce this observation though overexpression of Kin4 does not cause this effect **(Chapter 5, Figure 5.10)**. Moreover, we also found that Frk1-GFP, WT and T209A mutant, both localise to the vacuole. This suggests that Frk1 has an independent function in vacuole fusion. In future, it would be intriguing to understand the role of Frk1 in overall vacuole dynamics. Since Frk1 is a kinase it will be interesting to identify its substrates to gain more mechanistic insights in its activity. Genetic screen(s) can be employed to unravel the pathways through which Frk1 regulates vacuole morphology. This screen might identify potential Frk1 substrates.

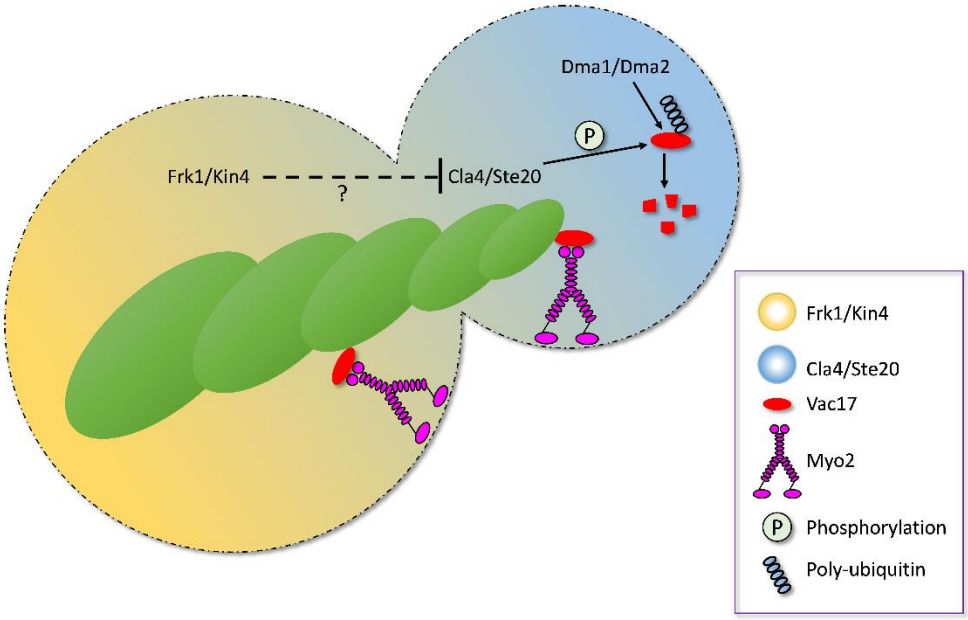

Figure 6.1 Model showing regulation of vacuole transport. Kin4 and Frk1 mainly localise to mother whereas Cla4 and Ste20 to the bud. Thus, they monitor vacuole transport in a spatial temporal manner.

6.4 Dma1 and Cla4 regulate peroxisome inheritance

In *dma1Δdma2Δ* cells Vac17 protein levels are elevated and that causes inappropriate positioning of vacuole at the bud neck in late cell cycle. Similarly, mis-positioning of peroxisomes in *dma1Δdma2Δ* cells has been reported (Yau et al., 2014). However, change (if any) in Inp2 protein levels has not been described. We tested Inp2-ProtA levels in wild type and *dma1Δdma2Δ* cells. Indeed, the level of Inp2 was strongly increased in *dma1Δdma2Δ* compared to in wild type cells **(Figure 6.2 A)**. Overexpression of *CLA4* causes defect in vacuole inheritance via excessive Vac17 breakdown (Bartholomew and Hardy, 2009). Therefore, peroxisome inheritance was analysed in these cells expressing *TEF2-mCherry-CLA4*. Interestingly, there was a clear defect in peroxisome inheritance and the phenotype observed was like in that observed in *inp2Δ* cells **(Figure 6.2 B)**. Furthermore, the level of Inp2-ProtA is reduced. In contrast, cells expressing *TEF2-mCherry-FRK1* showed increased Inp2-ProtA level **(Figure 6.2 C)**. Moreover, in *frk1Δkin4Δ* cells Inp2 levels are also low as observed for Vac17 **(Chapter 4, Figure 4.19)**. Therefore, from all the above results we conclude that the machinery that regulates vacuole transport also regulates peroxisome transport in very similar manner. Though further in detail studies are required to corroborate above hypothesis. The predicted PEST sequences in Inp2 are not as strong as in Vac17. However, Inp2 is stabilised in *dma1Δdma2Δ* cells. Hence, it will be interesting first test whether Dma1 can interact with Inp2 *in vivo*, test whether it is ubiquitinated dependent upon Dma1 activity. It would subsequently be interesting to perform mass spectrometry analysis on Inp2 from *dma1Δdma2Δ* cells. This may identify threonine residues that can undergo phosphorylation and thus can act as a docking site for Dma1 and Dma2 fork head domains. Moreover, some of the phosphosites hint towards being direct target of Cla4 kinase.

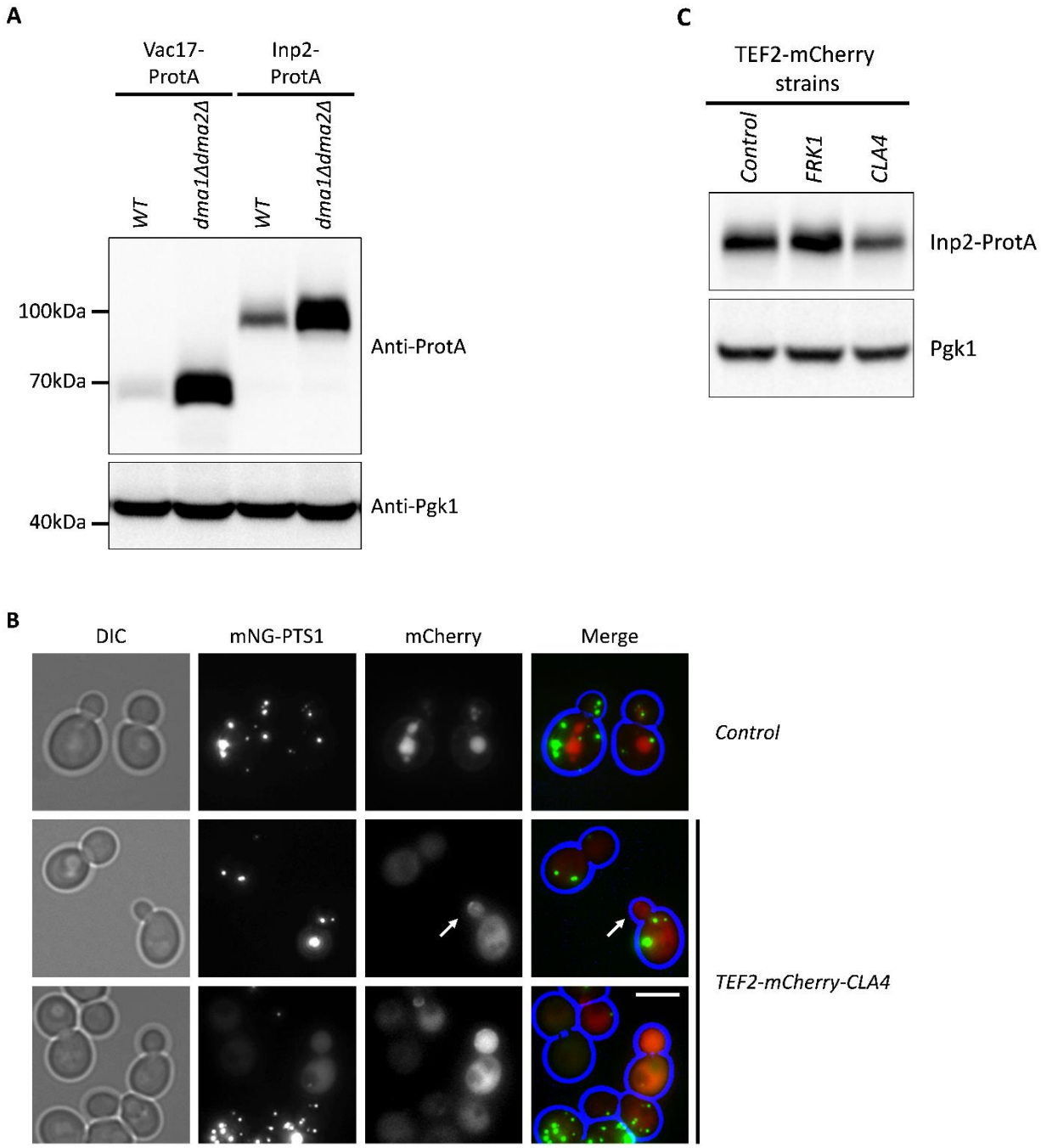

Figure 6.2 Dma1 and Cla4 regulate peroxisome transport. (A) Inp2-ProtA and Vac17-ProtA were expressed in wild type and *dma1Δdma2Δ* cells. TCA lysates were analysed by immunoblotting. (B) Microscopy images for peroxisome inheritance in cells expressing TEF2-mCherry-Cla4 where mNG-PTS1 was used to label peroxisomes. Arrow indicates the bud devoid of peroxisomes and shows mCherry-Cla4 concentrated at the bud tip. Scale bar is 5µm. (C) *TEF2-mCherry-CLA4* and *FRK1* expression cause a reduction or increase in Inp2 level respectively.

6.5 Kin4 and Cla4 act antagonistically in multiple pathways

The termination of nuclear inheritance involves activation of the mitotic exit network (MEN) in late anaphase. Once the SPB is segregated to the bud, this signals to activate the MEN via Tem1-GTPase. Bfa1 is the GAP for Tem1 and hence negatively regulates MEN activation. Bfa1 phosphorylation by Kin4 is required for GAP activity. Thus, Kin4 down regulates MEN activation. Therefore, overexpression of Kin4 is toxic to the cells because cells do not exit from mitosis. However, toxicity can be rescued via additional deletion of either *bfa1Δ* or *elm1Δ*. In wild type cells, Kin4 is kept inactive in the bud by Lte1. Here, Lte1 recruitment to the bud cortex and activity require the PAK kinase, Cla4 (Bertazzi et al., 2011; Falk et al., 2011; Hofken and Schiebel, 2002; Jensen et al., 2002). Moreover, Lte1 directly contributes to MEN activation. Hence, overexpression of Lte1 in mother cell leads to aneuploidy due to premature SPB segregation in the mother before it reaches to the bud. So, it is well established that Kin4 and Cla4 act antagonistically during mitosis or nuclear inheritance. In this study we show that Kin4 and Cla4 act in vacuole and peroxisome transport in opposing manner. Is this a general set up to spatially regulate transport processes?

Their contribution to organelle inheritance is accomplished by forming intracellular gradient in the cell in opposite direction, where Kin4 is mainly localised to mother cells whereas Cla4 to the bud. Thus, they regulate multiple processes in a spatial and temporal way. However, if the gradient is disturbed either by gene deletion or overexpression of *KIN4* or *CLA4*, it directly affects the tight monitoring of organelle maintenance. This tempted us to hypothesize that Kin4 and Cla4 are intracellular morphogens that decide the cell fate during asymmetric cell growth. Therefore, it is intriguing to understand how the Kin4 and Cla4 gradients are set up at the early stage of cell cycle.

The mechanisms unravelled by studying organelle dynamics in yeasts are of general relevance. For instance, in humans, PAK kinases have multiple important functions and these functions are crucial for smooth mitotic progression. In some cancers, PAKs are hyperactivated and this causes defects in chromosome segregation leading to multipolar spindle formation (Kumar et al., 2017). Melanosomes are organelle that synthesize and store melanin pigment. Dynamics of melanosomes between melanocytes and keratinocytes is crucial for hair and skin colour. Myo5a, a classV myosin, and its receptor Slac2 (Melanophilin) play important role in melanosome transport in actin rich dendrites of melanocytes (Marks and Seabra, 2001). Slac2 harbours PEST sequences which target it for degradation via activity of Calpain proteases. Slac2-PESTΔ mutant is defective in degradation and lead to perinuclear aggregation of

melanosomes (Fukuda and Itoh, 2004). Thus, melanosome transport resembles that of vacuoles (yeast lysosomes). Moreover, melanosome biogenesis is similar to that of lysosomes (Marks and Seabra, 2001). In conclusion, the regulatory principles of organelle dynamics seem to be conserved from the yeast to the higher eukaryotes. Therefore, study of organelle maintenance in *S. cerevisiae* provides molecular insights that can be extrapolated to higher eukaryotes including humans.

6.6 Pex27 is a regulator of Vps1 in peroxisome fission process

Pex11 family proteins are conserved from yeast to higher eukaryotes. They play vital role in maintaining peroxisome abundance. In yeast as well as in human Pex11 is required for elongation of peroxisomes during the fission process. Moreover, it also recruits Dlp1 in humans and enhances Dnm1 GTPase activity in *H. polymorpha* (Itoyama et al., 2013; Li and Gould, 2003; Williams et al., 2015). In *S. cerevisiae,* Vps1 contributes more than Dnm1 to peroxisome fission. We show that Pex27 acts as a limiting factor in Vps1 dependent peroxisome multiplication. In contrast, Pex27 is not required for Dnm1 activity since overexpression of *DNM1* in *pex27Δ* cells induce multiple small peroxisomes. This showed that *DNM1* is a multicopy suppressor of *pex27Δ*. We also show that Pex11 is dispensable for Dnm1 dependent fission if Dnm1 is overexpressed. Moreover, we showed that Pex27 and Vps1 interact *in vivo*. This further corroborated the *PEX27* and *VPS1* genetic interactions. Furthermore, Pex27-mNG is localised to potential fission sites in *dnm1Δvps1Δ* cells. The exact mechanism through which Pex27 and Vps1 regulate peroxisome division is still unclear. It will be interesting to analyse the beads on string peroxisomal structure in *dnm1Δvps1Δ* and *dnm1Δpex27Δ* cells whether there is a difference in the constrictions or change in localisation of other auxiliary factors (if there any). In addition, overexpression of *PEX27* in *dnm1Δvps1Δ* cells might reveal if it can modify the membrane as has been described for mitochondria in mammalian cells where Dlp1 constricts the outer membrane so that a second dynamin, Dyn2, can act on it. In *S. cerevisiae*, mitochondrial fission in blocked in *dnm1Δ* cells. Hence, if Pex27 is one of the (if not only) Vps1 recruitment factors on peroxisomal membrane, then it is intriguing to analyse mitochondrial fission in *dnm1Δ* cells where Pex27 is mistargeted to mitochondria and test if Vps1 can substitute for Dnm1. Furthermore, the enlarged and elongated peroxisome morphology in *dnm1Δvps1Δ* cells provides an opportunity to study tethers and contact sites that are not implicated previously and help to understand new aspects of cell metabolism.

References

Adams, I.R., and Kilmartin, J.V. (2000). Spindle pole body duplication: a model for centrosome duplication? Trends Cell Biol 10, 329-335.

Al-Saryi, N.A., Al-Hejjaj, M.Y., van Roermund, C.W.T., Hulmes, G.E., Ekal, L., Payton, C., Wanders, R.J.A., and Hettema, E.H. (2017). Two NAD-linked redox shuttles maintain the peroxisomal redox balance in Saccharomyces cerevisiae. Sci Rep 7, 11868.

Arai, S., Noda, Y., Kainuma, S., Wada, I., and Yoda, K. (2008). Ypt11 functions in bud-directed transport of the Golgi by linking Myo2 to the coatomer subunit Ret2. Curr Biol 18, 987-991.

Arlt, H., Perz, A., and Ungermann, C. (2011). An overexpression screen in Saccharomyces cerevisiae identifies novel genes that affect endocytic protein trafficking. Traffic 12, 1592-1603.

Bardin, A.J., Visintin, R., and Amon, A. (2000). A mechanism for coupling exit from mitosis to partitioning of the nucleus. Cell 102, 21-31.

Bartholomew, C.R., and Hardy, C.F. (2009). p21-activated kinases Cla4 and Ste20 regulate vacuole inheritance in Saccharomyces cerevisiae. Eukaryot Cell 8, 560-572.

Beach, D.L., Thibodeaux, J., Maddox, P., Yeh, E., and Bloom, K. (2000). The role of the proteins Kar9 and Myo2 in orienting the mitotic spindle of budding yeast. Curr Biol 10, 1497-1506.

Bertazzi, D.T., Kurtulmus, B., and Pereira, G. (2011). The cortical protein Lte1 promotes mitotic exit by inhibiting the spindle position checkpoint kinase Kin4. J Cell Biol 193, 1033-1048.

Bobola, N., Jansen, R.P., Shin, T.H., and Nasmyth, K. (1996). Asymmetric accumulation of Ash1p in postanaphase nuclei depends on a myosin and restricts yeast mating-type switching to mother cells. Cell 84, 699-709.

Bohl, F., Kruse, C., Frank, A., Ferring, D., and Jansen, R.P. (2000). She2p, a novel RNA-binding protein tethers ASH1 mRNA to the Myo4p myosin motor via She3p. EMBO J 19, 5514-5524.

Boldogh, I.R., Yang, H.C., Nowakowski, W.D., Karmon, S.L., Hays, L.G., Yates, J.R., 3rd, and Pon, L.A. (2001). Arp2/3 complex and actin dynamics are required for actin-based mitochondrial motility in yeast. Proc Natl Acad Sci U S A 98, 3162-3167.

Breslow, D.K., Cameron, D.M., Collins, S.R., Schuldiner, M., Stewart-Ornstein, J., Newman, H.W., Braun, S., Madhani, H.D., Krogan, N.J., and Weissman, J.S. (2008). A comprehensive strategy enabling high-resolution functional analysis of the yeast genome. Nat Methods 5, 711-718.

Bretscher, A. (2003). Polarized growth and organelle segregation in yeast: the tracks, motors, and receptors. J Cell Biol 160, 811-816.

Brown, L.A., and Baker, A. (2003). Peroxisome biogenesis and the role of protein import. J Cell Mol Med 7, 388-400.

Butland, G., Babu, M., Diaz-Mejia, J.J., Bohdana, F., Phanse, S., Gold, B., Yang, W., Li, J., Gagarinova, A.G., Pogoutse, O., et al. (2008). eSGA: E. coli synthetic genetic array analysis. Nat Methods 5, 789-795.

Catlett, N.L., Duex, J.E., Tang, F., and Weisman, L.S. (2000). Two distinct regions in a yeast myosin-V tail domain are required for the movement of different cargoes. J Cell Biol 150, 513-526.

Caydasi, A.K., Ibrahim, B., and Pereira, G. (2010a). Monitoring spindle orientation: Spindle position checkpoint in charge. Cell Div 5, 28.

Caydasi, A.K., Khmelinskii, A., Duenas-Sanchez, R., Kurtulmus, B., Knop, M., and Pereira, G. (2017). Temporal and compartment-specific signals coordinate mitotic exit with spindle position. Nat Commun 8, 14129.

Caydasi, A.K., Kurtulmus, B., Orrico, M.I., Hofmann, A., Ibrahim, B., and Pereira, G. (2010b). Elm1 kinase activates the spindle position checkpoint kinase Kin4. J Cell Biol 190, 975-989.

Caydasi, A.K., and Pereira, G. (2012). SPOC alert--when chromosomes get the wrong direction. Exp Cell Res 318, 1421-1427.

Chan, L.Y., and Amon, A. (2009). The protein phosphatase 2A functions in the spindle position checkpoint by regulating the checkpoint kinase Kin4. Genes Dev 23, 1639-1649.

Chernyakov, I., Santiago-Tirado, F., and Bretscher, A. (2013). Active segregation of yeast mitochondria by Myo2 is essential and mediated by Mmr1 and Ypt11. Curr Biol 23, 1818-1824.

Cohen, Y., and Schuldiner, M. (2011). Advanced methods for high-throughput microscopy screening of genetically modified yeast libraries. Methods Mol Biol 781, 127-159.

D'Aquino, K.E., Monje-Casas, F., Paulson, J., Reiser, V., Charles, G.M., Lai, L., Shokat, K.M., and Amon, A. (2005). The protein kinase Kin4 inhibits exit from mitosis in response to spindle position defects. Mol Cell 19, 223-234.

Dimmer, K.S., and Rapaport, D. (2017). Mitochondrial contact sites as platforms for phospholipid exchange. Biochim Biophys Acta 1862, 69-80.

Effelsberg, D., Cruz-Zaragoza, L.D., Schliebs, W., and Erdmann, R. (2016). Pex9p is a new yeast peroxisomal import receptor for PTS1-containing proteins. J Cell Sci 129, 4057-4066.

Erdmann, R., and Blobel, G. (1995). Giant peroxisomes in oleic acid-induced Saccharomyces cerevisiae lacking the peroxisomal membrane protein Pmp27p. J Cell Biol 128, 509-523.

Eshel, D., Urrestarazu, L.A., Vissers, S., Jauniaux, J.C., van Vliet-Reedijk, J.C., Planta, R.J., and Gibbons, I.R. (1993). Cytoplasmic dynein is required for normal nuclear segregation in yeast. Proc Natl Acad Sci U S A 90, 11172-11176.

Estrada, P., Kim, J., Coleman, J., Walker, L., Dunn, B., Takizawa, P., Novick, P., and Ferro-Novick, S. (2003). Myo4p and She3p are required for cortical ER inheritance in Saccharomyces cerevisiae. J Cell Biol 163, 1255-1266.

Eves, P.T., Jin, Y., Brunner, M., and Weisman, L.S. (2012). Overlap of cargo binding sites on myosin V coordinates the inheritance of diverse cargoes. J Cell Biol 198, 69-85.

Fagarasanu, A., Fagarasanu, M., Eitzen, G.A., Aitchison, J.D., and Rachubinski, R.A. (2006). The peroxisomal membrane protein Inp2p is the peroxisome-specific receptor for the myosin V motor Myo2p of Saccharomyces cerevisiae. Dev Cell 10, 587-600.

Fagarasanu, A., Mast, F.D., Knoblach, B., Jin, Y., Brunner, M.J., Logan, M.R., Glover, J.N., Eitzen, G.A., Aitchison, J.D., Weisman, L.S., et al. (2009). Myosin-driven peroxisome partitioning in S. cerevisiae. J Cell Biol 186, 541-554.

Fagarasanu, M., Fagarasanu, A., Tam, Y.Y., Aitchison, J.D., and Rachubinski, R.A. (2005). Inp1p is a peroxisomal membrane protein required for peroxisome inheritance in Saccharomyces cerevisiae. J Cell Biol 169, 765-775.

Falk, J.E., Campbell, I.W., Joyce, K., Whalen, J., Seshan, A., and Amon, A. (2016). LTE1 promotes exit from mitosis by multiple mechanisms. Mol Biol Cell 27, 3991-4001.

Falk, J.E., Chan, L.Y., and Amon, A. (2011). Lte1 promotes mitotic exit by controlling the localization of the spindle position checkpoint kinase Kin4. Proc Natl Acad Sci U S A 108, 12584-12590.

Fehrenbacher, K.L., Yang, H.C., Gay, A.C., Huckaba, T.M., and Pon, L.A. (2004). Live cell imaging of mitochondrial movement along actin cables in budding yeast. Curr Biol 14, 1996-2004.

Fidaleo, M. (2010). Peroxisomes and peroxisomal disorders: the main facts. Exp Toxicol Pathol 62, 615-625.

Fukuda, M., and Itoh, T. (2004). Slac2-a/melanophilin contains multiple PEST-like sequences that are highly sensitive to proteolysis. J Biol Chem 279, 22314-22321.

Gandre-Babbe, S., and van der Bliek, A.M. (2008). The novel tail-anchored membrane protein Mff controls mitochondrial and peroxisomal fission in mammalian cells. Mol Biol Cell 19, 2402-2412.

Ghaemmaghami, S., Huh, W.K., Bower, K., Howson, R.W., Belle, A., Dephoure, N., O'Shea, E.K., and Weissman, J.S. (2003). Global analysis of protein expression in yeast. Nature 425, 737-741.

Giaever, G., Chu, A.M., Ni, L., Connelly, C., Riles, L., Veronneau, S., Dow, S., Lucau-Danila, A., Anderson, K., Andre, B., et al. (2002). Functional profiling of the Saccharomyces cerevisiae genome. Nature 418, 387-391.

Gietz, R.D., and Woods, R.A. (2006). Yeast transformation by the LiAc/SS Carrier DNA/PEG method. Methods Mol Biol 313, 107-120.

Hanahan, D. (1983). Studies on transformation of Escherichia coli with plasmids. J Mol Biol 166, 557-580.

Hettema, E.H., Erdmann, R., van der Klei, I., and Veenhuis, M. (2014). Evolving models for peroxisome biogenesis. Curr Opin Cell Biol 29, 25-30.

Hettema, E.H., Girzalsky, W., van Den Berg, M., Erdmann, R., and Distel, B. (2000). Saccharomyces cerevisiae pex3p and pex19p are required for proper localization and stability of peroxisomal membrane proteins. EMBO J 19, 223-233.

Hill, S.M., Hao, X., Gronvall, J., Spikings-Nordby, S., Widlund, P.O., Amen, T., Jorhov, A., Josefson, R., Kaganovich, D., Liu, B., et al. (2016). Asymmetric Inheritance of Aggregated Proteins and Age Reset in Yeast Are Regulated by Vac17-Dependent Vacuolar Functions. Cell Rep 16, 826-838.

Hoepfner, D., Schildknegt, D., Braakman, I., Philippsen, P., and Tabak, H.F. (2005). Contribution of the endoplasmic reticulum to peroxisome formation. Cell 122, 85-95.

Hoepfner, D., van den Berg, M., Philippsen, P., Tabak, H.F., and Hettema, E.H. (2001). A role for Vps1p, actin, and the Myo2p motor in peroxisome abundance and inheritance in Saccharomyces cerevisiae. J Cell Biol 155, 979-990.

Hofken, T., and Schiebel, E. (2002). A role for cell polarity proteins in mitotic exit. EMBO J 21, 4851-4862.

Hohfeld, J., Veenhuis, M., and Kunau, W.H. (1991). PAS3, a Saccharomyces cerevisiae gene encoding a peroxisomal integral membrane protein essential for peroxisome biogenesis. J Cell Biol 114, 1167-1178.

Huber, A., Koch, J., Kragler, F., Brocard, C., and Hartig, A. (2012). A subtle interplay between three Pex11 proteins shapes de novo formation and fission of peroxisomes. Traffic 13, 157-167.

Huh, W.K., Falvo, J.V., Gerke, L.C., Carroll, A.S., Howson, R.W., Weissman, J.S., and O'Shea, E.K. (2003). Global analysis of protein localization in budding yeast. Nature 425, 686-691.

Hutchins, M.U., Veenhuis, M., and Klionsky, D.J. (1999). Peroxisome degradation in Saccharomyces cerevisiae is dependent on machinery of macroautophagy and the Cvt pathway. J Cell Sci 112 (Pt 22), 4079-4087.

Hwang, E., Kusch, J., Barral, Y., and Huffaker, T.C. (2003). Spindle orientation in Saccharomyces cerevisiae depends on the transport of microtubule ends along polarized actin cables. J Cell Biol 161, 483-488.

Ishikawa, K., Catlett, N.L., Novak, J.L., Tang, F., Nau, J.J., and Weisman, L.S. (2003). Identification of an organelle-specific myosin V receptor. J Cell Biol 160, 887-897.

Itoh, T., Toh, E.A., and Matsui, Y. (2004). Mmr1p is a mitochondrial factor for Myo2p-dependent inheritance of mitochondria in the budding yeast. EMBO J 23, 2520-2530.

Itoh, T., Watabe, A., Toh, E.A., and Matsui, Y. (2002). Complex formation with Ypt11p, a rab-type small GTPase, is essential to facilitate the function of Myo2p, a class V myosin, in mitochondrial distribution in Saccharomyces cerevisiae. Mol Cell Biol 22, 7744-7757.

Itoyama, A., Michiyuki, S., Honsho, M., Yamamoto, T., Moser, A., Yoshida, Y., and Fujiki, Y. (2013). Mff functions with Pex11pbeta and DLP1 in peroxisomal fission. Biol Open 2, 998-1006.

Jensen, S., Geymonat, M., Johnson, A.L., Segal, M., and Johnston, L.H. (2002). Spatial regulation of the guanine nucleotide exchange factor Lte1 in Saccharomyces cerevisiae. J Cell Sci 115, 4977-4991.

Jin, Y., Sultana, A., Gandhi, P., Franklin, E., Hamamoto, S., Khan, A.R., Munson, M., Schekman, R., and Weisman, L.S. (2011). Myosin V transports secretory vesicles via a Rab GTPase cascade and interaction with the exocyst complex. Dev Cell 21, 1156-1170.

Jin, Y., and Weisman, L.S. (2015). The vacuole/lysosome is required for cell-cycle progression. Elife 4.

Johnston, G.C., Prendergast, J.A., and Singer, R.A. (1991). The Saccharomyces cerevisiae MYO2 gene encodes an essential myosin for vectorial transport of vesicles. J Cell Biol 113, 539-551.

Jones, J.M., Morrell, J.C., and Gould, S.J. (2004). PEX19 is a predominantly cytosolic chaperone and import receptor for class 1 peroxisomal membrane proteins. J Cell Biol 164, 57-67.

Joshi, A.S., Nebenfuehr, B., Choudhary, V., Satpute-Krishnan, P., Levine, T.P., Golden, A., and Prinz, W.A. (2018). Lipid droplet and peroxisome biogenesis occur at the same ER subdomains. Nat Commun 9, 2940.

Kaur, N., and Hu, J. (2009). Dynamics of peroxisome abundance: a tale of division and proliferation. Curr Opin Plant Biol 12, 781-788.

Kiel, J.A., Veenhuis, M., and van der Klei, I.J. (2006). PEX genes in fungal genomes: common, rare or redundant. Traffic 7, 1291-1303.

Kim, P.K., Mullen, R.T., Schumann, U., and Lippincott-Schwartz, J. (2006). The origin and maintenance of mammalian peroxisomes involves a de novo PEX16-dependent pathway from the ER. J Cell Biol 173, 521-532.

Klionsky, D.J. (1997). Protein transport from the cytoplasm into the vacuole. J Membr Biol 157, 105-115.

Klouwer, F.C., Berendse, K., Ferdinandusse, S., Wanders, R.J., Engelen, M., and Poll-The, B.T. (2015). Zellweger spectrum disorders: clinical overview and management approach. Orphanet J Rare Dis 10, 151.

Knoblach, B., and Rachubinski, R.A. (2015a). Sharing the cell's bounty - organelle inheritance in yeast. J Cell Sci 128, 621-630.

Knoblach, B., and Rachubinski, R.A. (2015b). Transport and retention mechanisms govern lipid droplet inheritance in Saccharomyces cerevisiae. Traffic 16, 298-309.

Knoblach, B., Sun, X., Coquelle, N., Fagarasanu, A., Poirier, R.L., and Rachubinski, R.A. (2013). An ER-peroxisome tether exerts peroxisome population control in yeast. EMBO J 32, 2439-2453.

Knoops, K., de Boer, R., Kram, A., and van der Klei, I.J. (2015). Yeast pex1 cells contain peroxisomal ghosts that import matrix proteins upon reintroduction of Pex1. J Cell Biol 211, 955-962.

Knoops, K., Manivannan, S., Cepinska, M.N., Krikken, A.M., Kram, A.M., Veenhuis, M., and van der Klei, I.J. (2014). Preperoxisomal vesicles can form in the absence of Pex3. J Cell Biol 204, 659-668.

Kobayashi, S., Tanaka, A., and Fujiki, Y. (2007). Fis1, DLP1, and Pex11p coordinately regulate peroxisome morphogenesis. Exp Cell Res 313, 1675-1686.

Kumar, R., Sanawar, R., Li, X., and Li, F. (2017). Structure, biochemistry, and biology of PAK kinases. Gene 605, 20-31.

Kunau, W.H., Dommes, V., and Schulz, H. (1995). beta-oxidation of fatty acids in mitochondria, peroxisomes, and bacteria: a century of continued progress. Prog Lipid Res 34, 267-342.

Kuravi, K., Nagotu, S., Krikken, A.M., Sjollema, K., Deckers, M., Erdmann, R., Veenhuis, M., and van der Klei, I.J. (2006). Dynamin-related proteins Vps1p and Dnm1p control peroxisome abundance in Saccharomyces cerevisiae. J Cell Sci 119, 3994-4001.

Lazarow, P.B., and Fujiki, Y. (1985). Biogenesis of peroxisomes. Annu Rev Cell Biol 1, 489-530.

Lee, J.E., Westrate, L.M., Wu, H., Page, C., and Voeltz, G.K. (2016). Multiple dynamin family members collaborate to drive mitochondrial division. Nature 540, 139-143.

Legesse-Miller, A., Zhang, S., Santiago-Tirado, F.H., Van Pelt, C.K., and Bretscher, A. (2006). Regulated phosphorylation of budding yeast's essential myosin V heavy chain, Myo2p. Mol Biol Cell 17, 1812-1821.

Li, X., and Gould, S.J. (2003). The dynamin-like GTPase DLP1 is essential for peroxisome division and is recruited to peroxisomes in part by PEX11. J Biol Chem 278, 17012-17020.

Li, Y.Y., Yeh, E., Hays, T., and Bloom, K. (1993). Disruption of mitotic spindle orientation in a yeast dynein mutant. Proc Natl Acad Sci U S A 90, 10096-10100.

Lipatova, Z., Tokarev, A.A., Jin, Y., Mulholland, J., Weisman, L.S., and Segev, N. (2008). Direct interaction between a myosin V motor and the Rab GTPases Ypt31/32 is required for polarized secretion. Mol Biol Cell 19, 4177-4187.

Long, R.M., Gu, W., Lorimer, E., Singer, R.H., and Chartrand, P. (2000). She2p is a novel RNA-binding protein that recruits the Myo4p-She3p complex to ASH1 mRNA. EMBO J 19, 6592-6601.

Longtine, M.S., McKenzie, A., 3rd, Demarini, D.J., Shah, N.G., Wach, A., Brachat, A., Philippsen, P., and Pringle, J.R. (1998). Additional modules for versatile and economical PCR-based gene deletion and modification in Saccharomyces cerevisiae. Yeast 14, 953-961.

Maekawa, H., Priest, C., Lechner, J., Pereira, G., and Schiebel, E. (2007). The yeast centrosome translates the positional information of the anaphase spindle into a cell cycle signal. J Cell Biol 179, 423-436.

Marks, M.S., and Seabra, M.C. (2001). The melanosome: membrane dynamics in black and white. Nat Rev Mol Cell Biol 2, 738-748.

Marshall, P.A., Krimkevich, Y.I., Lark, R.H., Dyer, J.M., Veenhuis, M., and Goodman, J.M. (1995). Pmp27 promotes peroxisomal proliferation. J Cell Biol 129, 345-355.

Mast, F.D., Herricks, T., Strehler, K.M., Miller, L.R., Saleem, R.A., Rachubinski, R.A., and Aitchison, J.D. (2018). ESCRT-III is required for scissioning new peroxisomes from the endoplasmic reticulum. J Cell Biol 217, 2087-2102.

Mast, F.D., Jamakhandi, A., Saleem, R.A., Dilworth, D.J., Rogers, R.S., Rachubinski, R.A., and Aitchison, J.D. (2016). Peroxins Pex30 and Pex29 Dynamically Associate with Reticulons to Regulate Peroxisome Biogenesis from the Endoplasmic Reticulum. J Biol Chem 291, 15408-15427.

Menendez-Benito, V., van Deventer, S.J., Jimenez-Garcia, V., Roy-Luzarraga, M., van Leeuwen, F., and Neefjes, J. (2013). Spatiotemporal analysis of organelle and macromolecular complex inheritance. Proc Natl Acad Sci U S A 110, 175-180.

Miller, R.K., Cheng, S.C., and Rose, M.D. (2000). Bim1p/Yeb1p mediates the Kar9p-dependent cortical attachment of cytoplasmic microtubules. Mol Biol Cell 11, 2949-2959.

Miller, R.K., and Rose, M.D. (1998). Kar9p is a novel cortical protein required for cytoplasmic microtubule orientation in yeast. J Cell Biol 140, 377-390.

Moore, J.K., Chudalayandi, P., Heil-Chapdelaine, R.A., and Cooper, J.A. (2010). The spindle position checkpoint is coordinated by the Elm1 kinase. J Cell Biol 191, 493-503.

Motley, A.M., Galvin, P.C., Ekal, L., Nuttall, J.M., and Hettema, E.H. (2015). Reevaluation of the role of Pex1 and dynamin-related proteins in peroxisome membrane biogenesis. J Cell Biol 211, 1041-1056.

Motley, A.M., and Hettema, E.H. (2007). Yeast peroxisomes multiply by growth and division. J Cell Biol 178, 399-410.

Motley, A.M., Nuttall, J.M., and Hettema, E.H. (2012a). Atg36: the Saccharomyces cerevisiae receptor for pexophagy. Autophagy 8, 1680-1681.

Motley, A.M., Nuttall, J.M., and Hettema, E.H. (2012b). Pex3-anchored Atg36 tags peroxisomes for degradation in Saccharomyces cerevisiae. EMBO J 31, 2852-2868.

Motley, A.M., Ward, G.P., and Hettema, E.H. (2008). Dnm1p-dependent peroxisome fission requires Caf4p, Mdv1p and Fis1p. J Cell Sci 121, 1633-1640.

Munck, J.M., Motley, A.M., Nuttall, J.M., and Hettema, E.H. (2009). A dual function for Pex3p in peroxisome formation and inheritance. J Cell Biol 187, 463-471.

Musacchio, A., and Salmon, E.D. (2007). The spindle-assembly checkpoint in space and time. Nat Rev Mol Cell Biol 8, 379-393.

Nagotu, S., Saraya, R., Otzen, M., Veenhuis, M., and van der Klei, I.J. (2008). Peroxisome proliferation in Hansenula polymorpha requires Dnm1p which mediates fission but not de novo formation. Biochim Biophys Acta 1783, 760-769.

Nunnari, J., and Walter, P. (1996). Regulation of organelle biogenesis. Cell 84, 389-394.

Opalinski, L., Kiel, J.A., Williams, C., Veenhuis, M., and van der Klei, I.J. (2011). Membrane curvature during peroxisome fission requires Pex11. EMBO J 30, 5-16.

Otera, H., Wang, C., Cleland, M.M., Setoguchi, K., Yokota, S., Youle, R.J., and Mihara, K. (2010). Mff is an essential factor for mitochondrial recruitment of Drp1 during mitochondrial fission in mammalian cells. J Cell Biol 191, 1141-1158.

Otzen, M., Rucktaschel, R., Thoms, S., Emmrich, K., Krikken, A.M., Erdmann, R., and van der Klei, I.J. (2012). Pex19p contributes to peroxisome inheritance in the association of peroxisomes to Myo2p. Traffic 13, 947-959.

Pan, X., and Goldfarb, D.S. (1998). YEB3/VAC8 encodes a myristylated armadillo protein of the Saccharomyces cerevisiae vacuolar membrane that functions in vacuole fusion and inheritance. J Cell Sci 111 (Pt 15), 2137-2147.

Pan, X., Roberts, P., Chen, Y., Kvam, E., Shulga, N., Huang, K., Lemmon, S., and Goldfarb, D.S. (2000). Nucleus-vacuole junctions in Saccharomyces cerevisiae are formed through the direct interaction of Vac8p with Nvj1p. Mol Biol Cell 11, 2445-2457.

Paumi, C.M., Menendez, J., Arnoldo, A., Engels, K., Iyer, K.R., Thaminy, S., Georgiev, O., Barral, Y., Michaelis, S., and Stagljar, I. (2007). Mapping protein-protein interactions for the

yeast ABC transporter Ycf1p by integrated split-ubiquitin membrane yeast two-hybrid analysis. Mol Cell 26, 15-25.

Pedersen, J.I. (1993). Peroxisomal oxidation of the steroid side chain in bile acid formation. Biochimie 75, 159-165.

Peng, Y., and Weisman, L.S. (2008). The cyclin-dependent kinase Cdk1 directly regulates vacuole inheritance. Dev Cell 15, 478-485.

Pereira, G., and Schiebel, E. (2005). Kin4 kinase delays mitotic exit in response to spindle alignment defects. Mol Cell 19, 209-221.

Pernice, W.M., Vevea, J.D., and Pon, L.A. (2016). A role for Mfb1p in region-specific anchorage of high-functioning mitochondria and lifespan in Saccharomyces cerevisiae. Nat Commun 7, 10595.

Pitts, K.R., Yoon, Y., Krueger, E.W., and McNiven, M.A. (1999). The dynamin-like protein DLP1 is essential for normal distribution and morphology of the endoplasmic reticulum and mitochondria in mammalian cells. Mol Biol Cell 10, 4403-4417.

Platta, H.W., and Erdmann, R. (2007). Peroxisomal dynamics. Trends Cell Biol 17, 474-484.

Raychaudhuri, S., and Prinz, W.A. (2008). Nonvesicular phospholipid transfer between peroxisomes and the endoplasmic reticulum. Proc Natl Acad Sci U S A 105, 15785-15790.

Rechsteiner, M., and Rogers, S.W. (1996). PEST sequences and regulation by proteolysis. Trends Biochem Sci 21, 267-271.

Riedl, J., Crevenna, A.H., Kessenbrock, K., Yu, J.H., Neukirchen, D., Bista, M., Bradke, F., Jenne, D., Holak, T.A., Werb, Z., et al. (2008). Lifeact: a versatile marker to visualize F-actin. Nat Methods 5, 605-607.

Roguev, A., Wiren, M., Weissman, J.S., and Krogan, N.J. (2007). High-throughput genetic interaction mapping in the fission yeast Schizosaccharomyces pombe. Nat Methods 4, 861-866.

Rottensteiner, H., Stein, K., Sonnenhol, E., and Erdmann, R. (2003). Conserved function of pex11p and the novel pex25p and pex27p in peroxisome biogenesis. Mol Biol Cell 14, 4316-4328.

Saraya, R., Cepinska, M.N., Kiel, J.A., Veenhuis, M., and van der Klei, I.J. (2010). A conserved function for Inp2 in peroxisome inheritance. Biochim Biophys Acta 1803, 617-622.

Schrader, M., Bonekamp, N.A., and Islinger, M. (2012). Fission and proliferation of peroxisomes. Biochim Biophys Acta 1822, 1343-1357.

Sellers, J.R., and Veigel, C. (2006). Walking with myosin V. Curr Opin Cell Biol 18, 68-73.

Shai, N., Schuldiner, M., and Zalckvar, E. (2016). No peroxisome is an island - Peroxisome contact sites. Biochim Biophys Acta 1863, 1061-1069.

Shai, N., Yifrach, E., van Roermund, C.W.T., Cohen, N., Bibi, C., L, I.J., Cavellini, L., Meurisse, J., Schuster, R., Zada, L., et al. (2018). Systematic mapping of contact sites reveals tethers and a function for the peroxisome-mitochondria contact. Nat Commun 9, 1761.

Simon, V.R., Karmon, S.L., and Pon, L.A. (1997). Mitochondrial inheritance: cell cycle and actin cable dependence of polarized mitochondrial movements in Saccharomyces cerevisiae. Cell Motil Cytoskeleton 37, 199-210.

Smaczynska-de, R., II, Allwood, E.G., Aghamohammadzadeh, S., Hettema, E.H., Goldberg, M.W., and Ayscough, K.R. (2010). A role for the dynamin-like protein Vps1 during endocytosis in yeast. J Cell Sci 123, 3496-3506.

Smith, J.J., and Aitchison, J.D. (2013). Peroxisomes take shape. Nat Rev Mol Cell Biol 14, 803-817.

Smith, J.J., Marelli, M., Christmas, R.H., Vizeacoumar, F.J., Dilworth, D.J., Ideker, T., Galitski, T., Dimitrov, K., Rachubinski, R.A., and Aitchison, J.D. (2002). Transcriptome profiling to identify genes involved in peroxisome assembly and function. J Cell Biol 158, 259-271.

Steinberg, S.J., Dodt, G., Raymond, G.V., Braverman, N.E., Moser, A.B., and Moser, H.W. (2006). Peroxisome biogenesis disorders. Biochim Biophys Acta 1763, 1733-1748.

Subramani, S. (1993). Protein import into peroxisomes and biogenesis of the organelle. Annu Rev Cell Biol 9, 445-478.

Sugiura, A., Mattie, S., Prudent, J., and McBride, H.M. (2017). Newly born peroxisomes are a hybrid of mitochondrial and ER-derived pre-peroxisomes. Nature 542, 251-254.

Takizawa, P.A., and Vale, R.D. (2000). The myosin motor, Myo4p, binds Ash1 mRNA via the adapter protein, She3p. Proc Natl Acad Sci U S A 97, 5273-5278.

Tam, Y.Y., Torres-Guzman, J.C., Vizeacoumar, F.J., Smith, J.J., Marelli, M., Aitchison, J.D., and Rachubinski, R.A. (2003). Pex11-related proteins in peroxisome dynamics: a role for the novel peroxin Pex27p in controlling peroxisome size and number in Saccharomyces cerevisiae. Mol Biol Cell 14, 4089-4102.

Tanaka, C., Tan, L.J., Mochida, K., Kirisako, H., Koizumi, M., Asai, E., Sakoh-Nakatogawa, M., Ohsumi, Y., and Nakatogawa, H. (2014). Hrr25 triggers selective autophagy-related pathways by phosphorylating receptor proteins. J Cell Biol 207, 91-105.

Tang, F., Kauffman, E.J., Novak, J.L., Nau, J.J., Catlett, N.L., and Weisman, L.S. (2003). Regulated degradation of a class V myosin receptor directs movement of the yeast vacuole. Nature 422, 87-92.

Titorenko, V.I., and Rachubinski, R.A. (2001). The life cycle of the peroxisome. Nat Rev Mol Cell Biol 2, 357-368.

Tong, A.H., Evangelista, M., Parsons, A.B., Xu, H., Bader, G.D., Page, N., Robinson, M., Raghibizadeh, S., Hogue, C.W., Bussey, H., et al. (2001). Systematic genetic analysis with ordered arrays of yeast deletion mutants. Science 294, 2364-2368.

Tower, R.J., Fagarasanu, A., Aitchison, J.D., and Rachubinski, R.A. (2011). The peroxin Pex34p functions with the Pex11 family of peroxisomal divisional proteins to regulate the peroxisome population in yeast. Mol Biol Cell 22, 1727-1738.

Typas, A., Nichols, R.J., Siegele, D.A., Shales, M., Collins, S.R., Lim, B., Braberg, H., Yamamoto, N., Takeuchi, R., Wanner, B.L., et al. (2008). High-throughput, quantitative analyses of genetic interactions in E. coli. Nat Methods 5, 781-787.

van den Bosch, H., Schutgens, R.B., Wanders, R.J., and Tager, J.M. (1992). Biochemistry of peroxisomes. Annu Rev Biochem 61, 157-197.

van der Zand, A., Gent, J., Braakman, I., and Tabak, H.F. (2012). Biochemically distinct vesicles from the endoplasmic reticulum fuse to form peroxisomes. Cell 149, 397-409.

Vater, C.A., Raymond, C.K., Ekena, K., Howald-Stevenson, I., and Stevens, T.H. (1992). The VPS1 protein, a homolog of dynamin required for vacuolar protein sorting in Saccharomyces cerevisiae, is a GTPase with two functionally separable domains. J Cell Biol 119, 773-786.

Vida, T.A., and Emr, S.D. (1995). A new vital stain for visualizing vacuolar membrane dynamics and endocytosis in yeast. J Cell Biol 128, 779-792.

Vizeacoumar, F.J., Torres-Guzman, J.C., Bouard, D., Aitchison, J.D., and Rachubinski, R.A. (2004). Pex30p, Pex31p, and Pex32p form a family of peroxisomal integral membrane proteins regulating peroxisome size and number in Saccharomyces cerevisiae. Mol Biol Cell 15, 665-677.

Vizeacoumar, F.J., Torres-Guzman, J.C., Tam, Y.Y., Aitchison, J.D., and Rachubinski, R.A. (2003). YHR150w and YDR479c encode peroxisomal integral membrane proteins involved in the regulation of peroxisome number, size, and distribution in Saccharomyces cerevisiae. J Cell Biol 161, 321-332.

Wanders, R.J.A. (2018). Peroxisomal disorders: Improved laboratory diagnosis, new defects and the complicated route to treatment. Mol Cell Probes 40, 60-69.

Wang, S., Idrissi, F.Z., Hermansson, M., Grippa, A., Ejsing, C.S., and Carvalho, P. (2018). Seipin and the membrane-shaping protein Pex30 cooperate in organelle budding from the endoplasmic reticulum. Nat Commun 9, 2939.

Wang, Y.X., Catlett, N.L., and Weisman, L.S. (1998). Vac8p, a vacuolar protein with armadillo repeats, functions in both vacuole inheritance and protein targeting from the cytoplasm to vacuole. J Cell Biol 140, 1063-1074.

Warren, G., and Wickner, W. (1996). Organelle inheritance. Cell 84, 395-400.

Williams, C., Opalinski, L., Landgraf, C., Costello, J., Schrader, M., Krikken, A.M., Knoops, K., Kram, A.M., Volkmer, R., and van der Klei, I.J. (2015). The membrane remodeling protein

Pex11p activates the GTPase Dnm1p during peroxisomal fission. Proc Natl Acad Sci U S A 112, 6377-6382.

Wilsbach, K., and Payne, G.S. (1993). Vps1p, a member of the dynamin GTPase family, is necessary for Golgi membrane protein retention in Saccharomyces cerevisiae. EMBO J 12, 3049-3059.

Wroblewska, J.P., Cruz-Zaragoza, L.D., Yuan, W., Schummer, A., Chuartzman, S.G., de Boer, R., Oeljeklaus, S., Schuldiner, M., Zalckvar, E., Warscheid, B., et al. (2017). Saccharomyces cerevisiae cells lacking Pex3 contain membrane vesicles that harbor a subset of peroxisomal membrane proteins. Biochim Biophys Acta 1864, 1656-1667.

Yamamoto, A., Nagai, K., Yamasaki, M., and Matsuhashi, M. (1990). Solubilization of aster-forming proteins from yeast: possible constituents of spindle pole body and reconstitution of asters in vitro. Cell Struct Funct 15, 221-228.

Yau, R.G., Peng, Y., Valiathan, R.R., Birkeland, S.R., Wilson, T.E., and Weisman, L.S. (2014). Release from myosin V via regulated recruitment of an E3 ubiquitin ligase controls organelle localization. Dev Cell 28, 520-533.

Yau, R.G., Wong, S., and Weisman, L.S. (2017). Spatial regulation of organelle release from myosin V transport by p21-activated kinases. J Cell Biol 216, 1557-1566.

Yifrach, E., Chuartzman, S.G., Dahan, N., Maskit, S., Zada, L., Weill, U., Yofe, I., Olender, T., Schuldiner, M., and Zalckvar, E. (2016). Characterization of proteome dynamics during growth in oleate reveals a new peroxisome-targeting receptor. J Cell Sci 129, 4067-4075.

Yofe, I., Soliman, K., Chuartzman, S.G., Morgan, B., Weill, U., Yifrach, E., Dick, T.P., Cooper, S.J., Ejsing, C.S., Schuldiner, M., et al. (2017). Pex35 is a regulator of peroxisome abundance. J Cell Sci 130, 791-804.

Yofe, I., Weill, U., Meurer, M., Chuartzman, S., Zalckvar, E., Goldman, O., Ben-Dor, S., Schutze, C., Wiedemann, N., Knop, M., et al. (2016). One library to make them all: streamlining the creation of yeast libraries via a SWAp-Tag strategy. Nat Methods 13, 371-378.

Yoshida, Y., Niwa, H., Honsho, M., Itoyama, A., and Fujiki, Y. (2015). Pex11p mediates peroxisomal proliferation by promoting deformation of the lipid membrane. Biol Open.